Title

Liquid phase epitaxial growth and characterization of germanium far infrared blocked impurity band detectors

Author

Bandaru, Jordana

Publication Date

2001-05-12

Liquid Phase Epitaxial Growth and Characterization of Germanium Far Infrared Blocked Impurity Band Detectors

by

Jordana Bandaru

B.S.E. (University of Pennsylvania) 1994
M.S. (University of California, Berkeley) 1997

A dissertation submitted in partial satisfaction of the requirements for the degree of

Doctor of Philosophy

in

Engineering – Materials Science & Mineral Engineering

in the

GRADUATE DIVISION

of the

UNIVERSITY OF CALIFORNIA, BERKELEY

committee in charge:

Professor Eugene E. Haller, Chair

Professor Oscar D. Dubón, Jr.

Professor Chenming Hu

Spring 2001

Abstract

Liquid Phase Epitaxial Growth and Characterization of Germanium
Far Infrared Blocked Impurity Band Detectors
by
Jordana Bandaru
Doctor of Philosophy in Engineering – Materials Science & Mineral Engineering
University of California, Berkeley
Professor Eugene E. Haller, Chair

Germanium Blocked Impurity Band (BIB) detectors require a high purity blocking layer (< 10^{13} cm^{-3}) approximately 1 μm thick grown on a heavily doped active layer (~ 10^{16} cm^{-3}) approximately 20 μm thick. Epilayers were grown using liquid phase epitaxy (LPE) of germanium out of lead solution.

The effects of the crystallographic orientation of the germanium substrate on LPE growth modes were explored. Growth was studied on substrates oriented by Laue x-ray diffraction between 0.02° and 10° from the {111} toward the {100}. Terrace growth was observed, with increasing terrace height for larger misorientation angles.

It was found that the purity of the blocking layer was limited by the presence of phosphorus in the lead solvent. Unintentionally doped Ge layers contained ~ 10^{15} cm^{-3} phosphorus as determined by Hall effect measurements and Photothermal Ionization Spectroscopy (PTIS). Lead purification by vacuum distillation and dilution reduced the phosphorus concentration in the layers to ~ 10^{14} cm^{-3} but further reduction was not

observed with successive distillation runs. The graphite distillation and growth components as an additional phosphorus source cannot be ruled out.

Antimony (~ 10^{16} cm^{-3}) was used as a dopant for the active BIB layer. A reduction in the donor binding energy due to impurity banding was observed by variable temperature Hall effect measurements. A BIB detector fabricated from an Sb-doped Ge layer grown on a pure substrate showed a low energy photoconductive onset (~ 6 meV). Spreading resistance measurements on doped layers revealed a nonuniform dopant distribution with Sb pile-up at the layer surface, which must be removed by chemomechanical polishing. Sb diffusion into the pure substrate was observed by Secondary Ion Mass Spectroscopy (SIMS) for epilayers grown at 650 °C. The Sb concentration at the interface dropped by an order of magnitude over ~ 1.5 µm. Layers grown at 550 °C did not show significant Sb diffusion.

Sn doped In_2O_3 (ITO) was studied for use in far infrared transparent low temperature contacts for BIB arrays. It was found that ~100 nm of ITO deposited on Ge remains electrically conducting at 4 K and is ~ 90% transparent in the far infrared. ITO should be suitable for passivating contacts to Ge BIB arrays.

Table of Contents

Acknowledgements

I would first like to thank Professor Haller for providing me with the opportunity to conduct this research, and for his support and guidance throughout. I am thankful for the wonderful experience I have had at Berkeley and at LBL. Thanks to Jeff Beeman for contributing his time to my project, and for imparting some of his laboratory knowledge on me. Thanks to Bill Hansen whose experience in the lab has been a benefit to this project. I would like to thank Dr. Hartmut Bracht and Stefan Voss for their help with spreading resistance measurements. Thanks to David for ensuring that administrative work always ran smoothly. Thanks to all of my fellow graduate students for creating such an enjoyable work environment, and for their willingness to devote time to helping out fellow students. Special thanks to Prabhakar for helping in so many ways, both scientific and personal, and for putting up with our living in separate cities so that I could pursue this research.

I would like to acknowledge financial support from the Intel Robert Noyce Fellowship in Microelectronics. Financial support for this project was provided by the California Institute of Technology Jet Propulsion Laboratory in conjunction with NASA (Contract #1218214), and by NASA Washington D.C. Headquarters, Order #W19530, through the U.S. Department of Energy under Contract No. DE-AC03-76SF00098.

1 Introduction

1.1 Far Infrared Detectors

1.1.1 Motivation for Development of Far Infrared Detectors

The far infrared region of the electromagnetic spectrum (25 - 200 µm) is of great interest to astronomers, astrophysicists, and cosmologists [Lemke, 2000, Pilbratt, 1994, Rieke, 1986,]. In this spectral range much of the universe remains unexplored. The earth's atmosphere is opaque in this region of the spectrum, and therefore it is necessary to make infrared observations from high altitude sites or earth-orbiting satellites. Such missions include the Infrared Astronomy Satellite (IRAS) launched in 1983, the Cosmic Background Explorer (COBE) launched in 1989 [Mather, 1994], the Infrared Space Observatory (ISO) launched in 1995 [Lemke, 2000], the Space Infrared Telescope Facility (SIRTF) to be launched in 2001 [Rieke, 1986, 2000, Brandl, 2000], the Stratospheric Observatory for Infrared Astronomy (SOFIA), an airplane to be flown starting in 2003 [Becklin, 2000], and the Far InfraRed and Submillimetre Space Telescope (FIRST) to be launched in 2007 [Pilbratt, 1994, 2000].

Far infrared observations play an important role in understanding such scientific phenomena as the birth and evolution of planetary systems, star formation, and active galactic nuclei. Emissions from galaxies in the infrared part of the spectrum range from 30% in normal galaxies to 100% in active star-forming galaxies [Efstanathiou, 2000], and about 40% of stellar output is emitted in the far infrared peaking in the 100–140 µm wavelength region [Dwek, 2000]. The sites of star formation are cold clouds of interstellar dust which absorb starlight and re-emit in the far infrared. Far infrared emissions corresponding to excited states of molecules (e.g. rotational transitions of HeH^+, OH, NH_3, H_3O^+) as shown in Figure 1 could provide information on the composition, temperature, and ionization state of species in interstellar clouds. As more and more observations are made, astronomers expect to gain a better understanding of the processes at work in forming the complex structures in the universe.

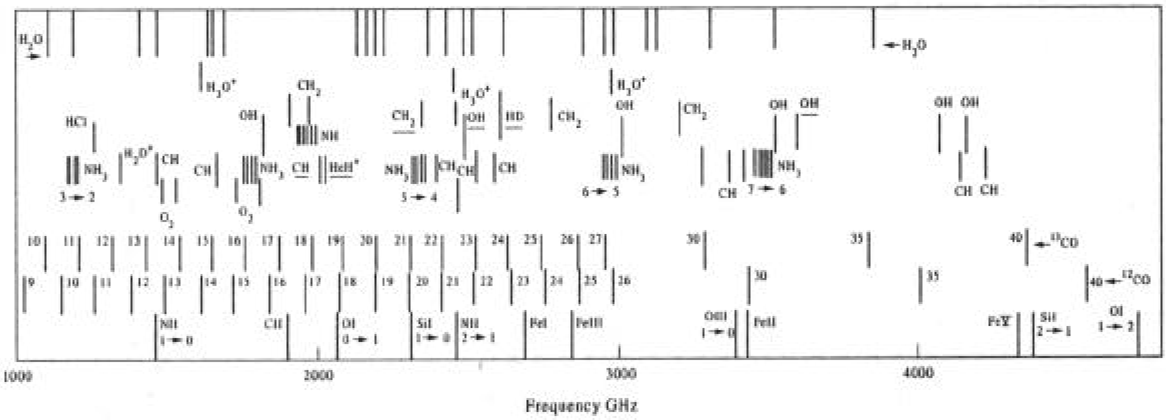

Figure 1. Some important atomic and molecular transitions. Rotational lines are marked with an upper J-value; underlining indicates transitions connected to the ground state. From Pilbratt, 1994

1.1.2 Current Detector Technology

Observations that could provide insight into the processes described above require sensitive far infrared detectors operating on satellites high in or above the earth's atmosphere. ISO was capable of photometry in broad and narrow spectral bands ranging from 2.5 – 240 μm and spectroscopy from 50 to nearly 200 μm [Kessler, 2000]. While ISO provided high resolution spectroscopy, SIRTF will focus on large format, high performance infrared arrays suited to advances in infrared surveys [Rieke, 2000]. The detectors that will be used on SIRTF are described in Table 1.

Wavelength	**Detector**	**Supplier**	**Instrument**
3.6 - 4.5 μm	Two 256 x 256 pixel InSb arrays	Raytheon/Santa Barbara Research Corporation	Infrared Array Camera (IRAC)
5.8 – 8 μm	Two 256 x 256 pixel Si:As BIB arrays	Raytheon/Santa Barbara Research Corporation	Infrared Array Camera (IRAC)
5.3 – 40 μm	128 x 128 pixel Si:As and Si:Sb BIB arrays	Boeing North America & Cornell University	Infrared Spectrograph (IRS), long wavelength part uses Si:Sb BIB
24 μm	128 x 128 pixel Si:As BIB array	Boeing North America & Cornell University	Multiband Imaging Photometer for SIRTF (MIPS)
70 μm	32 x 32 pixel Ge:Ga array	Lawrence Berkeley National Laboratory, University of Arizona, and Hughes Aircraft/Raytheon	Multiband Imaging Photometer for SIRTF (MIPS)
160 μm	2 x 20 pixel stressed Ge:Ga array	Lawrence Berkeley National Laboratory, University of Arizona, and Hughes Aircraft/Raytheon	Multiband Imaging Photometer for SIRTF (MIPS)

Table 1. Detectors to be used on SIRTF. Data from Rieke, 2000.

Figure 2 shows how a photoconductor can be tailored to the wavelength of interest by adding a suitable dopant. Si with dopant binding energies ~ 50 meV is typically used for mid infrared detectors, and Ge which has shallower dopants (~ 10 meV) is used for far infrared detectors. The response of Ge photoconductors can be extended to longer wavelengths by applying a uniaxial compressive stress which splits the degeneracy of the light and heavy hole bands, leading to a reduced binding energy for shallow acceptors. The drawback of the stressed Ge detector is the difficulty in fabrication of large 2-dimensional arrays.

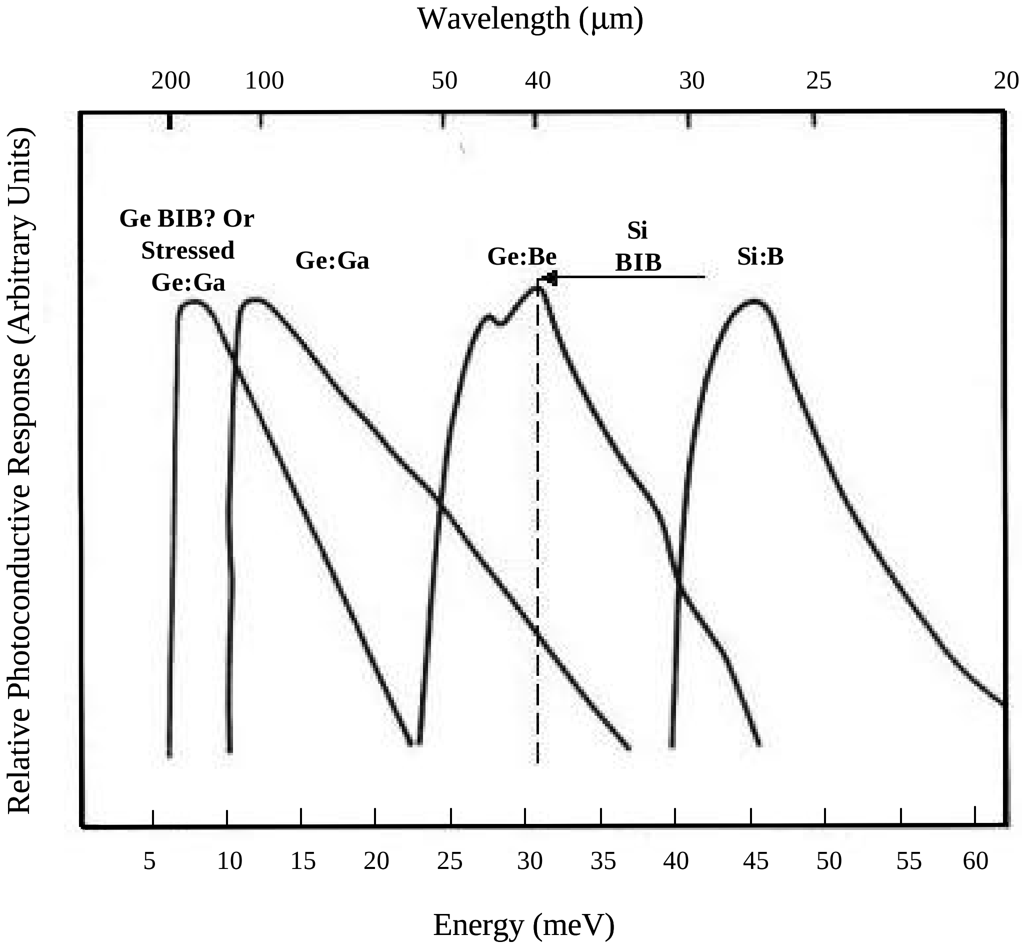

Figure 2. Relative photoconductive response for some Si and Ge photoconductors. Each spectrum has been normalized independently.

The goal of this project is to develop a Ge BIB detector that could satisfy the necessary requirements for far infrared astronomical observation. In principle, there is no fundamental lower limit to the energy photoresponse of a BIB, although there may be practical limitations. Such a detector could potentially replace stressed Ge:Ga detectors as well as unstressed Ge photoconductors. BIB detectors have been realized in silicon where they show longer wavelength response and higher absorption than normal silicon photoconductors. Adapting BIB technology to Ge requires achieving higher purity than Si (due to shallower dopants with larger Bohr orbits) as well as a thorough study of layer growth and impurity banding of shallow dopants in Ge. These important issues are studied in this work.

1.1.3 Photoconductor Parameters

Some important characteristics of photoconductors which are often used as figures of merit are spectral response, dark current, responsivity, responsive quantum efficiency, noise equivalent power (NEP), and detective quantum efficiency.

The **spectral response** characterizes the intensity of the photoconductive signal at different photon wavelengths. The spectra for shallow dopants in semiconductors, as shown in Figure 2, have a sharp onset at the ionization energy of the dopant. The intensity falls off on the higher energy side since the dopant level only occupies a finite width in k-space (for absorption of a photon the transition cannot change k value).

Dark current is defined as the electrical current that flows through the biased detector in the absence of light. It should be kept as low as possible since it contributes to noise. Some sources of dark current are surface leakage, leakage through defects such as cracks, and hopping conductivity.

Responsivity (R) is defined in A/W as the ratio of photoconductive current to incident photon power.

$$\mathrm{R} = \frac{\mathrm{e}}{h\nu} G\eta \qquad \text{Equation 1}$$

where e is the charge of an electron, h is Planck's constant, ν is the frequency of incident photons, G is the photoconductive gain (carriers detected /carriers produced), and η is the responsive quantum efficiency (carriers produced/photons incident).

The photoconductive gain is defined as the ratio of carrier lifetime (τ) to transit time (t) in the detector under applied bias.

$$G = \frac{\tau}{t} \qquad \text{Equation 2}$$

For a Blocked Impurity Band (BIB) detector the gain is 1 because carriers cannot recombine before crossing the device as discussed in section 1.1.4.

Responsive quantum efficiency (η) is a unitless quantity defined as the ratio of flux of absorbed photons to incident photons.

$$\eta = \frac{(1-r)\{1-\exp(-\alpha L)\}}{1-r\{\exp(-\alpha L)\}} \qquad \text{Equation 3}$$

where r = reflectivity, α is the linear absorption coefficient, and L is the thickness of the material. The linear absorption coefficient is the neutral dopant concentration, N_D, times the ionization cross section which is ~ 10^{-14} cm^{-2} for shallow dopants in germanium [Rotsaert, 1989]. The responsive quantum efficiency should be as high as possible. It can be increased by using higher dopant concentrations, thicker material, or by lowering the surface reflectivity by adding antireflective coatings. The reflectivity (r) is given by:

$$r = \frac{(n_1 - n_2)^2}{(n_1 + n_2)^2} \qquad \text{Equation 4}$$

where n_1 is the medium the light is traveling from and n_2 is the medium the light is traveling into. For vacuum (n=1) to germanium (n=4), r = 0.36.

Noise Equivalent Power (NEP) is given in W/√Hz and is defined as the photon power required to produce a signal to noise ratio of one per unit bandwidth ($\text{NEP} = \frac{\text{P}}{\text{S/N}}$) where P = signal power (W), S = signal (A) and N = background noise (A/√Hz). A low NEP is necessary for operation in extremely low background conditions. Such conditions prevail on satellites probing the darkest regions of space. The lowest value that the NEP can have is the background limited value known as NEP_{BLIP}. This background value is due to fluctuations in the photon stream and is given by

$$NEP_{BLIP} = 2\sqrt{Phu} \qquad \text{Equation 5}$$

Detective Quantum Efficiency (DQE or h $_{\text{detective}}$) is defined as the square of the ratio of the experimental and background limited NEP and is a measure of noise in the device above the background limited noise.

$$DQE = \left(\frac{NEP_{BLIP}}{NEP_{Measured}}\right)^2 \qquad \text{Equation 6}$$

A DQE of 1 means that there is no excess noise from the detector or electronics above the background photogenerated noise. A DQE < 1 can, for example, originate from electronic or device contact generated noise. For a further treatment of noise in photodetectors, see Haegel, 1983.

1.1.4 Blocked Impurity Band Detector Operation

The Blocked Impurity Band (BIB) detector concept was first proposed in 1980 by Petroff and Stapelbroek at the Rockwell International Science Center. A schematic of an n-type Blocked Impurity Band (BIB) detector is shown in Figure 3. The infrared absorbing layer of the device is a heavily doped semiconductor with impurity levels broadened to form an impurity band. This allows photons with lower energies to be detected. If an impurity band semiconductor were used as a traditional photoconductor, a large dark current (current in the absence of light) would flow because electrons would move in the impurity band even though they would not have enough energy to enter the conduction band (these devices are operated at low temperatures such that electrons do not have thermal energy to enter the conduction band). This dark current would cause noise far above the signal level. To overcome this problem and block the dark current the BIB detector uses a blocking layer, an intrinsic semiconductor, inserted between the absorbing layer and one of the electrical contacts. The blocking layer must be very pure to effectively block dark current ($< 10^{13}$ cm^{-3} impurities for germanium).

The operation of the BIB device can be understood from Figure 3. Although the absorbing layer is an n-type semiconductor it will always contain some p-type impurities.

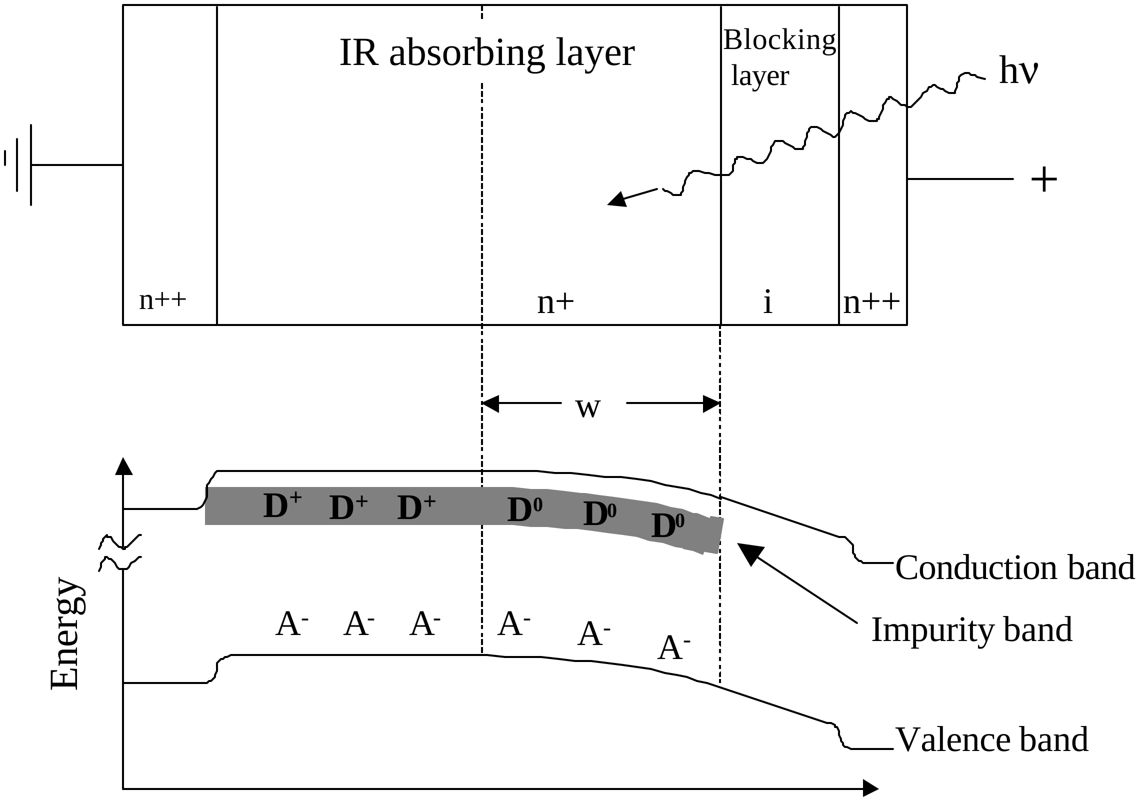

Figure 3. Schematic of an n-type Blocked Impurity Band detector with band diagram below, shown for a device with an electric field applied. Contacts are labeled n^{++}. D^+ = ionized donor, D^0 = neutral donor, A^- = ionized acceptor, w = depletion width.

These acceptors can accept electrons from the donors, leaving ionized donor and acceptor states distributed through the layer. When an electric field is applied, the electrons move in the impurity band toward the positive contact where they are stopped by the blocking layer. The electrons thereby fill in the ionized donor states closest to the positive contact. In this region (the depletion width, w), there will then be a net negative space charge due to the negatively charged impurity acceptors. This depletion width is the active region of the device. The absorbed photons excite electrons from the donor band into the conduction band where they can then be collected at the positive contact.

The Ge BIB detector will have several advantages over the standard extrinsic Ge photoconductor. The obvious advantage is the lowering of minimum detectable energy by impurity band broadening without the need for applying stress. The second advantage is that the dopant level required for impurity banding (~10^{16} cm^{-3} in germanium) is two orders of magnitude larger than the typical dopant level in a Ge photoconductor (~10^{14} cm^{-3}). The optical absorption coefficient is therefore proportionally larger. This means that the active region of the BIB detector can be ~ 100 times smaller than the photoconductor. This renders the device smaller and therefore less susceptible to interfering cosmic radiation. Another advantage is the lack of recombination of electrons crossing the depletion region. This results in a unity photoconductive gain compared to a gain which varies with bias in a traditional photoconductor.

1.1.5 Germanium Blocked Impurity Band Detector Requirements

The width of the depletion region (w) in a BIB depends on the applied bias (V_a), the built in bias (V_{bi}), the minority dopant concentration (N_A), and the blocking layer thickness (b):

$$\mathrm{w} = \left[\sqrt{\frac{2\varepsilon\varepsilon_0 (\mathrm{V_a} - \mathrm{V_{bi}})}{\mathrm{eN_A}} + b^2} \right] - b \qquad \text{Equation 7}$$

The built in bias (the difference in Fermi level between the active layer and blocking layer which are both n-type) is very small and can be neglected. A derivation of the electric field and depletion width in a BIB is given in appendix A.

The depletion width dependence on applied bias for various N_A and b values are calculated for germanium and shown in Figure 4. A typical Ge:Sb photoconductor contains [Sb] = 2×10^{14} cm^{-3} and has an active volume of 2.25 mm^3 [Beeman, 1996]. A BIB detector would be doped ~ 100 times higher, and therefore would require a volume ~ 0.0225 mm^3. The depletion width needed varies depending on the pixel size. For example, a 2×2 mm^2 pixel size would require a 5.6 μm depletion width to achieve an active volume of 0.0225 mm^3. Several pixel sizes are indicated in Figure 4 for reference. Of the requirements for the active layer, the minority dopant concentration (N_A) has the largest effect on depletion width and should be as low as possible. The thickness of the blocking layer appears to have less of an effect, but it should be kept as thin as possible for achieving high electric fields with low bias.

The active layer of the BIB should be doped to a level where impurity band conduction occurs. For shallow dopants in germanium, banding begins at $\sim 10^{16}$ cm^{-3} and metallic conductivity occurs at $\sim 10^{17}$ cm^{-3}. Both the optical absorption and the photoconductive response of the BIB are expected to increase as the doping concentration increases. Ideally, it would be possible to tailor the onset of spectral response to any value between zero and the ionization energy. There are expected to be some practical limitations, for example local fluctuations in concentration could leave some regions metallic even if the overall concentration is not. It is expected that dark current will

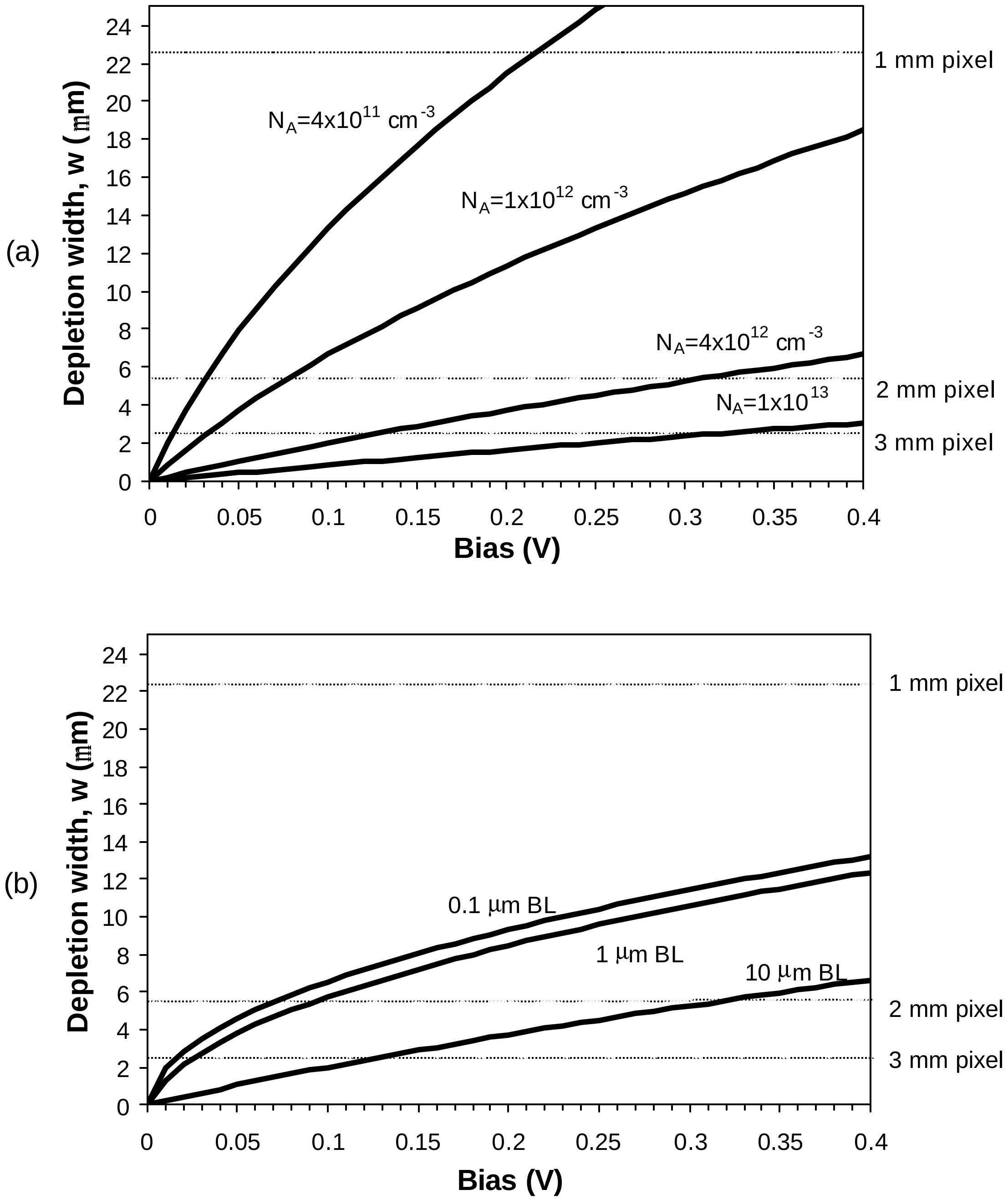

Figure 4. Depletion width vs. applied bias for (a) varying minority dopant concentrations with fixed blocking layer thickness = 10 μm and (b) varying blocking layer (BL) thickness with fixed $N_A = 4 \times 10^{12}$ cm^{-3}. Dashed lines indicate the required depletion width for the indicated pixel size (e.g. 2 mm indicates a 2 x 2 mm^2 pixel requiring a 5.6 μm depletion width to achieve a 0.0225 mm^3 active volume).

become unacceptably large for very low energies between the dopant band and the conduction band edge. However, it should be reasonable to achieve a photoconductive onset of ~ 6 meV (as low as stressed Ge:Ga detectors). The theoretical spectral response for Ge:Sb BIB detectors of varying Sb concentration has been calculated [Olsen, 1998] based on two models which estimated the broadening of the impurity band with doping concentration [Petroff 1984, Shklovski, 1984]. The broadening was modeled as proportional to N_D in one case and $N_D^{1/2}$ in the second case. Modeling can give an approximation of the onset in spectral response of ~ 200 μm (50 cm^{-1}). The actual onset must be determined experimentally by absorption or spectral response measurements on BIB structures.

Traditional Ge photoconductors contain ~ 10^{14} cm^{-3} dopants without incurring significant dark currents. This would therefore seem to be an appropriate concentration for the BIB blocking layer. However, modeling has shown that the electric field distribution in the BIB creates a more stringent requirement of < 10^{13} cm^{-3}. A BIB model has been developed using a numerical finite difference approach and taking into account space charge effects and spatial doping variations [Haegel, 2000]. The purity of the blocking layer and diffusion at the blocking/active layer interface are shown to be important factors. Modeling has focused on p-type Ge:Ga BIB structures but can be extended to other dopants. Increasing the acceptor concentration in the blocking layer increases the space charge in the blocking layer. This space charge is from negatively charged ionized acceptors which will always be present to some degree. For an ideally pure blocking layer the resulting field slope $dE/dx = \rho/\varepsilon\varepsilon_0$ is negligible. However, if the

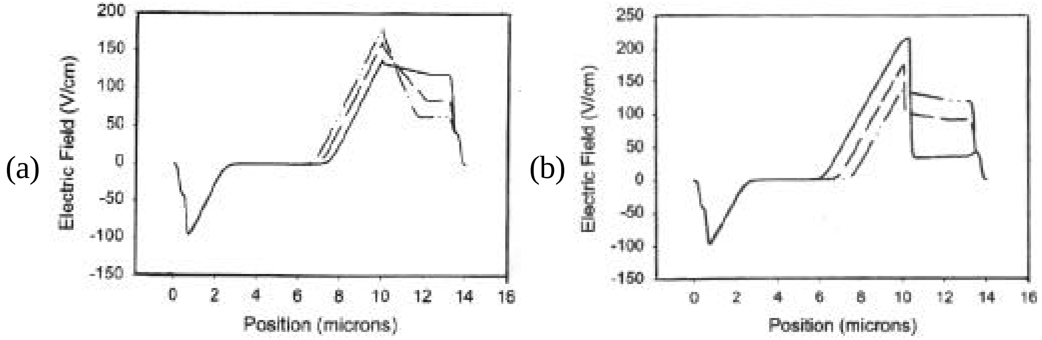

Figure 5. Effect of increasing (a) the acceptor concentration in the blocking layer (N_A = 1 x 10^{12} cm^{-3} solid line, 5 x 10^{12} cm^{-3} dashed line, and 1 x 10^{13} cm^{-3} dash-double dot-dashed line) and (b) the grade parameter (increasing grade parameter from dash-double dot-dashed line to dashed line to solid line) on the electric field distribution in a Ge:Ga BIB device. Increasing the grade parameter broadens the interface between the blocking layer and the active layer. [Haegel, 2000]

concentration in the blocking layer is too high the electric field can be reduced to a negligible amount in the part of the blocking layer closest to the electrical contact as shown in Figure 5. This should lower the responsivity of the device and will occur with lower concentration blocking layers than used in traditional photoconductors. It was also shown that a graded interface (as obtained from interdiffusion between the doped and blocking layers) could yield similar results leading to a collapse of the electric field in the device as shown in Figure 5.

1.1.6 Review of Silicon Blocked Impurity Band Detectors

Before the advent of the Si BIB, bulk Ge:Be detectors were the state of the art in the wavelength region from 30 to 50 µm [Haegel, 1985]. The silicon BIB has the advantage of a smaller detector volume and smaller mass and therefore lower sensitivity to cosmic radiation. The silicon BIB detector has been developed for space-based low background conditions and applied in infrared arrays using arsenic [Reynolds, 1989] and antimony [Huffman, 1992, Sirmain, 1992]. Boron [Leotin, 1999] has also been studied as a dopant but is not currently being used in Si BIBs for missions. Si:As BIB detectors have shown high responsivity and low signal-to-noise between 2.5 and 28 µm. Si:Sb responds between 2.5 and 40 µm. The reasons for choosing one shallow dopant over another for photoconductors are unclear from the literature, however As and Sb seem to have shown the best performance in silicon. In germanium the situation is different, and Ga is the most widely used shallow dopant. Ga possesses several desirable properties. For example, it is isocoric, it has a low vapor pressure, and it has a resistance to oxidation (as compared to B and Al). One could also speculate that diffusivity of dopants may play a role. In silicon the n-type dopants are slow diffusers compared to the p-type dopants while in germanium the p-type dopants are the slow diffusers [Stolwijk, 1998, Murch, 1984]. Diffusion could lead to nonuniform dopant distributions in photoconductors. For BIB devices, diffusion at the blocking layer-active layer interface would destroy the electric field distribution.

The development of the silicon BIB was made possible by the large research and development effort spent on pure silicon thin film growth. Si:Sb layers have been grown by CVD using $SiHCl_3$ [Sirmain, 1992] or $Si_2H_2Cl_2$ [Huffman, 1992] and $SbCl_5$. Doping of the IR active layer for Si:Sb and Si:As detectors is typically in the range of 1-7 x 10^{17} cm^{-3} and the pure blocking layer and compensating acceptor concentration is 5 x 10^{12} cm^{-3}. The germanium BIB has more stringent requirements than silicon, and high purity growth of germanium thin films has not been well established. A germanium BIB detector with the same blocking layer concentration would be expected to have a higher leakage current than the silicon device (operating at the same temperature) due to the smaller donor ionization energy in germanium. An effort in growing high purity epilayers is required before the Ge BIB structure can be realized.

1.1.7 Array Requirements

As infrared cameras become more advanced, there is a drive to increase the number of pixels and fabricate larger arrays. A growth method for BIB devices should take into account the ability to extend the process to large format array fabrication. Two possible BIB array structures are the front-illuminated and back-illuminated devices as

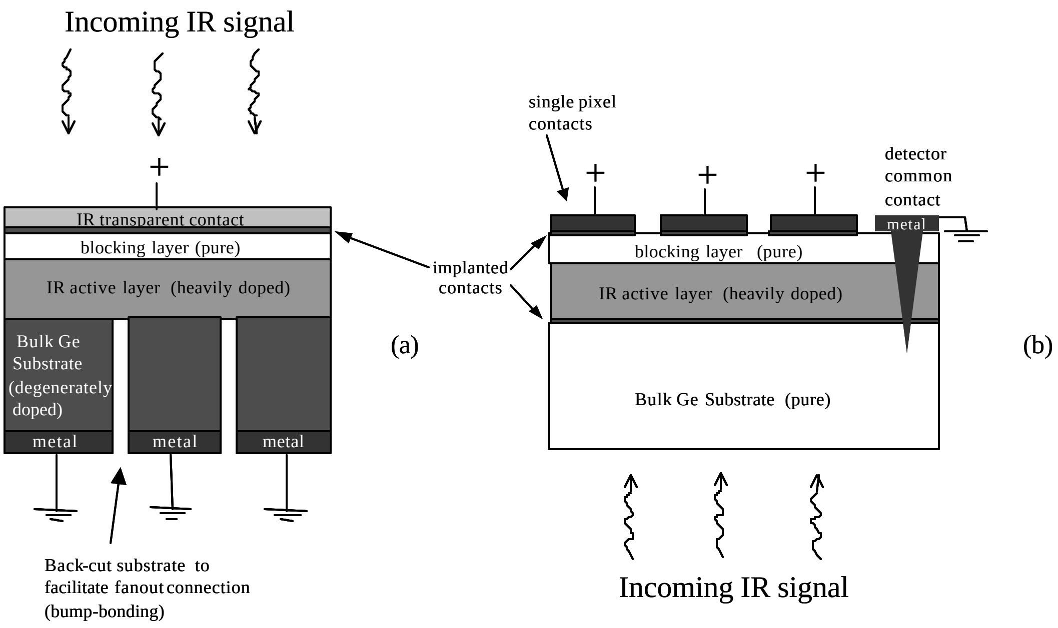

Figure 6. Schematic of (a) front-illuminated BIB array (b) back-illuminated BIB array.

shown in Figure 6. In the front illuminated structure, the doped IR active layer and pure blocking layer are grown on a degenerately doped substrate. A transparent contact is then deposited on the entire top surface. This can be a thin layer of indium tin oxide sputtered onto the surface. The substrate can then be patterned into pixels by dicing on the back side. The wafer is then bump bonded to a fanout connection. In the back-illuminated configuration, both layers are grown on a pure infrared transparent substrate. The substrate is implanted to form a thin back contact. The top contacts to the blocking layer are implanted and metalized and need not be transparent. The top contact is bump bonded to a fanout connection. The common back contact can be made by cutting into the wafer from the top using a dicing saw and depositing metal into the cut. The back illuminated structure has been used in Si:As BIB arrays [Reynolds, 1989]. Either structure should be feasible for the germanium BIB provided both the blocking layer and active layer can be grown epitaxially.

1.2 Liquid Phase Epitaxy

1.2.1 Previous Growth Efforts & Motivation for LPE

Growth techniques for achieving ultra high purity epitaxial germanium have not yet been established, although growth of ultra pure ($< 10^{10}$ cm^{-3}) bulk germanium crystals has been a major achievement [Haller, 1981]. Initial growth of the layers required for Ge BIB detectors at Berkeley was by chemical vapor deposition (CVD). Residual dopants were found to be acceptors, leading to the choice of growing pure layers on Ga-doped substrates. The main problems encountered in CVD growth were gas phase nucleation and inhomogeneous growth [Rossington, 1988, Lutz, 1991]. Structural defects in the epilayers contributed to deep acceptor levels ~ 5 x 10^{16} cm^{-3}. Copper concentrations were ~ 3 x 10^{13} cm^{-3} and shallow levels were present at ~ 6 x 10^{11} cm^{-3}. The high temperatures required to crack $GeCl_4$ precursors caused diffusion at the interface between blocking layer and active layer. Oxygen and carbon were found at the layer-substrate interface. BIB detectors fabricated from these epilayers had high leakage currents and did not show extended wavelength response.

Efforts at the Rockwell International Science Center and the University of Rochester [Huffman, 1992, Watson, 1993] have led to Ge:Ga BIB detectors by CVD using $GeCl_4$. Growth temperatures ~ 800 °C were used and growth rates as high as 18µm/hr were achieved. Purity of epilayers was measured using room temperature spreading resistance, and it was only possible to report purity ≤ 2 x 10^{13} cm^{-3} (intrinsic concentration). A bulk Ga doped crystal was used for the active region in devices that were tested. Compensation for the Ga doped crystal was determined by capacitance-voltage measurements of the BIB device and found to be ~ 5 x 10^{12} cm^{-3}. The depletion width (w) of their devices as calculated from Equation 7 is 2 µm. While they were able to achieve some detectors which responded down to 50 cm^{-1}, results were not reproducible and the detectors suffered from large dark current due to unpassivated surfaces. As a result of the small depletion width, the bulk of the substrate was absorbing but did not contribute to BIB response. This effective high series resistance slowed down the device considerably. This problem could potentially be solved by increasing the size of the depletion width and using a thinner epitaxial doped layer.

Liquid Phase Epitaxy (LPE) was seen as a promising technique by Olsen [1998] who designed and built the LPE reactor at Berkeley. The most attractive aspect of LPE growth is the fact that most impurities prefer to segregate to the liquid phase rather than incorporate in the growing layer. Segregation coefficients of 10^{-2} to 10^{-3} are common. This offers possibilities for high purity growth. Growth could potentially take place at low temperature, also desirable for high purity. In addition, LPE layers of 1-100 µm thick are commonly grown, an advantage for growing both the thick active layer and the thin blocking layer.

Growth efforts by LPE have focused on Pb as a solvent (a group IV element with a low melting point). However, the purity of commercially available Pb was found to be a problem, with n-type impurities ~ 10^{15} cm^{-3}. Devices were fabricated by Olsen [1998] using Sb doped LPE layers grown on pure substrates. The substrates were thinned to form the blocking layer. The devices tested showed some extended wavelength response. This was seen as an indication that the LPE process could be improved to meet the requirements for Ge BIB devices. Optimization of blocking layer thickness and concentration would be necessary. Solvent purity was identified as an important area of research, as high purity would be required for growth of both the pure and active layers.

1.2.2 Review of Germanium Liquid Phase Epitaxy

The main focus of semiconductor LPE reported in the literature has been on the growth of doped layers. The solvents used in growth have either been dopants or have contained high quantities of dopants. For example, silicon has been grown out of solutions of Ga [Linnebach, 1982], In [Konuma, 1993], and Sn [Shi, 1995].

Germanium has been grown from liquid metals including Ga, In, Sn, As, Sb, and Bi [Keck, 1953, Spitzer, 1961, Kijima, 1970]. Germanium has also been grown from Pb [Immorlica, 1980] on GaAs substrates, yielding layers with high concentrations of Ga and As. There has been recent interest in growth of ultra pure GaAs layers for x-ray and infrared detectors [Wynne, 1999] out of a Ga solution. Gallium can be obtained with very high purity (8N). A solvent of such high purity has not been available for LPE growth of Si and Ge.

The first attempt at growing high purity germanium by liquid phase epitaxy [Olsen, 1998] was from a solution using 6N commercially available Pb. A residual donor concentration of $\sim 10^{15}$ cm^{-3} was shown to be originating in the Pb solution. Pb was chosen as a solvent because it has a low melting point, is not electrically active in Ge, and has a relatively low solubility in Ge. Sn also meets the first two criteria, but has a high solubility (4×10^{20} cm^{-3} at 650 °C) in Ge leading to defects and polycrystalline growth [Trumbore, 1956]. Attempts were made at measuring the Pb concentration in LPE layers by Secondary Ion Mass Spectrometry (SIMS) and x-ray fluorescence. In both cases, the Pb concentration was below the detection limit of $\sim 10^{17}$ cm^{-3}. An electron mobility at 77 K lower than that of bulk crystals was observed in LPE layers and was attributed to Pb incorporation. It was reasoned that the strain induced by the Pb atoms in the Ge lattice inhomogeneously perturbs the conduction band enough to account for the lowering of the mobility by scattering from band edge fluctuations.

The surface morphology of GaAs and Si layers as well as the critical angles for terrace formation have been well studied as described in section 1.2.4. Growth modes have been shown to impact epilayer quality and are expected to impact device performance. The morphology of Ge homoepitaxial LPE layers has not been studied in detail until this work.

1.2.3 Liquid Phase Epitaxy Process

Liquid Phase Epitaxy involves the precipitation of a solute out of solution onto a substrate. For Ge growth from a Pb solvent, Ge is dissolved in Pb at an elevated temperature (e.g. 650 °C). The Pb becomes saturated with Ge according to the phase diagram shown in Figure 7. The solution is then brought into contact with a single crystal Ge substrate and cooled. As cooling takes place, the composition of the solution follows the liquidus line with Ge precipitating out of solution. Nucleation on the Ge substrate is energetically preferable to homogeneous nucleation (although for slow cooling rates some homogeneous nucleation is observed).

Several methods of LPE have been developed, and each uses a different equipment design and growth technique [Astles, 1990]. Some of these techniques include the tipping boat system, the dip system, the sliding boat system, and more recently, the centrifuge system [Konuma, 1996]. The tipping boat system was chosen for this project because it is a relatively simple mechanical design and it avoids direct contact with the substrate in order to remove the solvent. A schematic of the tipping boat system is shown in Figure 8. A graphite crucible contains the growth materials. Growth begins when the solvent is tipped onto the germanium substrate and the temperature is lowered. The system is tipped back to the starting position to terminate growth.

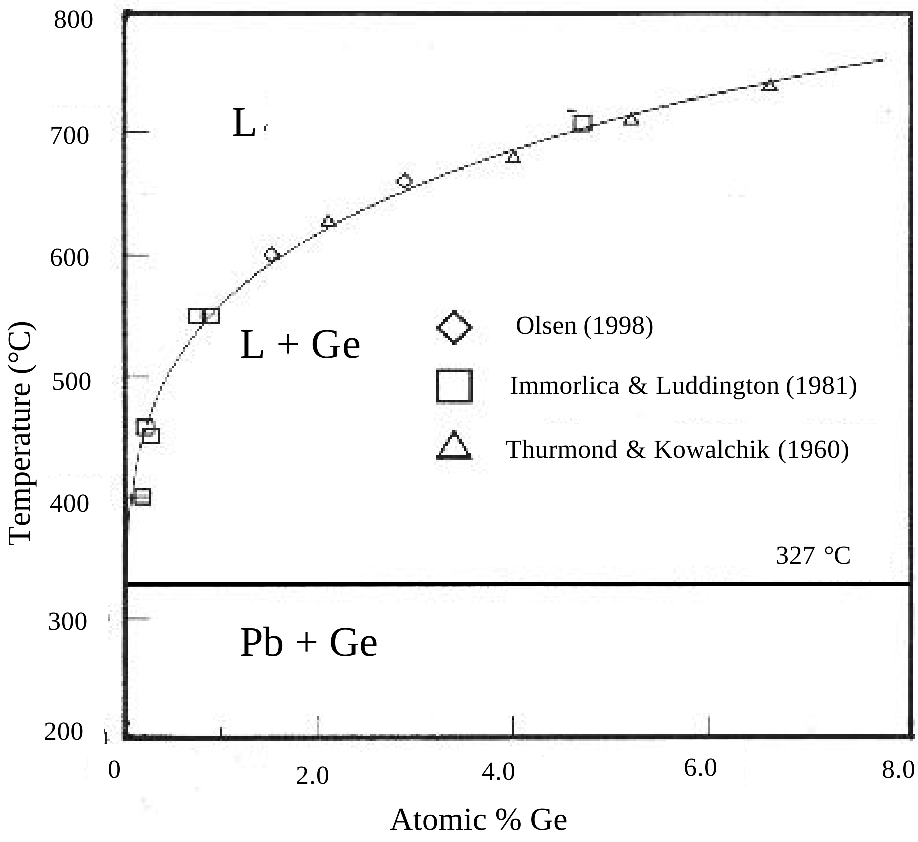

Figure 7. The Pb-rich side of the Pb-Ge phase diagram.

The incorporation of impurities or dopant atoms into the growing layer is characterized by a segregation coefficient (k). The segregation coefficient is defined as the concentration of dopant in the solid layer divided by the concentration of dopant in the liquid solvent. Direct measurement of k is possible by dissolving a known amount of

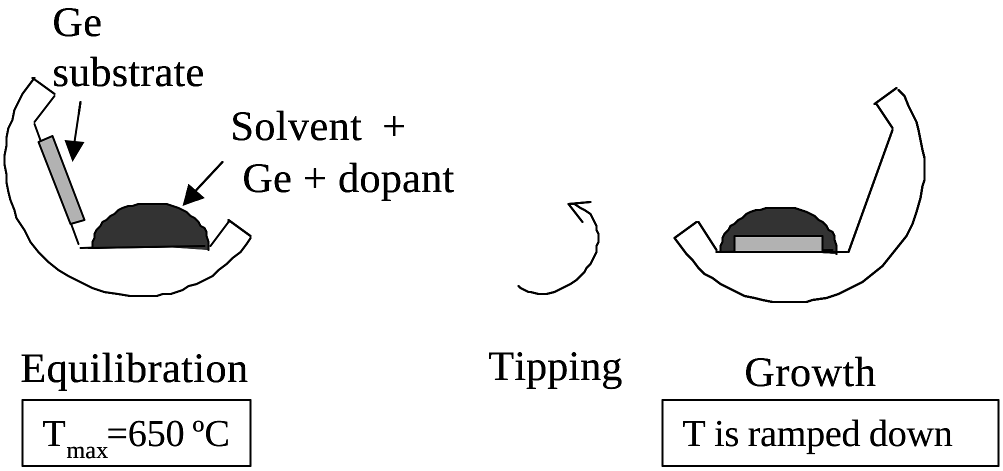

Figure 8. Liquid Phase Epitaxy growth procedure showing growth materials in a graphite crucible. The solvent is tipped onto the substrate to begin growth and tipped off to terminate growth

dopant in the solvent and measuring (e.g. by Hall effect) the amount incorporated in the solid layer after growth. An approximation was developed for estimating the segregation coefficient based on information obtainable from phase diagrams [Rosenberger, 1979].

The effective segregation coefficient k_{eff} given here for Sb in the Pb-Ge system is approximated with:

$$k_{eff} \approx \frac{X_{Ge}^{sat} Pb}{X_{Sb}^{sat} Pb} \qquad \text{Equation 8}$$

where $X_{Ge}^{sat} Pb$ is the saturation concentration of Ge in Pb at a given temperature and $X_{Sb}^{sat} Pb$ is the saturation concentration of Sb in Pb at a given temperature. For impurities that dissolve completely in Pb, the segregation coefficient at 650°C will be less than 2.8% (the solubility of Ge in Pb at 650°C). This includes Sb, As, Bi, and Ga.

1.2.4 Growth Modes and Crystal Orientation Dependence

Growth mechanisms and surface morphology of LPE layers are highly dependent on the orientation of the substrate. The free energy of a surface increases as the number of dangling bonds increases. In an FCC crystal, the energy of the {111} < {100} < {110}. In the case of Ge growth on a {100} Ge substrate, pyramids will form on the surface to expose the lower energy {111} faces. This morphology was observed experimentally. For this reason {111} substrates were chosen for this project. The layer will grow in such a way as to minimize overall energy (exposing the {111} surface), however kinetics play a large role in morphology as described below. Although macroscopic growth occurs perpendicularly to the substrate surface, microscopic growth takes place laterally as atoms attach to step edges. Substrate orientation studies on silicon and gallium arsenide have shown that even within a very small angle of surface misorientation from a low index plane there can be a large effect on layer morphology. Silicon layers grown on {111} substrates misoriented by more than 0.17° were found to exhibit a terraced morphology [Linnebach, 1982]. For GaAs [Bauser, 1984] growth was demonstrated on a spherically polished {100} substrate as shown schematically in Figure 9. It was found that for angles much less than 0.1° layers were nearly atomically flat, even for layers that were microns thick. In this facet growth regime addition of atoms occurs at screw dislocations which act as step sources. This is the preferred growth mode as it produces the most uniform layers. If the substrate is dislocation free, no layer growth takes place at the facet since there are no nucleation sites. This has been observed in silicon grown in the vicinity of the [111] pole. If there is supersaturation, two dimensional nucleation can take place. As the miscut angle approached 0.1° layers were still close to atomically flat, however misorientation steps became the primary nucleation sites for growth. For miscut angles between 0.1° and 2° the terrace growth mechanism was observed. Terrace growth can be understood by considering that the heights and distances of surface steps are randomly distributed. During growth atoms attach to step ledges as shown in Figure 10. A small step will grow quickly as atoms attach to ledges, but a larger step will require many more atoms to attach. In this way, small steps will catch up with large steps and steps tend to bunch during growth. This process illustrated

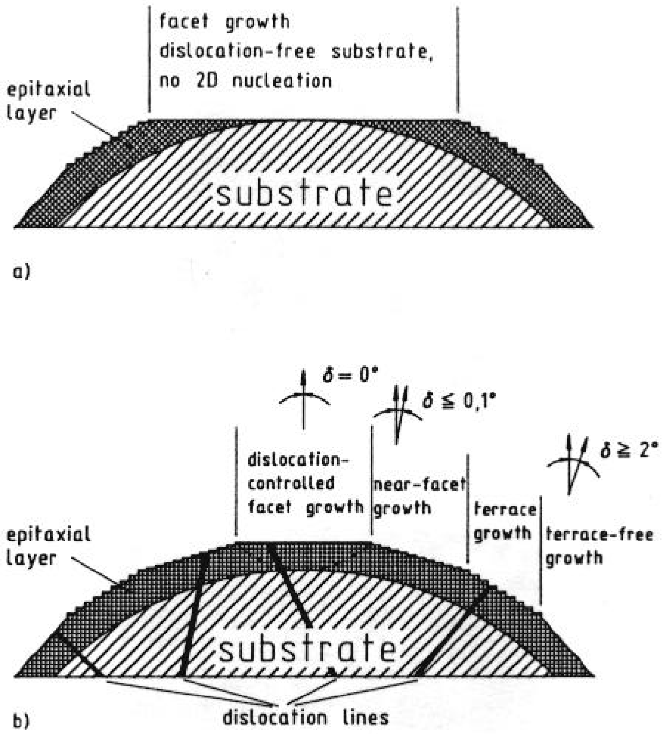

Figure 9. Schematic of growth regimes on a spherically shaped substrate. The misorientation angle δ is exaggerated. (a) Growth on a dislocation free substrate (b) Growth on a substrate with dislocations. [Bauser, 1994]

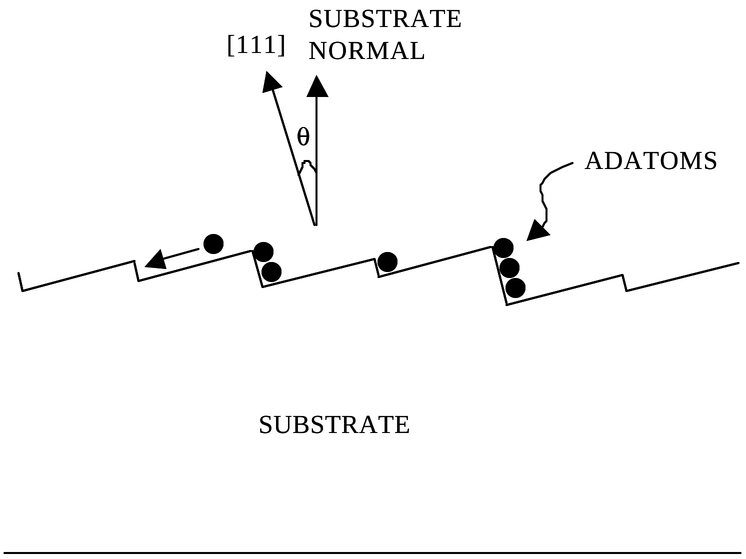

Figure 10. Schematic of lateral epitaxial growth as atoms are added to step ledges on a substrate miscut from a low index plane (e.g. (111)) by the angle θ.

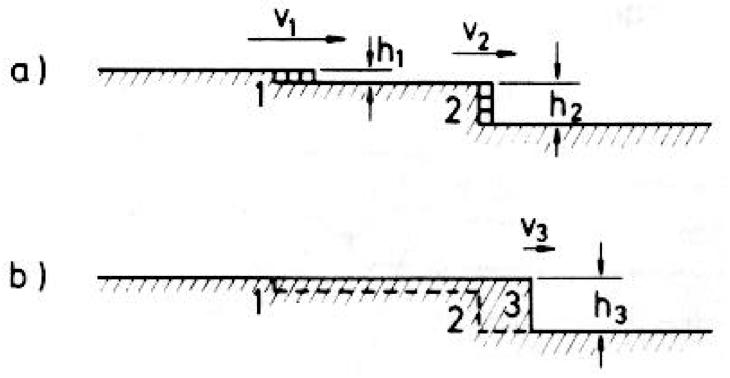

Figure 11. Schematic of step bunching. (a) steps 1 and 2 move laterally as atoms attach at their edges. (b) Step 1 catches up to step 2 and steps merge to form step 3. Lateral velocity is proportional to the inverse step height, $v_3 < v_2 < v_1$. [Bauser, 1985]

in Figure 11 leads to macroscopic terrace formation.

There are several undesirable aspects to the terrace growth mode. The surface of such a layer will be rough on the order of 1 µm. As growth takes place, small terraces merge with larger terraces making them taller. Eventually the lateral growth velocity will approach zero and deep grooves can form. They may even close on themselves leaving holes in the layer. The terrace growth mode is therefore morphologically unstable. Additionally, nonuniform incorporation of dopants during terrace growth has been observed. In GaP, photoluminescence of LPE layers in cross section has shown dark bands at terrace traces which were thought to be regions of depleted dopants for the case of Zn and O [Nishinaga, 1983] or regions of excess dopants for the case of S and N [Kajimura 1977]. Striations have been extensively observed in cross sections of Si and GaAs for both small and large terrace heights [Bauser]. These striations, which were revealed on etching, represent regions of dopant inhomogeneity from the bulk. Since they are observed even for small terraces it is concluded that one should avoid the terrace growth mode.

For angles greater than 2° in GaAs, a terrace-free growth mode was observed. At a large enough angle, the surface steps are so close together with so many dangling bonds present that steps do not have to grow very far laterally.

2 Experimental Methods

2.1 Liquid Phase Epitaxy Growth Procedures

Germanium films were grown by liquid phase epitaxy in a tipping boat system. Details of the system are described in the PhD thesis of Olsen [1998]. Prior to growth, materials were prepared by wet etching as shown in Table 2. The presence of an oxide on the surface of the Ge substrate prior to growth is a concern. The standard procedure for preparation of silicon wafers includes processing in dilute HF solution. After such a treatment the surface is H-terminated. For germanium, Cl termination has been found to be more stable than H [Lu, 1995]. Treating the substrate with 10% HCl (and no water rinse) is a possible means for eliminating the surface oxide. A comparison of layers grown with and without Cl termination using Secondary Ion Mass Spectroscopy (SIMS) should reveal the effects of Cl on oxygen at the interface.

Ge substrates 8x8x0.5 mm^3 were held by a graphite clip in a graphite crucible

Growth Material	**Etchant**	**Post-etch treatment**
Ge substrate	20:1 HNO_3: HF, 10 sec.	distilled H_2O + dilute HCL, rinse distilled H_2O, blow dry with N_2
Ge charge	3:1 HNO_3: HF, 1 min.; 20:1 HNO_3: HF, 10 sec. (streaming)	distilled H_2O, distilled methanol, blow dry with N_2
Pb shot 99.9999% pure (Cerac)	acetic acid + dilute hydrogen peroxide, 10 sec.	acetic acid, distilled H_2O, methanol, blow dry with N_2
PbSb alloy	acetic acid + dilute hydrogen peroxide, 10 sec.	acetic acid, distilled H_2O, methanol, blow dry with N_2

Table 2. Treatment of LPE growth materials

fabricated by Poco Specialty Materials, Inc[1]. The crucible was loaded into a single zone quartz tube furnace. The furnace was pumped and purged with argon gas and the system evacuated by a turbo pump to ~ 5 x 10^{-6} Torr. At 300 °C the gate valve was closed and H_2 was introduced at a flow rate of 1 L/min and 1/3 atmosphere overpressure. The melt was equilibrated at the starting growth temperature (generally 655 °C) for 5.5 hours. The system was tipped at an undercooling temperature of 3 °C to begin growth. Layer growth occurred as the furnace was ramped down to 340 °C over a 12 hour period. The solvent was then tipped off, and any solvent remaining on the surface was first removed by melting on a hotplate and then etching in a 1:1 acetic acid : hydrogen peroxide mixture.

2.2 Laue Diffraction for Wafer Orientation

Back-reflection Laue diffraction was used for orientation of substrate wafers. A detailed description of orientation by Laue diffraction is given in appendix C. A Ge crystal was mounted with epoxy onto a brass disc attached to a goniometer capable of tilting in two orthogonal directions. The goniometer was screwed onto a steel rod which was mounted in the Laue diffractometer. Orientation was achieved by comparing diffraction patterns at four in-plane rotation angles (0°, 90°, 180°, 270°) and measuring the offset of the 111 spot from the center or incident beam. To orient as close as possible parallel to the {111} plane, the crystal was tilted until the 111 spots on all four diffraction patterns overlaid with one another. This was more accurate than aligning the 111 spot with the center of the diffraction pattern since in back-reflection the incident beam does not form a spot on the detector (it is blocked), and it can be difficult to determine the

---

[1] Poco Specialty Materials, Inc, a Unocal company, 1601 South State St., Decatur, Texas 76234

center. After orientation, the goniometer assembly was mounted on a precision machined brass holder in an ID saw for cutting wafers.

The accuracy of the orientation process is limited by both the mounting assembly in the diffractometer and the ID saw. By measuring the offset of a wafer of GaAs with known misorientation of 0.05° it was determined that the error in the Laue assembly is ~ 0.5°. Wafers measured after cutting on the ID saw were within the 0.5° limit. The total misorientation of the process was deemed to be within ±0.5° accuracy. Higher precision orientation was obtained commercially at Eagle-Picher Industries, Inc.[2] where wafers were oriented to within ±0.02°.

2.3 Wafer Polishing & Flatness Determination

After cutting on the ID saw, Ge wafers were chemomechanically polished on a Logitech, Ltd.[3] polishing machine. Wafers were rough lapped using diamond coated lapping plates and polished with 7:3:1 H_2O: syton (colloidal silica): hydrogen peroxide on a polishing pad for 3 hours. Wafers were then rinsed with distilled water and gently blown dry with N_2. It was found that a final rinse with water left a surface free of particulates, while a rinse with distilled methanol left the surface covered with fine particulates that could be seen in dark field imaging under an optical microscope. The contamination appears to be from the LBNL nitrogen line since a clean wafer blown with the nitrogen gun would also show the particulates. Wafers blown dry in the Berkeley Microfabrication Laboratory did not leave particulates. A 1 µm particle filter was then

---

[2] Eagle-Picher Industries, Inc., 200 B.J. Tunnell Blvd., Miami, Oklahoma 74354

[3] Logitech, Ltd., Erskine Ferry Rd., Old Kilpatrick, Glasgow G60 5EU, Scotland, UK

attached to the LBNL nitrogen line as used in the Microlab to try to eliminate this effect. No change was observed so the particulates must be smaller than 1 µm. A final water rinse with a gentle blow dry with N_2 was found to be the cleanest option and was therefore used during substrate rinse steps.

Wafer flatness was determined by a Fizeau interferometer using a 5866 Å laser. Each fringe is 1/2 λ. A count of the number of fringes determines the thickness variation across the wafer. The variation across a 3.3 cm diameter wafer after polishing was found to be 4.5 µm from center to edge. This corresponds to a misorientation angle of 0.016°. For example, if the center of the wafer were oriented exactly on the (111) then the edge of the wafer would be misoriented by 0.016°. Any misorientation of the wafers was therefore presumed to be from the alignment and cutting process and was not limited by the polishing step.

2.4 Layer Thickness Determination

Layer thickness was determined using a Logitech depth probe. A base reading was taken at the substrate where growth was masked by the graphite clip. The thickness was then measured at nine points along the surface of the film and averaged. This method allowed measurement to within 1 µm. For several layers, measurements were also made on a profilometer as well as on an optical microscope to confirm the depth probe measurements.

2.5 Fabrication of Electrical Contacts

Contacts for 77K Hall effect and resistivity measurements consisted of indium pressed onto four corners of the sample with a small amount of In-Ga eutectic alloy rubbed into the surface of the germanium. Care was taken to make the contacts as small and as close to the edges as possible to minimize errors in the Hall measurement (as described in Appendix B).

Implanted contacts were used for variable temperature Hall effect, resistivity, and Photothermal Ionization Spectroscopy (PTIS) measurements. Samples were masked with copper or Kapton tape leaving four corners exposed. Since all LPE layers were n-type, 2 x 10^{14} /cm^2 phosphorus ions were implanted at 33 keV. Phosphorus was implanted at ~ 77K. Residues from the tape were removed in xylenes, acetone, and methanol. Samples were then annealed to activate the phosphorus. The furnace was ramped over 5 hours from 50 ° to 450 °C and held at 450 °C for 2 hours in flowing argon gas. After annealing the samples were masked again with tape, vapor etched with HF for 1 minute to remove any surface oxide, and then loaded directly into an e-beam evaporator. Metal contacts of 200 Å Pd / 4000 Å Au were deposited. Tape residues were removed in solvents and the contacts were annealed. The furnace was ramped from 250 ° to 300 °C over 30 minutes and held at 300 °C for 1 hour in flowing argon gas.

2.6 Hall Effect

Hall Effect measurements in the van der Pauw configuration [van der Pauw, 1958] were used to characterize shallow dopants in germanium. A detailed description of van der Pauw measurements on germanium samples is given in appendix B. In order to determine the shallow donor concentration and mobility in LPE films, 77K Hall effect measurements were used. Measurements were taken with a 100 Gauss electromagnet. The sample holder was immersed in liquid nitrogen. Currents through the sample ranged from 1 µA to 10 mA. Two currents were used for each sample to verify operation in the linear resistance regime.

Variable temperature Hall and resistivity measurements were made in a Lakeshore CT-210 continuous flow helium cryostat which cools down to 4.2 K. A magnetic field of 0.3 T was used in both the positive and negative polarity. The reversal of polarity allows for cancellation of any extraneous DC voltage that may be present. Currents were applied between 10^{-3} and 10^{-9} A. The temperature was stabilized by adjusting the He flow from room temperature down to approximately 50 K. Below 50 K a heater resistor was used to stabilize temperature. Data points were taken via computer control of a switchable current source and voltmeter at multiple currents to ensure that the sample was not heating up at low temperature. Current was lowered as the sample cooled in order to avoid heating.

2.7 **<u>Spreading Resistance</u>**

Spreading resistance measurements were taken at the University of Muenster by Dr. Hartmut Bracht and Stefan Voss. Samples were lapped on a shallow angle (5°44’) to allow depth profiling and then scanned with two 5 µm diameter tungsten-osmium probes spaced 100 µm apart. A constant voltage of 10 mV was applied and the spreading resistance measured at room temperature.

The spreading resistance can be related to resistivity, and in many cases the relationship is linear [Boussey, 1998]. For n-type Ge samples we observed that the relationship was not linear but showed a power dependence. Spreading resistance data on Ge determined by Chu et al in 1971 shows a power dependence which varies between p and n-type samples and changes slightly with surface preparation. We therefore maintained a constant surface preparation for all samples. In order to determine the spreading resistance – resistivity (and carrier concentration) relationship for use in this work, five n-type samples were characterized by Hall effect measurements and used as standards. Results are shown in Table 3 and are plotted in Figure 12. A calibration curve was taken for every sample to account for possible changes in the system from run to run. Calibration curves from different samples were within 10% of each other. It should be noted that the two samples with the lowest dopant concentrations do not follow the curve

Ge crystal #	**Concentration (cm^{-3})**	**Mobility (cm^2/Vs)**	**Temperature**	**Spreading Resistance* (Ω) at 293 K**	**Resistivity* (Ω-cm) at 293 K**
873-17 As <111>	9.3×10^{12}	4.2×10^{4}	77 K	1.12×10^{4}	56.540
866-6 Sb <111>	8.7×10^{13}	3.5×10^{4}	77 K	1.11×10^{4}	19.714
866-18.5 Sb <111>	5.3×10^{14}	3.0×10^{4}	77 K	8.19×10^{3}	2.757
867-8 Sb <111>	2.0×10^{16}	2.7×10^{3}	300 K	6.58×10^{2}	0.165
733-8 As <111>	8.6×10^{16}	2.0×10^{3}	300 K	1.30×10^{2}	0.0302

Table 3. Calibration data for spreading resistance measurements. A * indicates measurements made at the University of Muenster.

fit. This is probably due to non-Ohmic contacts between the probes and the germanium samples. The conversion of data from spreading resistance to concentration should therefore be considered correct only for the heavily doped layers and not for the pure substrates.

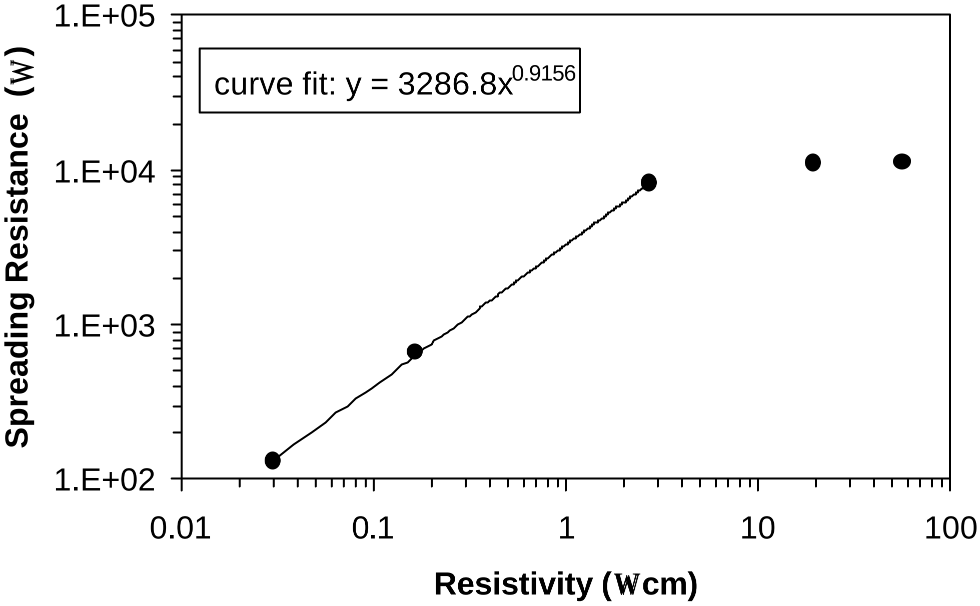

Figure 12. Spreading resistance – resistivity relationship for n-type germanium as determined from standard samples given in Table 3.

2.8 Absorption Measurements

The absorption of Sb doped Ge samples and the transmission of candidate transparent contacts in the far infrared were measured using a Fourier transform spectrometer. Fourier Transform Infrared Spectroscopy (FTIR) is discussed in appendix D. Samples were mounted in a rotatable wheel in an Infrared Labs dewar that can be cooled to 1.3 K by pumping on a liquid helium reservoir. Cold black poly is used at the window to the dewar to filter out bandgap light. The sample wheel can be rotated to place one of 6 samples between the spectrometer light and a Ge bolometric detector. Spectra are taken using the bolometer with each of the 6 samples in place. The spectra are then referenced to spectra measured with a pure Ge substrate in place to determine relative absorption.

Of the radiation incident on the sample, a fraction is reflected (R) from the surface, a fraction is transmitted through the sample (T), and a fraction is lost through absorption (A):

$$R+T+A=1 \qquad \text{Equation 9}$$

The linear absorption coefficient (α) is defined by:

$$\frac{I}{I_0} = e^{-ax} \qquad \text{Equation 10}$$

where I is the transmitted intensity, I_0 is the incident intensity, and x is the thickness of the material. In this work, pure Ge substrates are used as references. Therefore I_0 is not the incident intensity of radiation, but rather the intensity transmitted through a pure Ge substrate (where absorption is negligible). Since reflection from the surfaces of all of the Ge samples should be the same, Equation 10 can be used (with the modified I_0) to calculate the absorption coefficient.

2.9 Photothermal Ionization Spectroscopy

Photothermal Ionization Spectroscopy (PTIS) was used to identify the dopant species present in LPE layers. A discussion of PTIS is given in appendix E. Layers for PTIS were prepared with four phosphorus ion implanted contacts as for Hall effect measurements. In this case sets of two contacts were tied together. Spectra were taken using Fourier Transform Infrared Spectroscopy (FTIR). Samples were mounted in a brass holder that was pumped out and then backfilled with 5 Torr He to allow for heating of the sample using a heater resistor. The brass holder was immersed in liquid helium in a glass dewar. Samples were exposed to chopped light (~ 20 Hz) from a mercury arc lamp through an 8 mil black poly filter. The photoconductive signal from the sample was measured with a lock-in amplifier. Spectra were taken at temperatures between 4 and 10 K.

2.10 Blocked Impurity Band Detector Fabrication

Difficulty in achieving the desired purity of the blocking layer has led to device fabrication using an alternate method. Ideally, for simple fabrication of arrays, both the active layer and blocking layer should be grown. For research purposes, the active layer was grown on a pure substrate which was then thinned down to form the blocking layer. A schematic of the detector is shown in Figure 13.

An antimony doped layer was grown to form the IR active region and then the top 10 μm polished off to remove the highly doped surface region (see section 3.2.2.2 for details). Samples were mounted for polishing surrounded by germanium spacer material

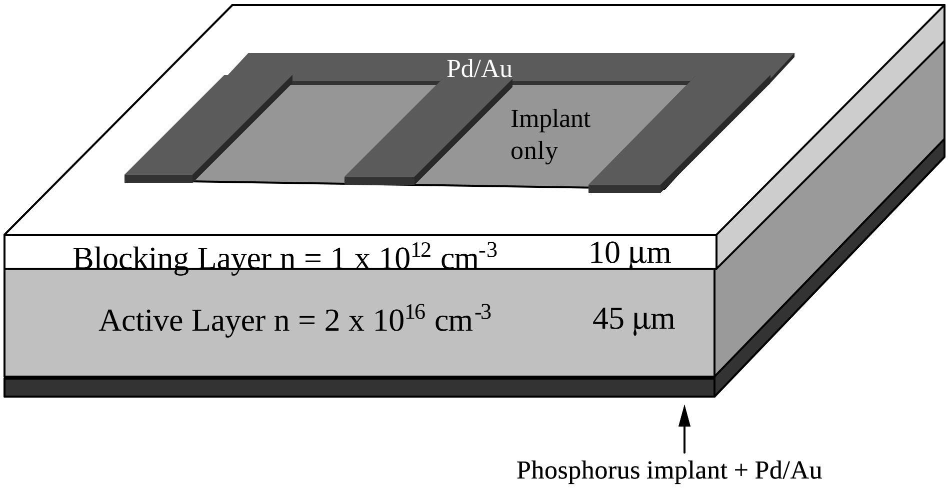

Figure 13. Schematic of BIB detector structure

to avoid rounding of the edges. In order to achieve a thicker final device for mechanical stability purposes, a double layer was sometimes grown. In this case the surface was polished off of the first layer before growing a second layer. The surface was implanted with phosphorus ions (2 x 10^{14} cm^{-2} at 40 kV and 4 x 10^{14} cm^{-2} at 100 kV). The sample was diced into rectangular pieces of 3 mm x 2.5 mm for easier handling when thinned. Notches were cut in the corners to help differentiate between the top and bottom of the detector when thinned. Samples were then mounted on the polishing block, doped layer down, with germanium spacers. Sample thickness was measured beforehand using the depth gauge, and then again after mounting on the holder. The substrate was lapped down and the final 20 µm polished away to leave the desired blocking layer thickness (e.g., 10 µm). The pure side was masked around the edges with picene wax and phosphorus ions were implanted (2 x 10^{14} cm^{-2} at 33 kV) in the center to avoid possible current leakage around edges. Phosphorus implants were annealed in Ar as described in section 2.5. Picene wax was used to paint a finger structure on the pure side and Pd/Au was deposited and contacts annealed as described in section 2.5. The Au finger structure was used to leave a portion of the surface transparent to IR while still applying a relatively uniform electric field to the top surface of the detector.

2.11 Blocked Impurity Band Detector Characterization

BIB devices were tested by measuring I-V characteristics, spectral response, and responsivity. Detectors were tested in an Infrared Labs HD-3 Helium dewar that can be cooled to 1.3K by pumping on the helium reservoir. The dewar electronics are described in appendix F. The detector is mounted on a piece of gold-coated sapphire on top of a cold stage. A brass clip forms the top contact. A shutter wheel on the dewar contains several apertures for allowing radiation to pass through. The shutter wheel was closed for dark I-V measurements. Spectra were taken using Fourier Transform Infrared Spectroscopy (FTIR) through a 1mm aperture. A cold 8 mil black polyethylene filter was used to suppress bandgap light. Responsivity measurements were taken through a narrow bandpass filter.

3 Results & Discussion

3.1 Substrate Orientation Effects on Germanium LPE Layers

3.1.1 Layer Morphology

Laue diffraction of wafers that were cut and polished without the use of x-ray orientation were found to be miscut from the (111) plane by as much as 2°. Wafers that

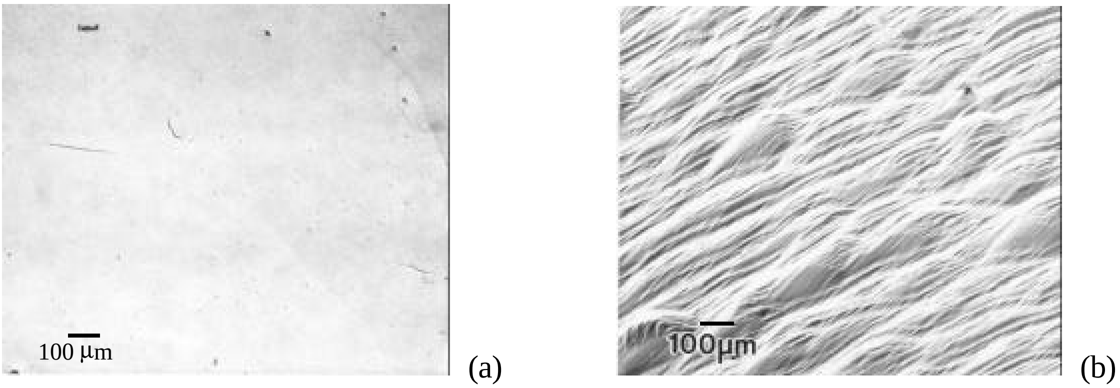

Figure 14. Optical interference contrast micrographs for (a) 23 µm Ge layer on a 0.02° miscut substrate and (b) 45 µm Ge layer on a 0.5° miscut substrate, terrace height = 0.5 µm

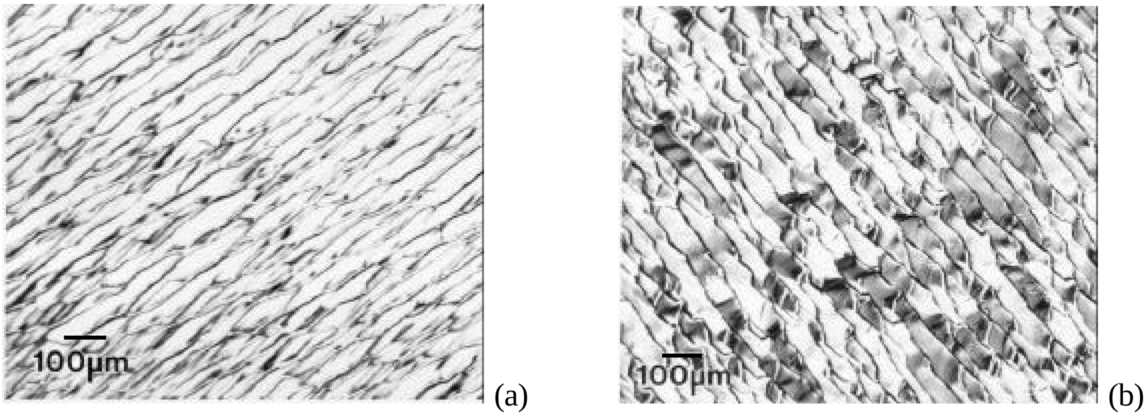

Figure 15. Optical interference contrast micrographs for (a) 30 µm Ge layer on a 3° miscut substrate, terrace height = 1 µm and (b) 35 µm Ge layer on a 6° miscut substrate, terrace height = 4 µm

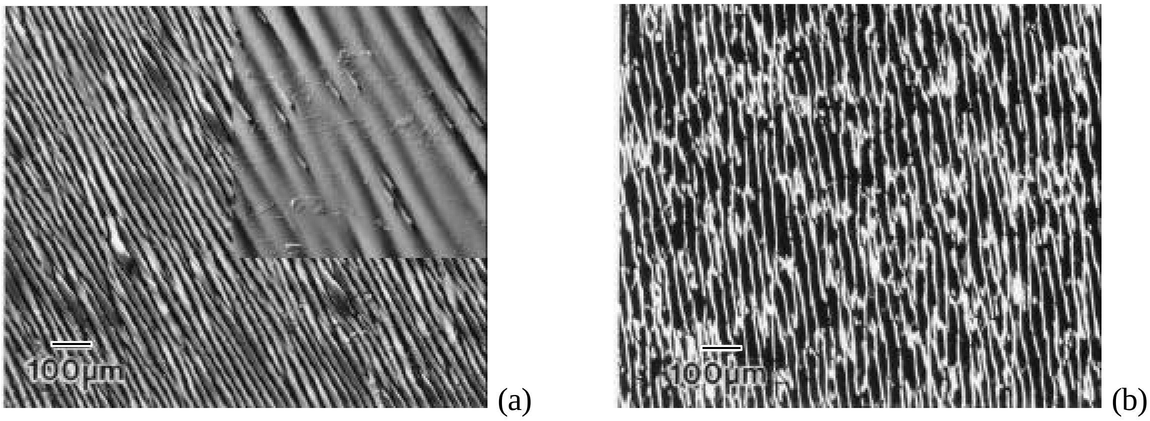

Figure 16. Optical interference contrast micrographs for (a) 30 μm Ge layer on a 8° miscut substrate, terrace height = 1 μm. The inset in the upper right corner shows a close-up of the surface. (b) 42 μm Ge layer on a 10° miscut substrate, terrace height = 4 μm

were oriented, cut, and polished were miscut within 0.5 °. In order to study the effect of miscut angle on the morphology of Ge layers grown by LPE, a series of layers were grown on substrates with miscut angles ranging from 0.5° to 10°. Intentionally miscut substrates were oriented away from the [111] in the [100] direction. Additionally, substrates were purchased from Eagle Picher, Inc. that were oriented to within 0.02° from the (111) which was beyond the capability of the instrument at Berkeley. Interference contrast optical micrographs of LPE layers grown on substrates with various miscut angles are shown in Figure 14, Figure 15, and Figure 16.

Terrace growth was observed in all cases except for that of the 0.02° substrate. The height of terraces was measured by profilometry and was taken from peak to valley. Terrace height was found to increase for larger miscut angles, however at 7° miscut the terrace height decreased. The morphology of the surface shows that in some regions of the layer the terraces are filling themselves in. This may correspond to the terrace free growth region seen in GaAs for large miscut angles.

For device fabrication, the 0.02° oriented substrate is preferred since the terrace growth mechanism does not dominate. A Ge crystal grown at LBNL containing 2 x 10^{12} cm^{-3} donors was oriented, cut, and polished at Eagle Picher, Inc. to within 0.02° for this work. When p-type wafers were required, as for PTIS and variable temperature Hall effect, wafers oriented at Berkeley to within 0.5° were used.

3.2 Doping of the Infrared Active Layer

Previous work [Olsen, 1998] found that residual impurities in undoped Ge LPE layers grown out of Pb solvent are donors. This led to the choice of fabricating n-type BIBs. Both Bi and Sb were studied as potential dopants.

3.2.1 Bi Doping

Initially, bismuth doping was investigated for use in the active layer. However, it was found that the solubility limit of Bi in Ge for growth starting at 650 °C was too low for sufficient impurity banding to occur. Bismuth was initially explored because previous work [Olsen, 1998] indicated that antimony evaporation during growth caused doping to be unpredictable. It is thought that this was simply an effect of nonuniform contact placement during Hall effect measurements. In the current work, antimony doping behaved in a predictable fashion. Antimony is more desirable for the BIB active layer because it is not solubility limited and it has a lower ionization energy than Bi.

3.2.2 Sb Doping

Unlike bismuth, antimony incorporation is not solubility limited in the doping range of interest. Therefore, in order to add small amounts of Sb to the Pb melt, a master Pb-Sb alloy was used. The metals were heated in a graphite crucible and sealed in a quartz ampoule with hydrogen gas. Ampoules were annealed for 24 hours at 700 °C and then quenched in ethylene glycol.

Experimentally, the segregation coefficient for Sb in the Pb-Ge system was found to be 5 x 10^{-3} in this work. This is lower than that determined experimentally by Olsen (1.5 x 10^{-2}). However, Olsen's Hall effect measurements were of samples with nonuniform dopant distributions (as discussed in section 3.2.2.2) yielding concentrations that were typically higher than the actual concentrations in the bulk of the layers. This difference is enough to account for the differences in segregation coefficient.

3.2.2.1 Carrier Concentration and Mobility

Variable temperature Hall and resistivity measurements on Sb doped layers as shown in Figure 17, Figure 18, and Figure 19 provide information on the antimony dopant concentration and activation energy as well as the conduction and mobility in impurity banded semiconductors. A theoretical fit of the Hall curve in Figure 17 gives a donor concentration of 1 x 10^{16} cm^{-3} and a donor binding energy of 10 meV. The full slope region required to determine the compensation does not show up because hopping conductivity in the impurity band occurs first. At low temperatures, the curve deviates from the theoretical fit due to hopping conductivity in the impurity band. The mobility curve in this temperature range is no longer meaningful. This phenomenon has been studied in Sb doped Ge ranging from 7 x 10^{15} – 2 x 10^{17} cm^{-3} by Davis and Compton in 1965. They have demonstrated the dependence of the resistivity vs. temperature on Sb concentration as well as compensation. The resistivity curve in Figure 18 exhibits a change in slope at some point below 5 K. This corresponds to a change in conduction mechanism. Above 5 K the slope corresponds to activated conduction band transport.

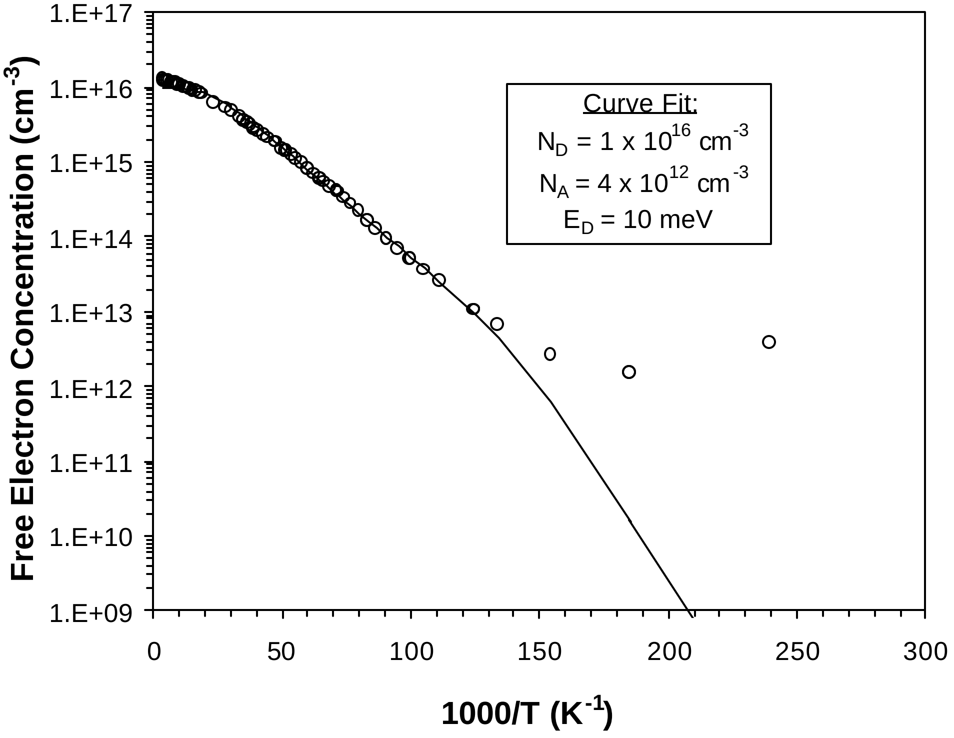

Figure 17. Variable temperature Hall effect measurements of the free electron concentration of a 21 μm thick LPE layer (LPE 396) grown on a 5 x 10^{10} cm^{-3} p-type substrate. Growth cycle: Equilibrate at 655 °C for 5.5 hours, grow from 652 °C-340 °C, 3° undercooling, 0.43°/min cooling rate. Growth materials: 9.9 g Pb, 0.313 mg Sb, 0.16 g Ge. The compensating acceptor concentration was chosen arbitrarily to illustrate the full slope regime. Hopping conductivity occurs before the full slope region can be observed.

Below 5 K conduction occurs by hopping in the impurity band. Davis and Compton have shown experimentally that the slope of the resistivity curve in the low temperature regime decreases as compensation increases. This can be understood by considering that hopping can only occur when states in the impurity band are empty. Adding compensation increases the number of empty states and therefore the energy required to hop from one state to the next is reduced. This trend is observed until compensation is

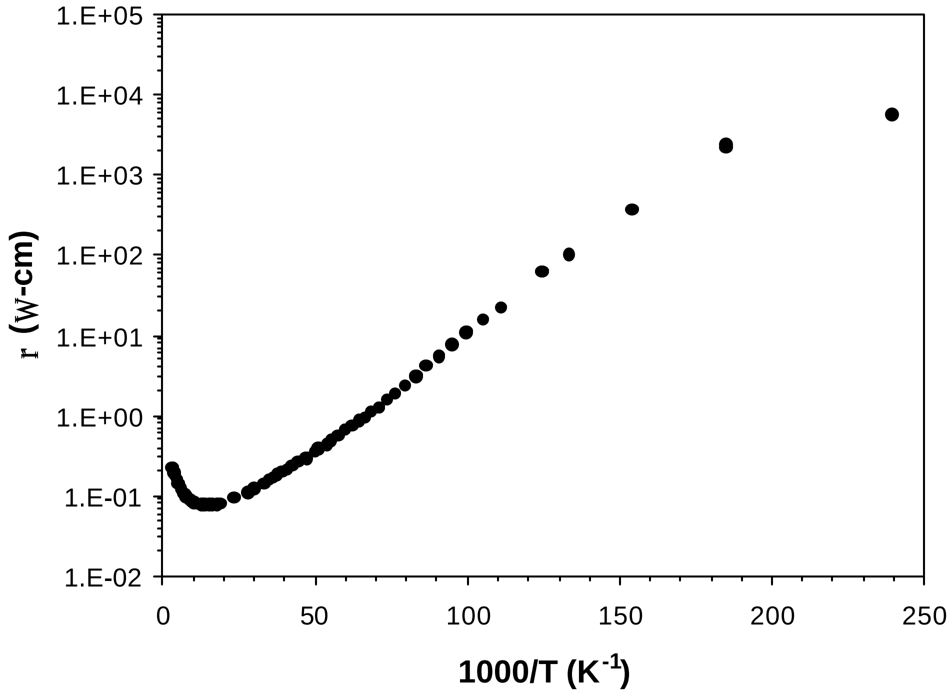

Figure 18. Variable temperature resistivity of LPE 396

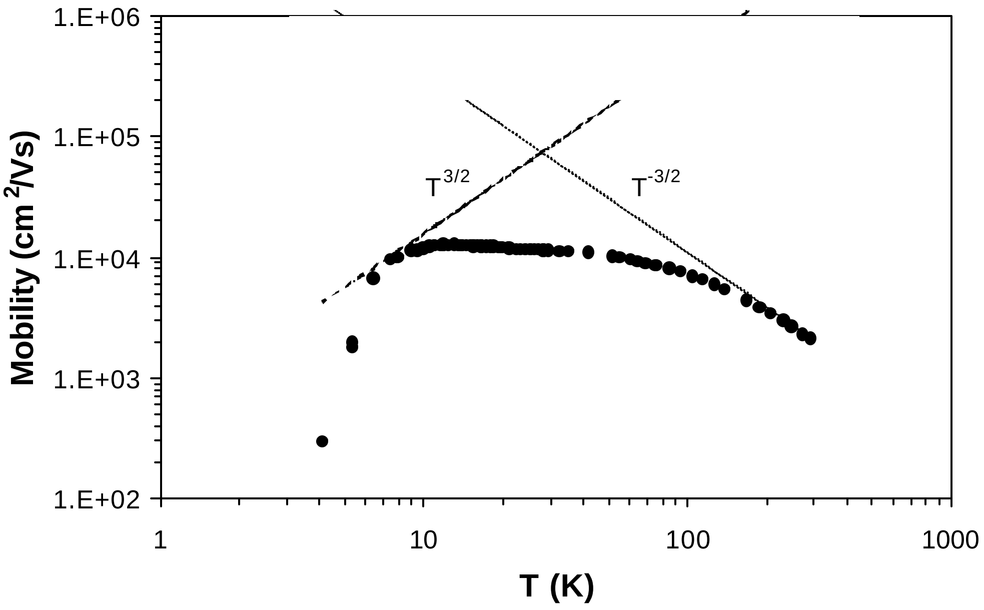

Figure 19. Variable temperature mobility of LPE 396. The high temperature regime behaves as predicted. Hopping conduction at low temperature gives a fictitious mobility.

above~ 50% at which point the resistivity increases. At low compensation (<~50%) there are only a few vacant sites for electrons to hop to, while at high compensation (>~50%) there are only a few electrons in the impurity band.

3.2.2.2 Doping Homogeneity

LPE growth of Ge layers takes place over a range of temperatures (a typical growth run begins at 650 °C and ends at 340 °C). It is therefore important to consider the temperature effect on dopant incorporation. Incorporation of Sb in the solid becomes limited by diffusion in the solution at low temperatures. At the initial growth temperature, Sb is distributed uniformly in the liquid, and incorporates in the growing Ge layer according to the segregation coefficient. At lower temperatures (at the end of a growth run), Sb cannot diffuse away sufficiently rapidly from the growth interface and becomes incorporated in the Ge layer at a higher concentration. This leads to a pile up of Sb at the layer surface. The curvature of the liquidus line of the Ge-Pb phase diagram determines the quantity of Ge that can precipitate out of solution at a given temperature. The slope becomes steeper at lower temperatures, indicating that the bulk of the layer is formed at higher temperatures, and the excess Sb is confined to the surface (top several microns).

The spreading resistance profile of a 34 μm thick Sb doped Ge layer at room temperature is shown in Figure 20. The data is converted into the concentration – depth profile shown in Figure 21 using the standard calibration from section 2.7. The pile up of Sb at the surface is apparent. The curvature of the substrate-layer interface is likely due to the finite diameter of the probes, and it is not possible to determine whether there is diffusion at the interface from this data. The spreading resistance data has important implications for detector fabrication as well as epilayer characterization. Hall effect measurements on nonuniform samples yield false results, and therefore the concentrations of layers grown prior to this result are unreliable. The top 10 μm of all layers were subsequently removed either by chemomechanical polishing or etching in 20:1 HNO_3:HF. To achieve the desired Sb concentration for detector fabrication, the amount of Sb added during growth was adjusted. For multiple layer growths, it is important to remove the surface of the first layer before growing the second to avoid a concentration spike in the center of the layer. It is likely that detectors fabricated from Ge:Sb LPE layers prior to this work had similar dopant distributions to the layer shown in

Figure 20. This would lead to a lower concentration than required for impurity banding (when the substrate is used as a blocking layer), and unoptimized BIB performance.

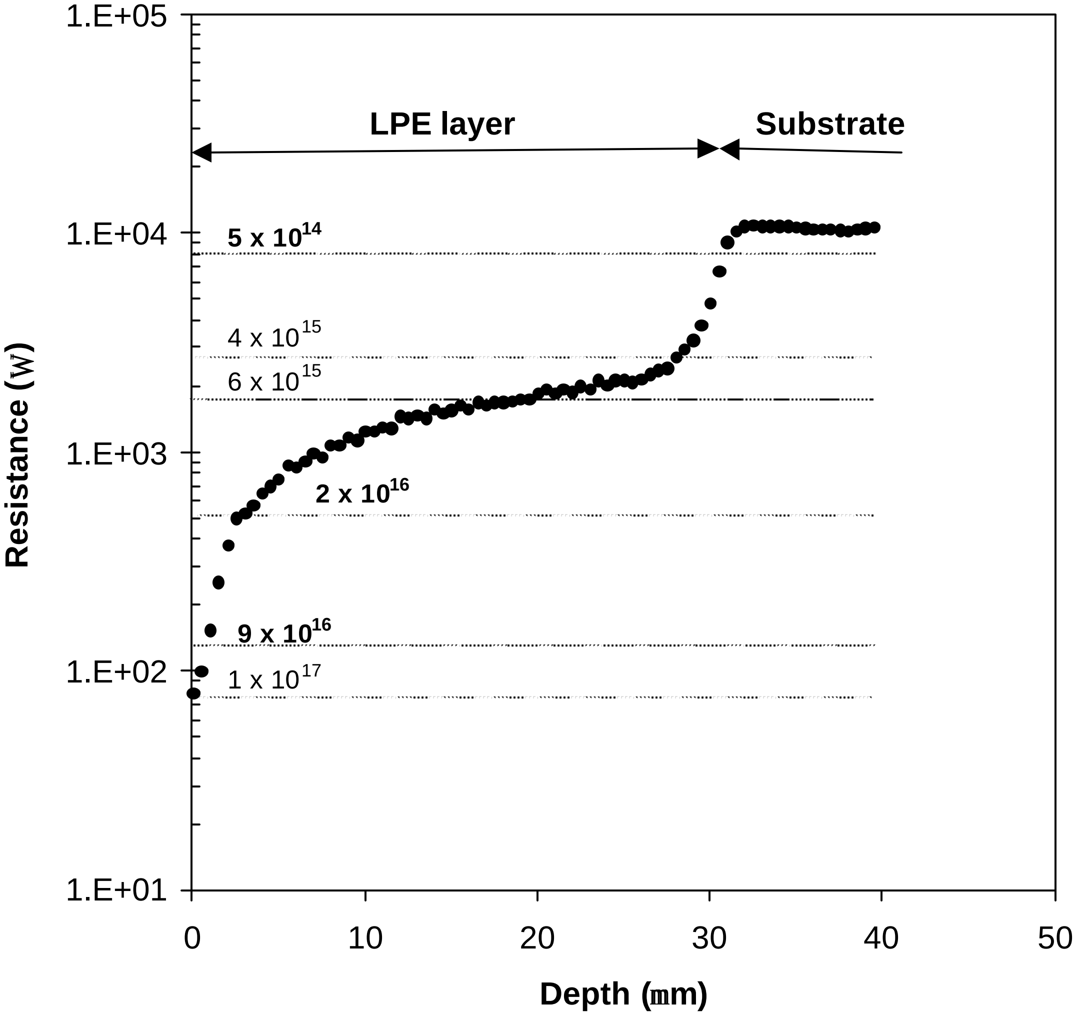

Figure 20. Spreading resistance profile of a 34 μm thick LPE layer (LPE 340) grown on an n-type substrate. Growth cycle: Equilibrate at 655 °C for 5.5 hours, grow from 652 °C-340 °C, 3° undercooling, 0.43°/min cooling rate. Growth materials: 11.35 g Pb, 0.162 mg Sb, and 0.18 g Ge. Dashed lines indicate concentration in cm^{-3}. Numbers in bold are determined from Hall effect measurements of standard samples. Other values are extrapolated. This measurement was performed at the University of Muenster.

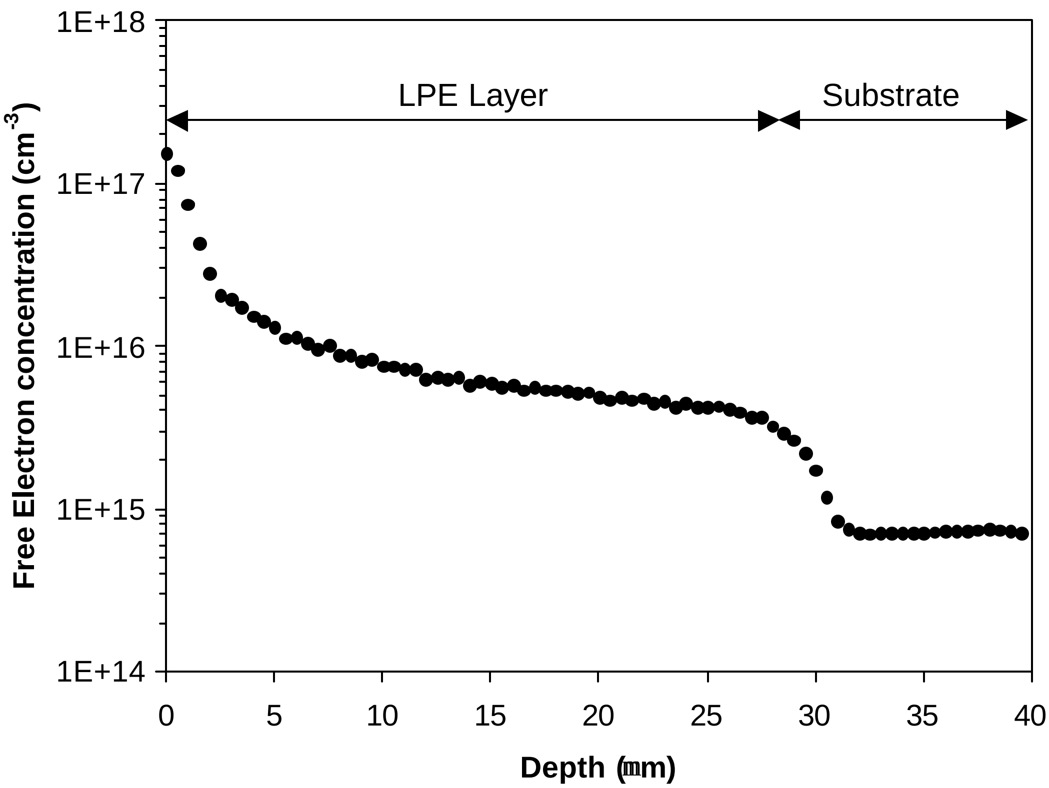

Figure 21. Electron concentration vs. depth for the sample shown in Figure 20 as determined using standard calibration. An average constant mobility determined from three standards (concentrations 8.6 x 10^{16}, 2.0 x 10^{16}, and 5.3 x 10^{14} cm^{-3}) was used. The concentration of the substrate is incorrect because the spreading resistance vs. resistivity no longer follows the curve fit for the low doped standard samples as described in section 2.7. The actual concentration in the substrate is below intrinsic.

The diffusion of Sb into the pure Ge during growth could not be addressed by spreading resistance due to the poor depth resolution. However, Sb diffusion should be considered as it can have effects on device performance. The diffusivity of Sb in Ge at 650 °C is 4 x 10^{-13} cm^2/s [Stolwijk, 1998]. The temperature cycle during growth is complex, however an estimate of $\sqrt{Dt}$ at 650°C for 2 hours is 0.8 μm. This distance could be significant for a BIB device. For Ga in Ge the diffusivity is 9 x 10^{-17} cm^2/s [Stolwijk, 1998]. For the same diffusion conditions Ga would diffuse only 8 nm.

Further experimental studies used Secondary Ion Mass Spectrometry (SIMS) to measure the Sb profile near the layer-substrate interface. LPE layers were chemomechanically polished to thicknesses suitable for SIMS analysis (all layers were polished to < 4 µm). SIMS analysis was performed at the Materials Analysis Group at Accurel Systems

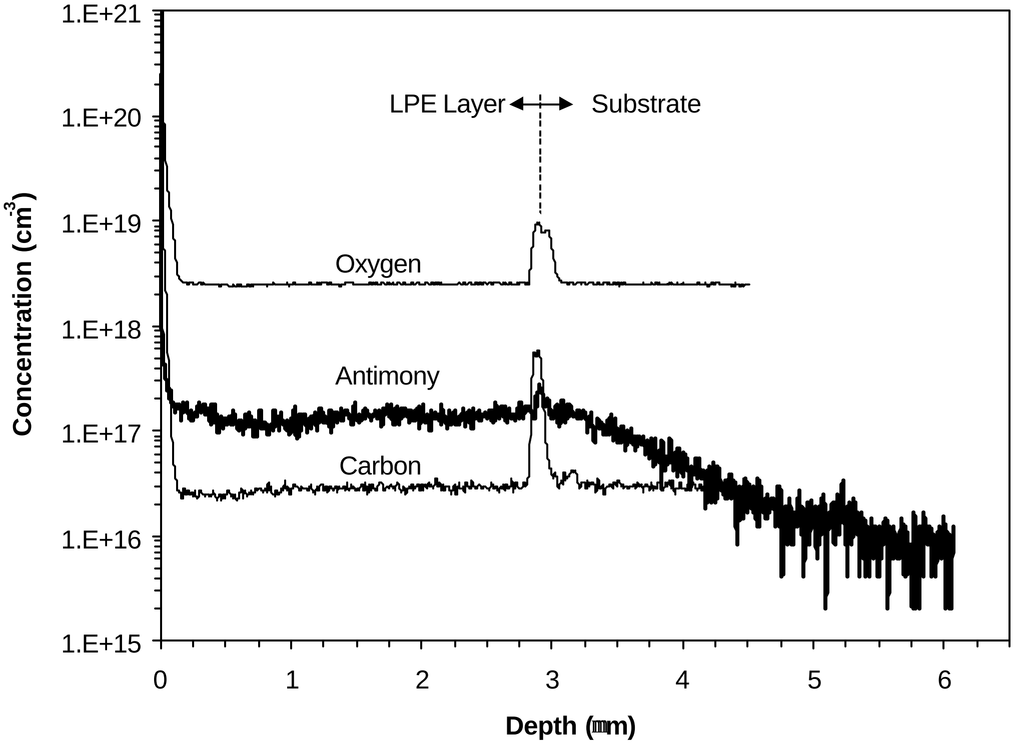

Figure 22. Concentration vs. depth obtained by SIMS analysis for Sb, O, and C in a Ge LPE layer (LPE 421) grown at a starting temperature of 650 °C on a pure Ge substrate. Oxygen and carbon are observed at the layer-substrate interface. SIMS sputter rate = 58 Å/sec

International, Inc.[4] using a Cs ion beam. A 2x10^{16} cm^{-3} Sb-doped Ge crystal was used as a standard to quantify Sb concentration. Figure 22 and Figure 23 show concentration profiles near the layer-substrate interface for Sb-doped layers grown at 650°C and 550°C. The layer grown at 650°C shows significant Sb diffusion into the substrate. The concentration drops an order of magnitude over ~ 1.5 μm. The layer grown at 550°C

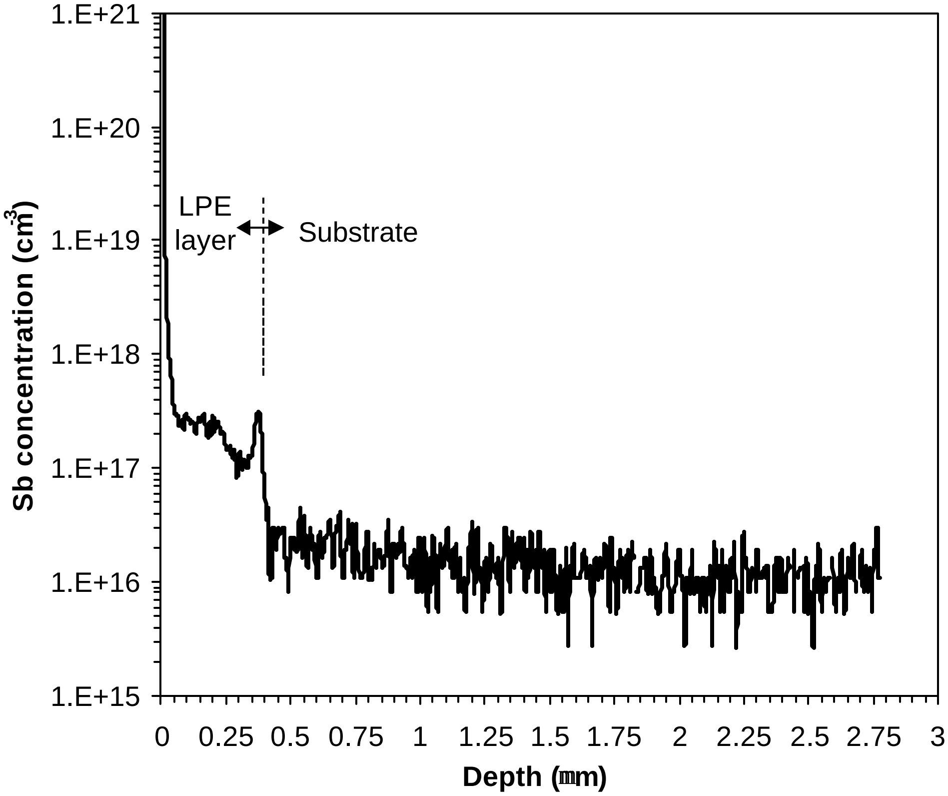

Figure 23. Concentration vs. depth obtained by SIMS analysis for Sb in a Ge LPE layer (LPE 423) grown at a starting temperature of 550 °C on a pure Ge substrate.

---

[4] Materials Analysis Group, Accurel, 350 Potrero Ave., Sunnyvale, CA 94086

does not show significant diffusion of Sb into the substrate. Oxygen and carbon are observed at the layer substrate interface. It should be noted that the oxygen and carbon concentrations observed away from the interface (~ 3 x 10^{18} cm^{-3} and 3 x 10^{16} cm^{-3}) are due to a high background present during SIMS. The actual values are expected to be approximately four orders of magnitude lower as has been observed in Czochralski crystal growth of germanium. The spike in Sb concentration observed at the interface could be due to segregation of Sb to the oxide layer, or to a SIMS artifact caused by the differences in sputter rates between the oxide and Ge. Future work should include a comparison of BIB devices fabricated from layers grown at low and high temperatures in order to observe the effects of diffusion that have been predicted by Haegel [2000].

3.3 Blocking Layer Growth

3.3.1 Impurity Distribution in Undoped Layers

Unintentionally doped layers were found to be n-type with a shallow donor concentration ~ 10^{15} cm^{-3}. Unlike the Sb doped samples, they did not show a pile-up of dopants on the surface. Spreading resistance measurements (see Figure 24 and Figure 25) on undoped layers revealed more uniform dopant incorporation with a slight deficiency at the surface.

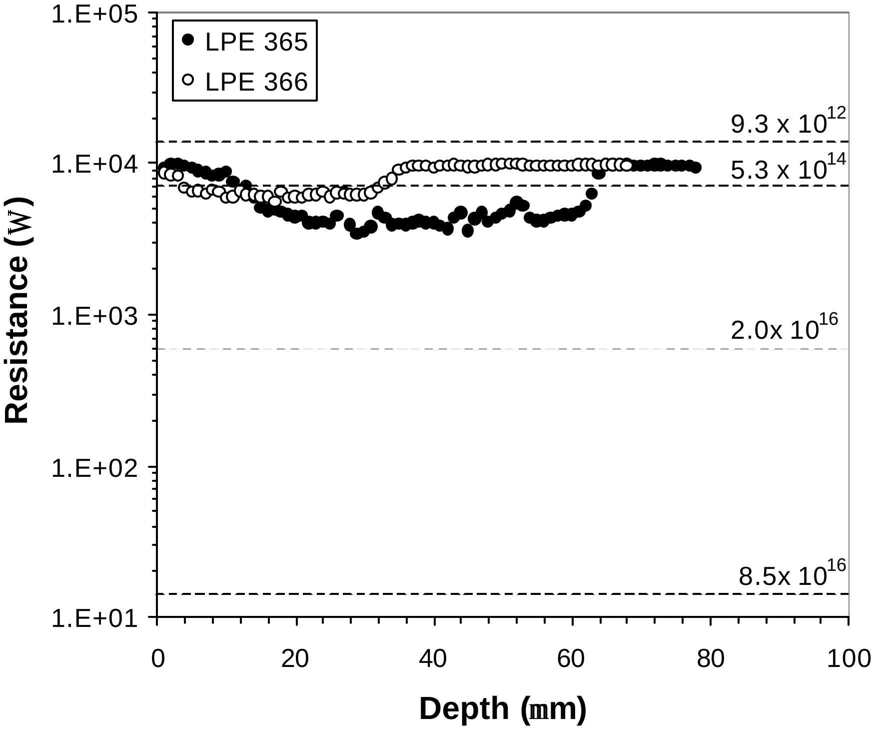

Figure 24. Spreading resistance profile of two LPE layers grown on n-type substrates. Growth cycle: Equilibrate at 655 °C for 5.5 hours, grow from 652 °C to 340 °C, 3° undercooling, 0.43°/min cooling rate. LPE 365 Growth materials: 9.5 g distilled Pb (3 times distilled) and 0.16 g Ge. LPE 366 Growth materials: 7 g distilled Pb (1 time distilled) and 0.16 g Ge. Dashed lines indicate concentration in cm^{-3}. This measurement was performed at the University of Muenster

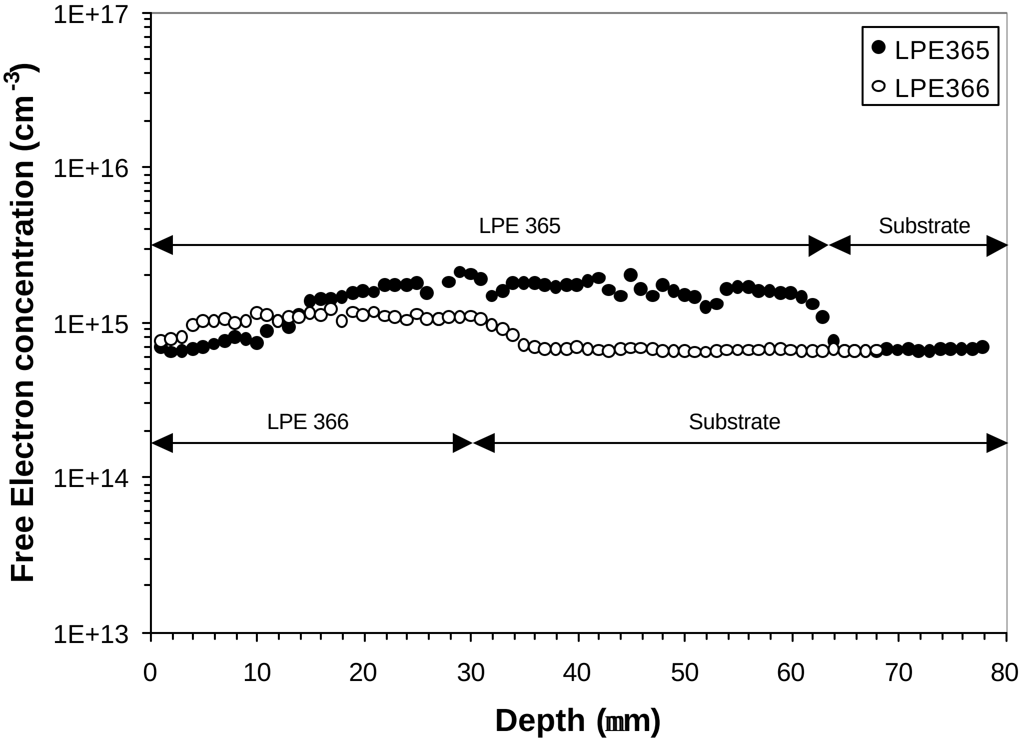

Figure 25. Electron concentration vs. depth for the samples shown in Figure 24 as determined using the standard calibration curve. The concentration of the substrate is again incorrect because the spreading resistance vs. resistivity no longer follows the curve fit for the low doped standard samples.

3.3.2 Purity Determination

3.3.2.1 Variable Temperature Hall Effect

In order to determine the base level and type of impurities in Ge LPE layers, variable temperature Hall effect measurements were used. The results are shown in Figure 26, Figure 27, and Figure 28.

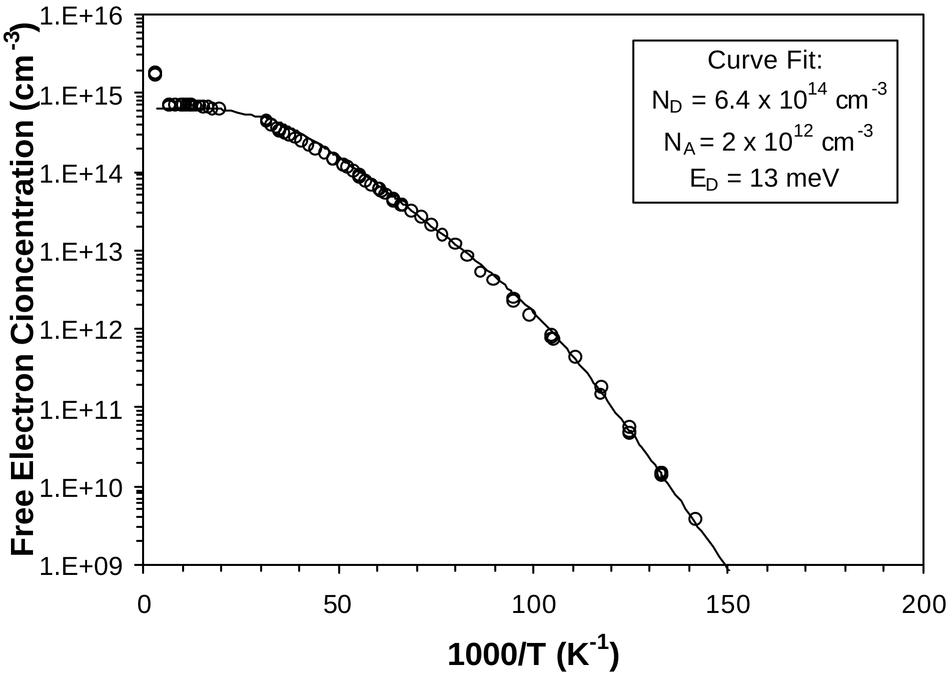

Figure 26. Carrier concentration vs. 1/T as determined by variable temperature Hall effect. The LPE layer (LPE 347) is 38 μm thick and is grown on a p-type substrate ($p = 5 \times 10^{10}$ cm^{-3}). Growth cycle: Equilibrate at 605 °C for 5.5 hours, grow from 602 °C-340 °C, 3° undercooling, 0.37°/min cooling rate. Growth materials: 10.5 g Pb and 0.17 g Ge. The surface of the layer was not removed.

The majority impurity species is a donor at a concentration of 6×10^{14} cm^{-3}. The compensation due to p-type impurities is 2×10^{12} cm^{-3}. The activation energy of 13 meV corresponds to phosphorus (as found by PTIS described in section 3.3.2.2). The mobility is lower than observed in bulk germanium which would be ~ 4×10^4 cm^2/Vs at 77 K. This is in agreement with Olsen's work. The shape of the mobility curve follows the form observed in low compensation germanium crystals [Hansen, 1993]. Phonon scattering dominates at all temperatures above ~ 10K. The decrease in slope of the

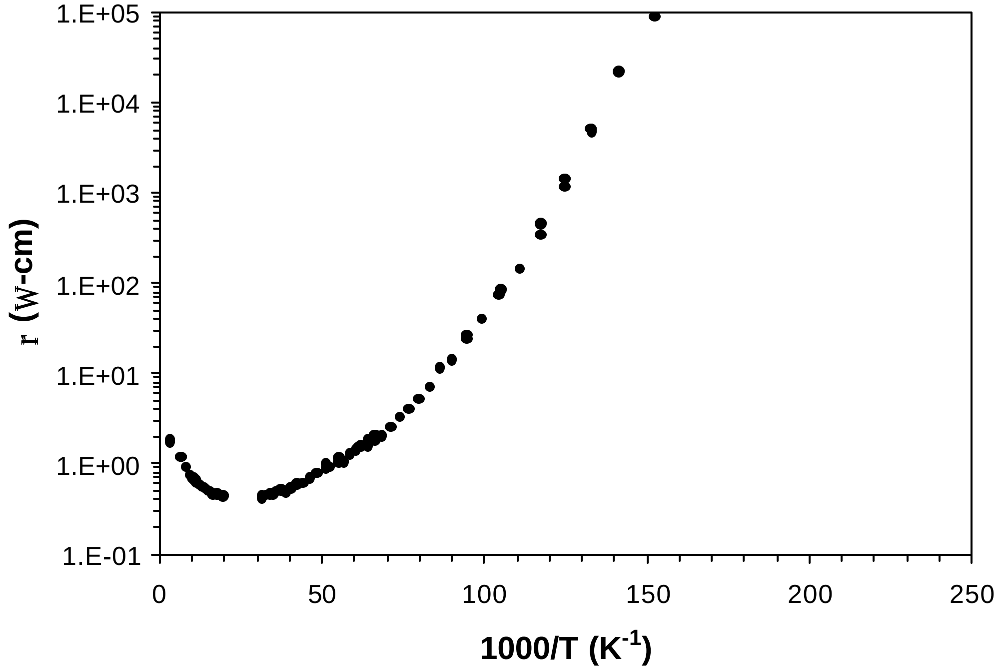

Figure 27. Variable temperature resistivity of LPE 347.

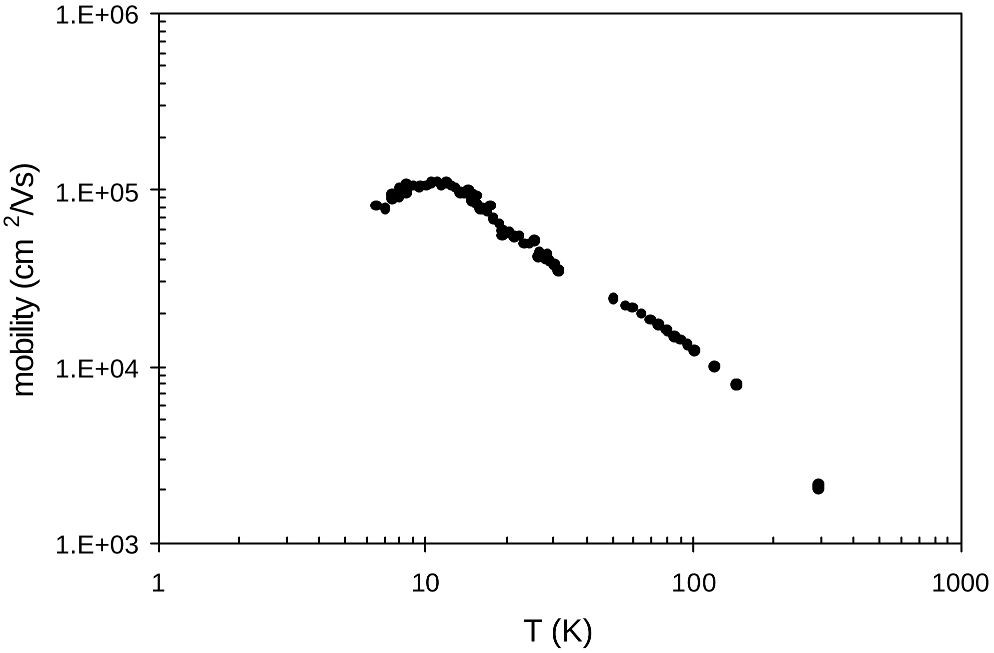

Figure 28. Mobility vs. T for LPE 347.

mobility curve at ~ 70K is due to contributions from ionized impurity scattering. Below ~ 20K the ionized impurities are freezing out and there is a rapid increase in slope.

3.3.2.2 Identification of Shallow Donors in Germanium Layers

In order to identify the donor species present in LPE germanium layers,

	P		**Sb**		**Bi**		**As**	
Transition from lower ground state to	Energy (meV)	ν (cm-1)	Energy (meV)	ν (cm-1)	Energy (meV)	ν (cm-1)	Energy (meV)	ν (cm-1)
$2P_0$	8.15	65.722	5.58	44.997	8	64.512	9.44	76.124
$3P_0$	10.33	83.301	7.75	62.496	10.2	82.253	11.61	93.623
2p±	11.156	89.962	8.74	70.479	11.08	89.349	12.44	100.316
3p±	11.844	95.510	9.42	75.963	11.72	94.510	13.15	106.042
4p±	12.127	97.792	9.7	78.221				
4f±	12.26	98.865	9.855	79.471				
5p±	12.408	100.058	9.99	80.559				
5f±	12.483	100.663	10.06	81.124				
6p±	12.559	101.276	10.13	81.688				
Ionization Energy	12.76	102.897	10.19	82.172	12.68	102.252	14.04	113.219
Ground state splitting	2.83	22.821	0.32	2.580	2.87	23.144	4.23	34.111
Transition from upper ground state to	Energy (meV)	ν (cm-1)	Energy (meV)	ν (cm-1)	Energy (meV)	ν (cm-1)	Energy (meV)	ν (cm-1)
$2P_0$	5.32	42.900	5.26	42.417	5.13	41.368	5.21	42.013
$3P_0$	7.5	60.480	7.43	59.916	7.33	59.109	7.38	59.512
2p±	8.326	67.141	8.42	67.899	8.21	66.205	8.21	66.205
3p±	9.014	72.689	9.1	73.382	8.85	71.366	8.92	71.931
4p±	9.297	74.971	9.38	75.640				
4f±	9.43	76.044	9.535	76.890				
5p±	9.578	77.237	9.67	77.979				
5f±	9.653	77.842	9.74	78.543				
6p±	9.729	78.455	9.81	79.108				

Table 4. Transitions from the ground state to bound excited states for shallow donors in germanium.(data from Kogan, 1977)

Photothermal ionization spectroscopy (PTIS) was used. The energies of shallow donor excited states in germanium are shown in Table 4. The spectra in Figure 29 were measured for n-type LPE germanium layers grown on p-type substrates. The shallow donor is identified as phosphorus. None of the other donors appear to be present. Phosphorus is present even in growths from distilled Pb (discussed in section 3.4).

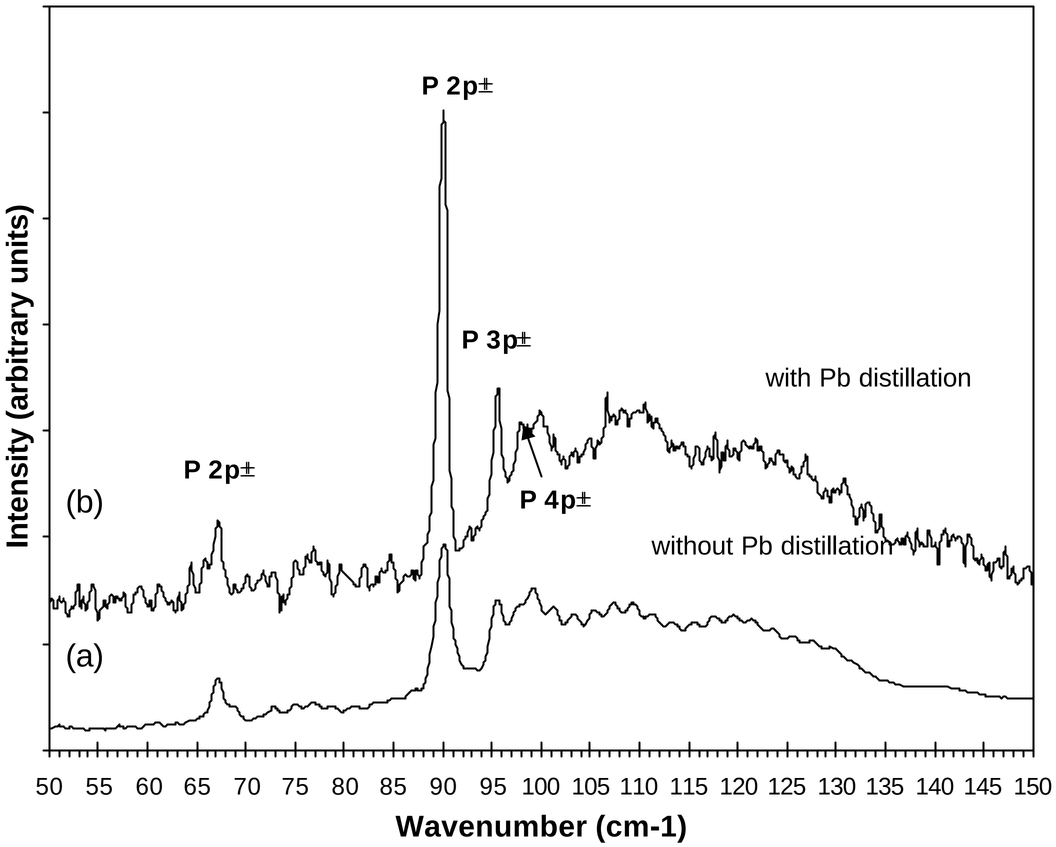

Figure 29. PTIS spectra of LPE layers taken at ~ 8K (a) grown from 6N Pb, n = 1 x 10^{15} cm^{-3} (b) grown from distilled 6N Pb, n = 1 x 10^{14} cm^{-3}. Phosphorus can be identified as the predominant donor impurity in both cases. The spectrum in (b) has been shifted up relative to (a) for clarity.

3.4 Lead Solvent Purification

3.4.1 Review of Pb Purification

The primary ore from which lead is extracted is PbS [Gilchrist, 1989, Engh, 1992]. Once the metal is extracted from the crude ore by heating in an oxygen environment, the metal is purified by a series of refinement steps to remove elements such as Cu, Sb, As, Sn, Ag, Au, Bi, Fe, and Zn. The main processes used are drossing (cooling and skimming impurities from the surface), softening (blowing oxygen through and skimming off impurity oxides from the surface), precipitation from solution by specific reagents, distillation, and electrolytic refining.

Although much information exists on Pb purification, there is little information available in the literature on phosphorus in lead and no information on methods for its removal. The P-Pb phase diagram has not been determined. The only available information indicates that molten Pb has been found to dissolve up to 1.5% phosphorus, and the formation of a compound PbP_2 by reacting white phosphorus with Pb has been observed [Van Wazer, 1958].

Several methods of Pb purification have been attempted [Olsen, 1998] including distillation, evaporation, oxidation, and zone refining. None of these methods specifically addressed phosphorus since it was thought at the time that Sb and Bi were also important impurities in Pb. Of these methods, distillation showed the most promise and was therefore chosen as a subject of further research.

3.4.2 Vacuum Distillation

The process of distillation makes use of the differences in vapor pressures of the components of a mixture. To separate a high vapor pressure component from other low vapor pressure components, the source material is heated to the boiling point of the high vapor pressure component which is then transported via a thermal gradient to a lower temperature region where it condenses and can be collected in a pure form. A multi-stage distillation apparatus can be built which allows this process to take place a large number of times, creating purer material at each stage. To separate out a low vapor pressure component, the same process is used but the source material or the material in the first distillation stage is collected at the end as the pure component. Removal of high vapor pressure impurities from Mg metal using vacuum distillation has been reported in the literature [Revel, 1978]. Na and Zn were detected in the starting material with the vapor pressures of the materials following the order $P_{Na} > P_{Zn} > P_{Mg}$. Na was reduced from 9.6 µg/g to 0.4 µg/g after two successive distillations. Zn, which had a vapor pressure closer to Mg, was reduced from 55 to 3 µg/g after two successive distillations. The distillation apparatus contained a graphite source crucible in the bottom of a vertical furnace evacuated to 10^{-3} Torr. The source was heated to 700 °C. Steel plates with apertures in the center were placed at various heights vertically and served as condensing plates. Magnesium with reduced Na and Zn concentrations was collected in the first condensing stage held at 400 °C. This process was used as a rough guide to designing the Pb distillation set-up. The vapor pressure curves for Pb and the group V elements are shown in Figure 30. They all have higher vapor pressures than Pb

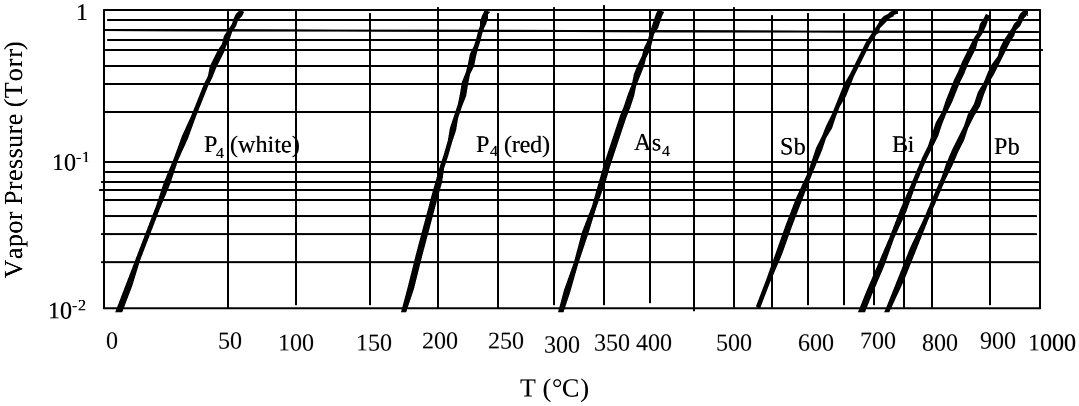

Figure 30. Vapor pressures of Pb and the shallow donor dopants in Ge (data taken from EPI MBE Products Group).

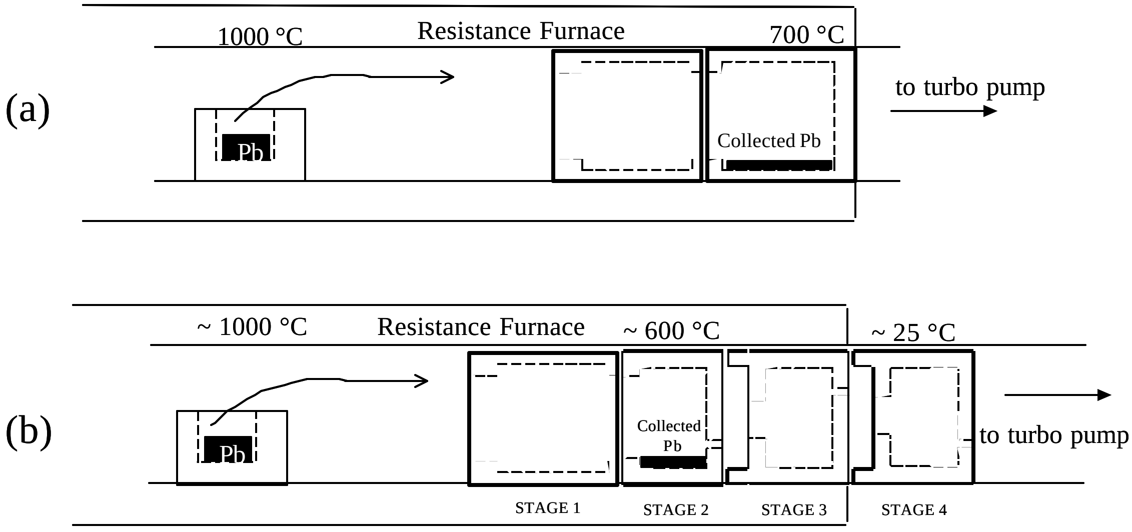

Figure 31. Schematic of graphite distillation stages in a quartz furnace tube. (a) preliminary distillation apparatus used by Olsen (1998) and (b) distillation apparatus design used in this work.

with the difference between Pb and P being the largest. It was therefore expected that the separation of Pb and P by distillation would be possible.

Previous work by Olsen on Pb distillation used one closed-ended stage for collection of the Pb as shown in Figure 31. It was found that germanium epilayers grown from twice distilled Pb had impurity concentrations as low as 5×10^{13} cm^{-3} for the best layer and typically around 10^{14} cm^{-3}.

Results of these initial Pb distillations led to ideas for improvements. Since phosphorus has a very high vapor pressure compared to Pb, it would be expected that in a multiple stage system, Pb collected from the first stage would contain the least amount of phosphorus. Based on this, a design using 4 distillation stages as shown in Figure 31 was used. Instead of having a closed ended system, each stage contains an opening to the next stage. The positioning of the 4 stages in the furnace determined the proportion of Pb condensed in each stage. This design would aid in the transport of phosphorus through the system to the turbo pump and Pb would be collected in the second stage (stage 1 is simply a hollow graphite cylinder used to prevent condensation on the outer wall of stage 2). It was expected that each subsequent stage would contain more phosphorus.

Growth from distilled Pb yielded layers as low as 4×10^{13} cm^{-3} but these values were not reproducible. A typical distillation run lowered the electron concentration in the Ge layer from 10^{15} cm^{-3} to 10^{14} cm^{-3} associated with a removal of phosphorus from the Pb. The segregation coefficient of P between Pb and Ge is not known, so the percent removed from the Pb cannot be known. Layers were periodically grown using undistilled Pb between growths using distilled Pb to verify that phosphorus was not simply being baked out of the crucible showing a reduction over time. Multiple distillation runs (using the amount condensed in stage 2 as the source for the next distillation) were repeated up to 4 times with no improvement seen after the first time.

Distillation runs collected between 3 and 25 g of Pb in stage 2. Neither the amount collected nor the amount remaining in the source after distillation was found to have an effect on the purity. The source temperature was varied from 700 °C to 1000 °C and distillation times ranged from 1 minute to 12 hours. Either lowering the source temperature or using a graphite cover on the source established slower distillation rates. Rates varied from 930 g/hr to 0.6 g/hr. It was thought that perhaps a slower rate was required for the phosphorus to move through the stages, however no difference in purity was observed as the rate was varied. The positions of the condensation stages were also varied in order to vary the amount of Pb collected in each stage. In some runs, Pb only condensed in stage 2, while with the stages placed deeper in the furnace, ~ 10% of the Pb condensed in stage 3. Growths using Pb that condensed in stage 2 were compared with growths using Pb that condensed in stage 3. No difference in purity was observed.

3.4.3 Evaporation and Dilution

A potential method for eliminating phosphorus from the melt is to mix the Pb with a low vapor pressure material that forms a compound with phosphorus. If this compound would stay in solution then the Pb could be evaporated out of the melt in a pure form. Since little is known about the Pb-P interaction, it is not possible to determine such a reaction quantitatively. For this experiment, aluminum was chosen based on its high vapor pressure and the existence of a line compound AlP. An important consideration was the possibility of incorporation of the alloying element into the Ge during growth. Aluminum would be a p-type dopant and increase the compensation, however methods for elimination of Al by oxidation during crystal growth have been established [Edwards, 1963]. This made aluminum a promising choice. In order to insure maximum contact between the aluminum and phosphorus, Pb and Al were melted in a covered graphite crucible. Temperatures between 700 and 950 °C and times from 40 minutes to 12 hours were used. During the mixing time Pb was evaporated from the source and condensed in distillation stage 2. No improvement in purity below 10^{14} cm^{-3} was observed. It is hypothesized that the P-Al bond in Pb solution is not strong enough to bind the excess P and prevent it from evaporating.

3.4.4 Summary of Pb Purification

Figure 32 is a chart of electron concentration in Ge LPE layers grown from purified Pb over time, including both distillation and evaporation runs. Multiple distillation runs are included as a single point. The distillation and evaporation methods described in the above sections were conducted in a random sequence. Except for a few stray points, the purity appears to improve slightly over time, however does not improve beyond ~10^{14} cm^{-3}. There are at least two possible causes for this phenomenon. The first is that there is an inherent limit to the distillation process occurring at low concentrations, for example a Pb-P compound which evaporates with Pb only at the low concentration limit. A second possible explanation is that there are two sources of phosphorus in the system: the Pb and the graphite stages/crucibles. Distillation may inherently reduce the phosphorus

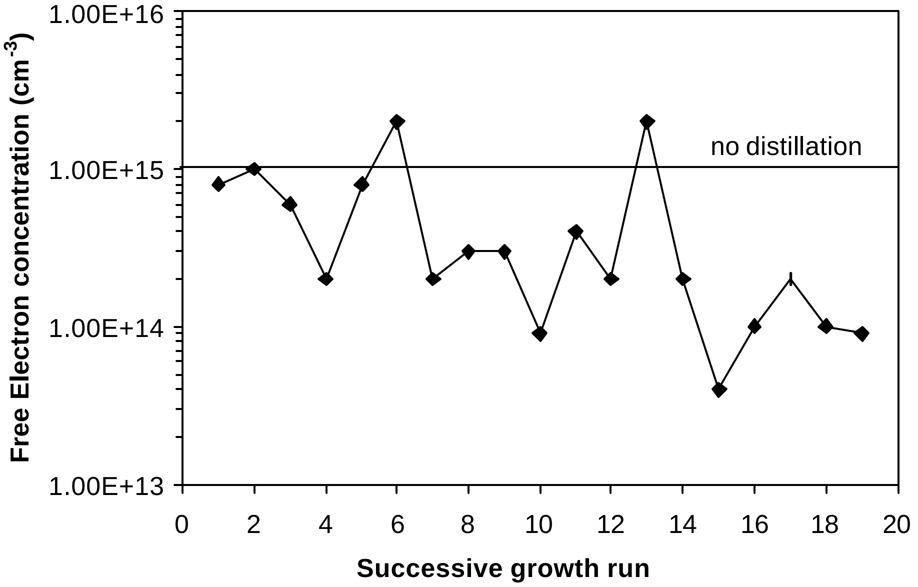

Figure 32. Electron concentration vs. successive growth runs after Pb purification as measured by 77K Hall effect. The solid line indicates an approximate concentration for growth from undistilled Pb. This graph includes single and multiple distillation runs as well as evaporation runs with Ge and Al. Distillation parameters such as source temperature and condensation temperature vary in a random way. The data show that no one particular method achieves higher purity, but the concentration goes down slowly over time, perhaps due to self cleaning of the system / graphite components.

to below 10^{14} cm^{-3}, but the graphite acts as a constant source always yielding layers with 10^{14} cm^{-3} P concentrations. In order to prove the second hypothesis it would be necessary to obtain very clean graphite parts (or non-graphite parts) for both the distillation and growth. A series of commercial high temperature bakeouts in a Cl atmosphere may be necessary. It may also be possible to machine a very thin graphite shell which would not hold as much P as a thick crucible. This could either be free standing or could fit in a quartz crucible. It may be possible in that way to remove more P with fewer bakeout steps. If pure graphite parts were obtained for both the distillation and the growth steps, then one could identify whether the purity limit is inherent to distillation or due to background concentrations from the graphite. Another possible method for determining whether the graphite parts are a source of phosphorus would be melting ultra pure germanium in the crucible and then determining the phosphorus concentration in the germanium by Hall effect and PTIS measurements. Although this process would take place at a higher temperature than growth it would serve as a strong indicator for the presence of phosphorus in the graphite. This procedure has been used in the past for determining the purity of graphite components used for growth of ultra high purity germanium crystals. The contamination from the components was ~ 10^{11} cm^{-3} and was typically from Al and B.

3.5 In_2O_3:Sn Transparent Contacts

Transparent contacts play an important role in BIB detectors used in the front illuminated configuration. For experimental purposes, partial metal contacts are often used leaving some parts of the implanted surface bare as discussed in section 2.10. However, since poor surface passivation has been considered to be a problem [Watson, 1993], it will be important for future array fabrication to develop far infrared transparent contacts which cover and passivate the surface of the blocking layer.

A good candidate for transparent contacts is Sn-doped In_20_3 (Indium Tin Oxide or ITO) which is an n-type oxide semiconductor. Sn^{4+} occupies the In^{3+} site thus acting as an n-type donor. ITO is a widely used material as it has a high optical transmittance in the visible range, good electrical conductivity, excellent substrate adherence, hardness, and chemical inertness [Hamberg, 1986]. Some of the technologically important uses are in window coatings and transparent electrodes. One of the properties that make ITO useful as a window coating is its high infrared reflectance. It is possible to lower the infrared reflectance by using very thin ITO films with low electron concentrations. The optical properties of ITO will depend on its semiconducting properties. The band gap is 3.75 eV. Using the Mott criteria for the metal insulator transition we expect metallic behavior at ~ 6 x 10^{18} cm^{-3} [Hamberg, 1986].

ITO thin films were rf sputtered at 300 W forward power in 10 mTorr Ar gas onto pure Ge substrates (n=5 x 10^{10} cm^{-3}). The sputtering target contained 90% In_2O_3 and 10% SnO_3. The films were characterized by profilometry, Hall effect, resistance at 300K and 4K, and optical transmission in the far infrared from 20 – 500 cm^{-1}. For transmission measurements, phosphorus implanted substrates were used to simulate the device structure.

The plasma frequency (ω_p) of a metal determines the cutoff wavelength of light which can be transmitted and is dependent on the free electron concentration (n) [Kittel, 1986]. A wave can propagate only if its free space frequency is above the plasma frequency. The plasma frequency in SI units is defined as:

$$\omega_p{}^2 = \frac{ne^2}{\varepsilon_0 m} \qquad \text{Equation 11}$$

where e is the electronic charge, m is the electron mass, and ε_0 is the permittivity of free space. For a metal with electron concentration 10^{22} cm^{-3} the plasma frequency is 5.7 x 10^{15} s^{-1} corresponding to a wavelength of 0.33 µm. For an electron concentration of 10^{18}

cm^{-3} (low for a metal) the plasma frequency is 5.7 x 10^{13} s^{-1} corresponding to a wavelength of 33 μm. So even a conductor with a concentration as low as 10^{18} cm^{-3} will not transmit wavelengths greater than 33 μm.

The penetration depth of light in a metal is known as the skin depth (δ) [Harrison, 1980]. The skin depth depends on the conductivity (σ) and the frequency of light (ω).

$$\delta = \sqrt{\frac{2\varepsilon_0 c^2}{\sigma\omega}} \qquad \text{Equation 12}$$

where c is the speed of light. Metals reflect visible light and are transparent in the ultraviolet. For example, the skin depth of silver for 0.5 μm visible light calculated using Equation 12 is 2.6 nm. A material with a large skin depth will have a low conductivity. For contacts which are transparent in the far infrared this is a tradeoff since they must also remain conducting at low temperatures. A standard metal cannot be used for far infrared transparent contacts. The calculated skin depth of Au at 200 μm is 61 nm. In practice, a 50 nm thick Au film sputtered on pure Ge did not show any transmission when tested in the far infrared.

3.5.1 Infrared Transmission and Electrical Properties of In_2O_3:Sn

The transmission of ITO layers was determined by dividing the intensity of signal transmitted through the ITO/Ge samples by the intensity transmitted through the pure Ge substrate. The relative spectra for samples sputtered from 0.5 to 5 minutes are shown in Figure 33. Note that the implanted substrate transmits 100%. Figure 34 shows the average transmission of the ITO samples as well as their resistance at 300K and 4K.

Resistance is given instead of resistivity because the thickness of the samples is not known (profilometry measurements were unclear for most samples). The only reliable thickness measurement of 1000 Å was made for the 1.5 minute sputtering time. Samples were 6 x 6 mm^2 with contacts along two edges. Based on this the resistivity of the 1000 Å thick sample would be 4.5 x 10^{-3} Ω-cm at 300K and 1.2 x 10^{-2} Ω-cm at 4K. Hall effect measurements at 300K on the same sample were in agreement and gave an electron concentration of 1.4 x 10^{18} cm^{-3} and a resistivity of 4.3 x 10^{-3} Ω-cm. This shows that this film is very close to the metal insulator transition. The skin depth calculated for this film

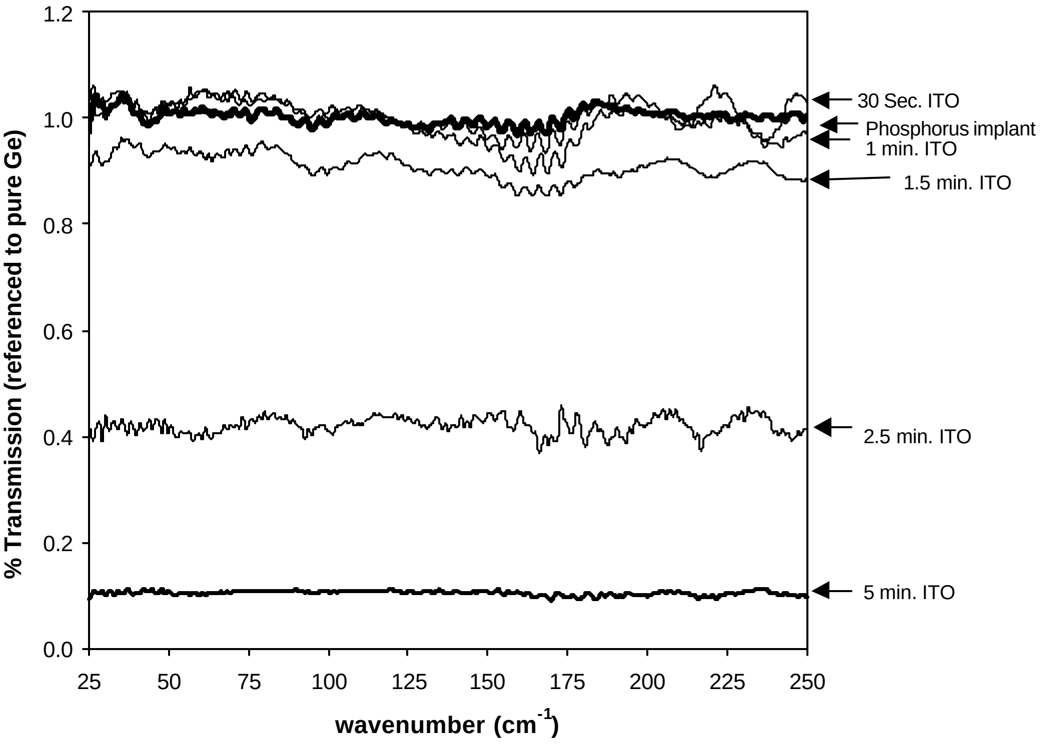

Figure 33. Transmission spectra of sputtered ITO films on phosphorus implanted Ge substrates referenced to bare Ge substrates (5 x 10^{10} cm^{-3} n-type). Sputtering time is given to the right of each curve.

using Equation 12 is ~ 3 μm. Since the resistivity of germanium photoconductors can be in the MΩ-cm range, the conductivity of this ITO sample should be sufficient. Using ITO films with higher electron concentrations would reduce the transmission.

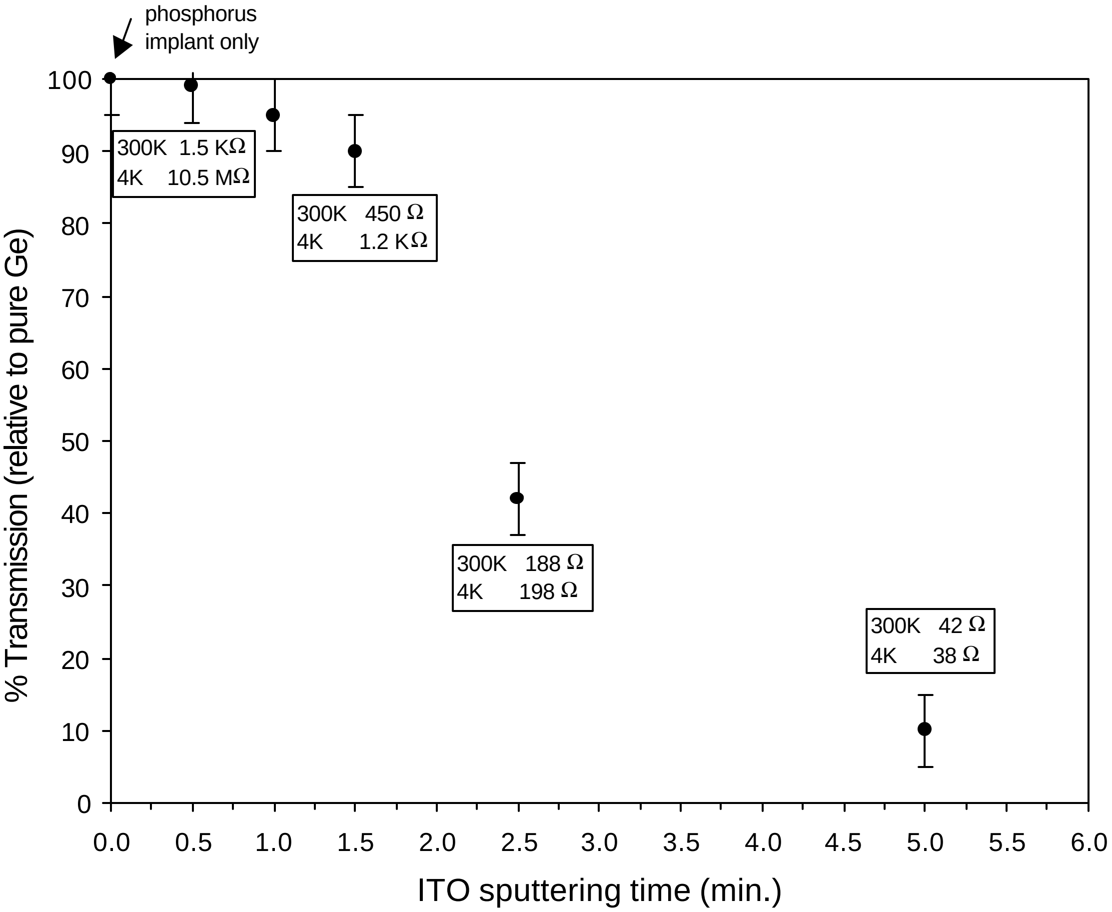

Figure 34. Relative transmission of ITO films grown on phosphorus implanted Ge substrates referenced to a pure Ge substrate (5 x 10^{10} cm^{-3} n-type). Phosphorus implant: 33kV, 2 x 10^{14} cm^{-2}. Transmission is an average from 25 to 500 wavenumber. Resistance for 4 of the samples at 300K and 4K is given next to the data points. The 1.5 minute sputtering time corresponds to 1000Å thickness (from profilometry), but other samples were difficult to measure.

The ITO film sputtered for 0.5 minutes is transparent to nearly 100 % but is not conducting at 4K. It is likely that the film is too thin to form a continuous layer. Thicker films stay very well conducting at 4K, but transmission is significantly reduced. The film sputtered for 5 minutes is only 10% transmitting.

Thin ITO films seem well suited for transparent contacts to Ge photoconductors. However, care must be taken to achieve repeatable sputtering conditions. Since the conductivity and transparency of the layers will depend highly on composition and thickness, a careful study of the repeatability of ITO sputtering should be undertaken.

3.6 Germanium Blocked Impurity Band Detector Measurements

The BIB devices discussed in this section are described below. The Sb concentration in the devices is ~ 2×10^{16} cm^{-3}.

Device	**Thickness**	**Starting growth temperature**
BIB1	45 µm active layer (double layer, surface polished both layers) 10µm blocking layer	650 °C
BIB4	22 µm active layer (surface not polished) 10 µm blocking layer	550°C

3.6.1 Current-Voltage Characteristics

The current – voltage behavior of BIB1 at 2 K is shown in Figure 35. Under positive bias (reverse bias for an n-type BIB) the device is blocking. It begins to break down at ~ 40 mV. Under negative bias the device behaves like a forward biased diode. Under positive bias below 40 mV the leakage current is below the detectable limit with this set-up.

Some of the other devices tested had higher dark current, even at low applied bias values. In order to determine whether this was a surface leakage effect, I-V was measured for BIB4 with and without a passivating amorphous germanium layer on the surface. The amorphous Ge was sputtered onto the device after Pd/Au contacts were

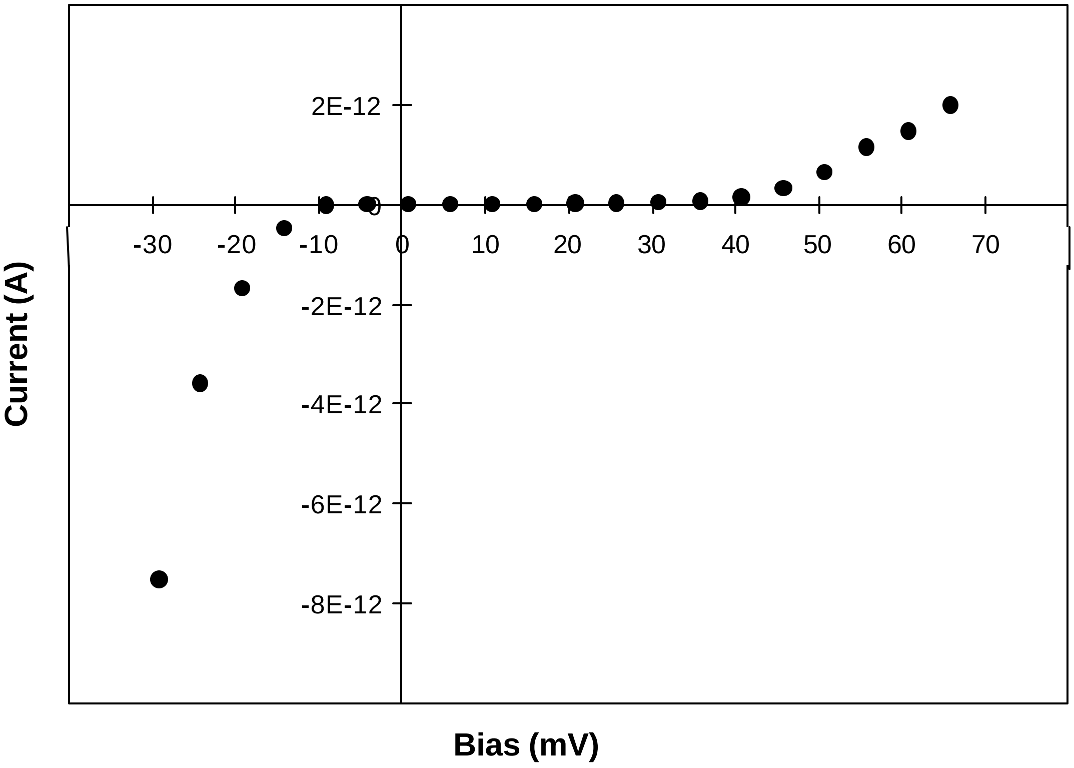

Figure 35. Dark current – voltage characteristics of BIB1. At 0 bias the dark current is below the detection limit for the electronics.

applied. Amorphous Ge is known to pin the Fermi level of the surface around mid-gap which makes the surface non-conducting at low temperatures [Hansen, 1980]. Even with the surface passivation the dark current was not significantly lowered (see Figure 36). Difficulty in removing picene wax after masking steps left a residue on the surface which may have contributed to leakage. In the future, a masking step that does not require

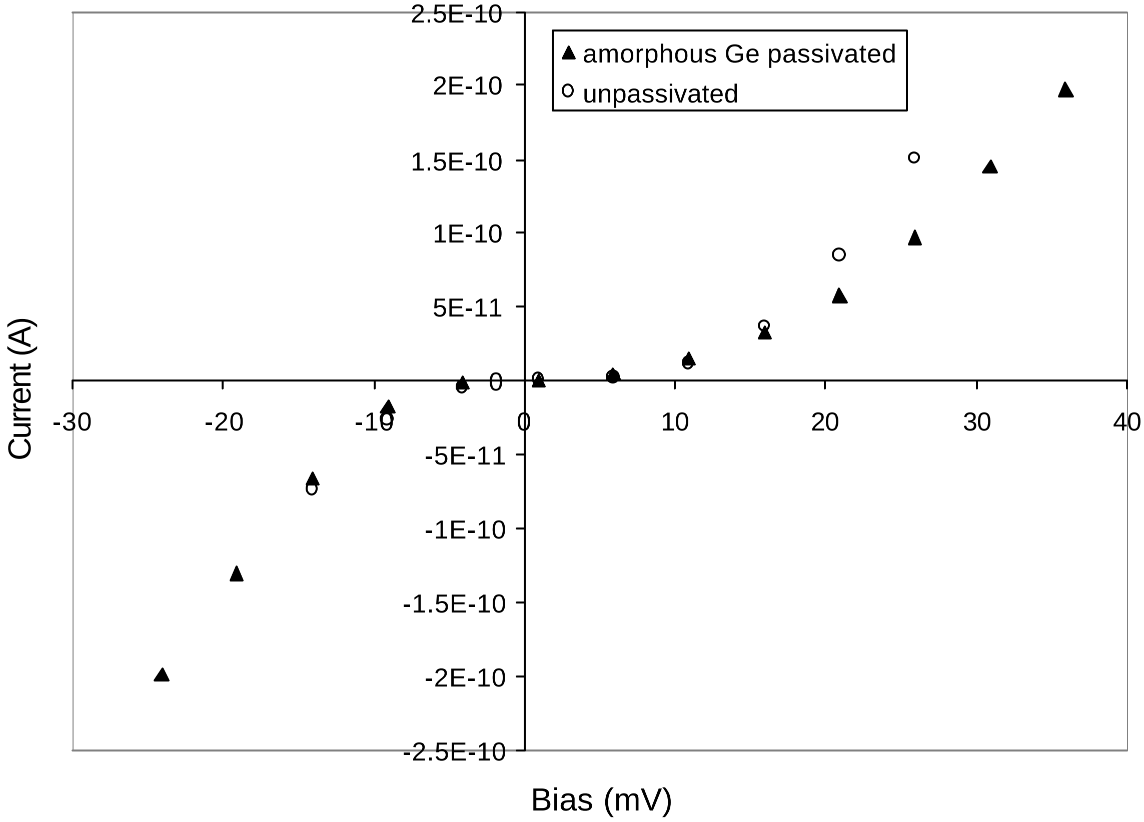

Figure 36. Dark current – voltage characteristics of BIB4 with and without a passivating amorphous Ge surface. The dark current close to 0 on the reverse bias side is ~ 10^{-13} A.

picene (such as a shadow mask) should be used. Another possibility is that there are defects at the surface of the LPE layer (the part grown at low temperature). For the layers that showed high leakage current, the surface was not polished away before device processing.

3.6.2 Spectral Response

The spectral response of BIB1 at 2K is shown in Figure 37 for three different applied bias values. The Fabry-Perot oscillations were too strong to be removed without

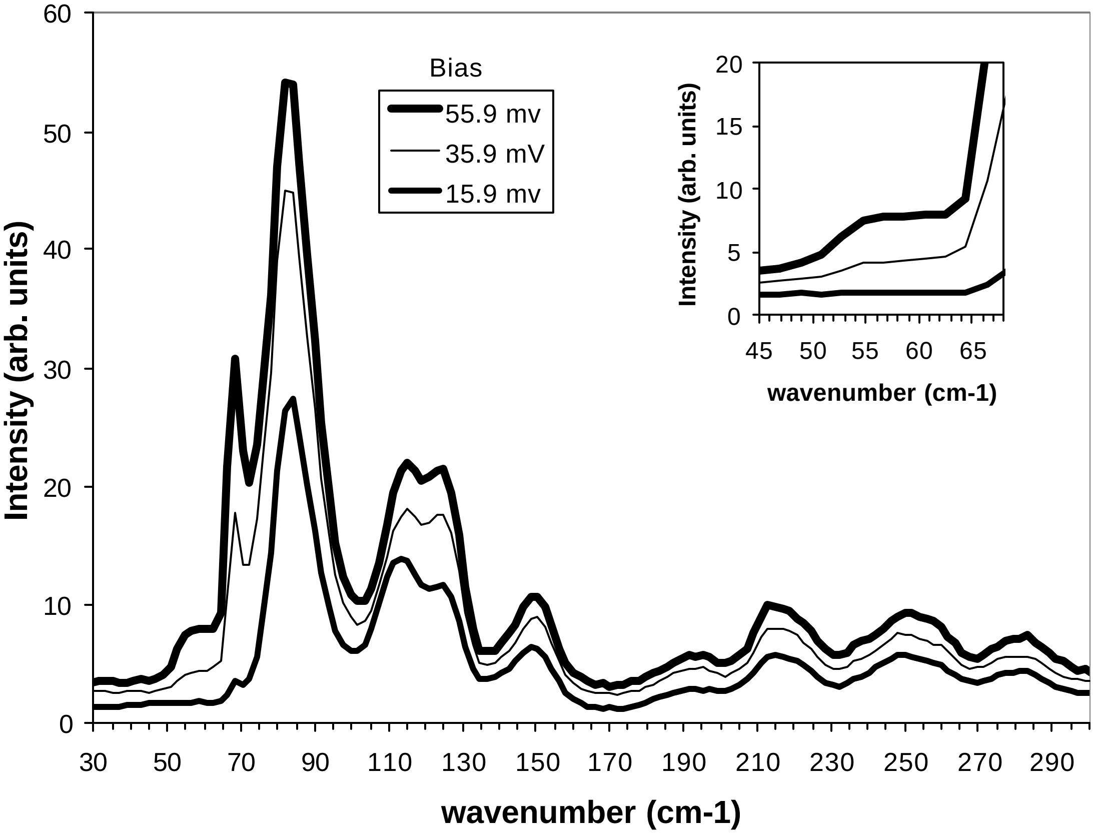

Figure 37 . Spectral response of BIB1.

eliminating too much real data. They are regularly spaced at ~ 40 cm^{-1} apart which corresponds to 30 µm of germanium. The sample is close to this thickness so it is thought that the phenomenon is likely to originate inside the sample.

Long wavelength response is observed relative to a standard Ge:Sb photoconductor. It can be seen that the onset of photoconductivity extends to lower wavenumbers (longer wavelength) as the bias is increased. This can be understood by considering the depletion in the active layer of the BIB. The exact compensation of this LPE layer is not known, but it is likely between 1 and 4 x 10^{12} cm^{3}. The depletion width obtained from Figure 4 is between 1 and 4 µm for 50 mV applied bias. Assuming there is a transition region between the pure substrate and the Sb-doped layer due to Sb diffusion during growth, the material being depleted at low applied bias will contain less Sb than the material depleted at high applied bias. A measurement of responsivity was attempted on BIB1 using a 163 µm filter with a 3.66 µm bandpass and 8% transmission, however it was not possible to obtain a large enough signal with this filter.

3.7 Ge:Sb Absorption Measurements

The interpretation of the extended wavelength response in a BIB detector can be complicated by the fact that the depletion width of the device may be small, and the Sb distribution may be nonuniform at the layer-substrate interface. Far infrared optical absorption coefficient vs. wavelength measurements for LPE Ge layers of various concentrations should help to determine the change in onset of Sb absorption with concentration. The optimal Sb concentration for a BIB device could be found in this way.

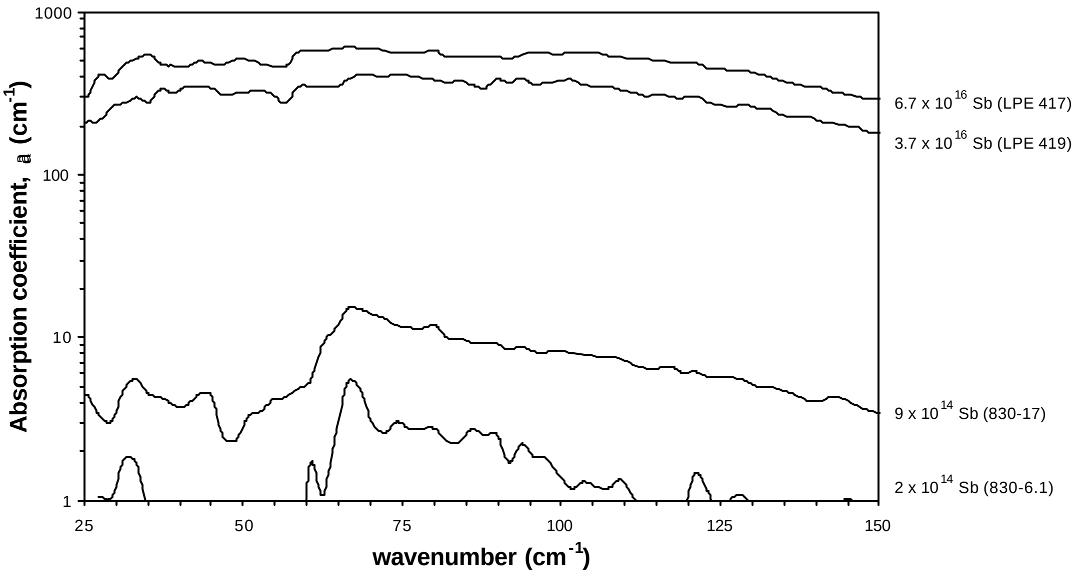

Figure 38. Optical absorption coefficients vs. wavenumber for Sb doped Ge samples of various Sb concentrations measured at 1.5K.

Absorption measurements as described in section 2.8 were performed on Ge samples containing 2 x 10^{14}, 9 x 10^{14}, 3.7 x 10^{16}, and 6.7 x 10^{16} cm^{-3} Sb. Spectra are shown in Figure 38. The first two samples are bulk Ge crystals and the second two are LPE layers. The concentrations cited were measured by Hall effect at 77K. The two bulk samples were used as controls. The absorption coefficients for these samples agree well with the results of Reuszer [1964] which show a peak absorption coefficient of ~ 12 cm^{-1} for Ge with ~ 7 x 10^{14} cm^{-1} Sb. The onset in spectral response for the two bulk samples occurs at ~ 65 cm^{-1}. Both LPE layers show broadband absorption indicating that they are close to metallic. An intermediate concentration should be found for use in BIB detectors.

4 Future Work

In order to fabricate large Ge BIB arrays using liquid phase epitaxy, it will be necessary to grow both the pure blocking layer and the doped active layer. The existence of a pure solvent for blocking layer growth is required before this can become a reality. Since it is clearly understood that phosphorus is the main contaminant, it would be worthwhile to perform a thorough study of the behavior of phosphorus in Pb. The level of phosphorus present in commercial Pb is too low for many experiments, so phosphorus should be intentionally added to Pb for these studies. The phase diagram could be established from a series of Pb-P samples heated to various temperatures in ampoules. Because phosphorus has a very high vapor pressure, a hole should be drilled in the Pb and the phosphorus enclosed in the hole and plugged in order to ensure contact between solid phosphorus and Pb. With such a setup the segregation coefficient of P in the Pb-Ge system should be determined. A Pb-P alloy (as described above) could be used as a solvent for growing LPE layers. The Phosphorus content in the Pb could be determined from Secondary Ion Mass Spectrometry (SIMS).

Zone refining is a unique technique which can be repeated many times in order to obtain very high purity material. The segregation coefficient for P in Pb is not known and should be determined by zone refining a Pb bar that is intentionally alloyed with P. In this way it could be determined whether the segregation coefficient is favorable for purification by zone refining. Zone refining of Pb for removal of other elements has been reported in the literature [Pfann, 1958]. Both active heating and cooling of the Pb bar are necessary to maintain a small confined liquid zone. An initial attempt at zone refining

[Olsen, 1998] did not use cooling, so it is hypothesized that the zone was too large for efficient refining to occur. A double walled quartz boat could be used for water cooling. If the Pb sticks to the quartz, a graphite shell or coating could be used.

A possible alternative to fabrication of BIB devices by liquid phase epitaxy is wafer bonding. If a pure germanium wafer could be bonded to a doped wafer, the pure side could be thinned to form the blocking layer. Direct bonding of Ge to Ge has been reported in the literature [Haisma, 1994]. This technique shows promise, provided the polishing and surface preparation techniques are well developed. Surface peak to valley roughness should be ~ 1nm.

Although growth of the pure layer is important for array fabrication, much can still be learned about the Ge:Sb BIB by growing only the active layer. A comparison should be made of the spectral response for various Sb concentrations. Although an extension of the long wavelength response of the Ge:Sb BIB near the metal insulator transition has been observed, the behavior of BIB devices with different Sb concentrations has not yet been characterized experimentally. Both absorption measurements and photoconductivity measurements should prove useful.

The diffusion of Sb into the blocking layer during growth should be studied in depth and a comparison should be made between devices grown at low vs. high temperatures. A comparison between Ge:Sb and Ge:Ga BIBs would be useful, since Ga has ~ 1000 times lower diffusivity than Sb. However, the ability to fabricate a p-type BIB is still limited by Pb purity.

Finally, the effects of surface passivation should be studied further by developing a reliable method for deposition of ITO layers as transparent contacts. Device performance should be compared for layers with and without ITO passivating surface layers.

Important issues in LPE growth of germanium for use as far infrared BIB detectors have been studied in detail in this work. A BIB device showing extended wavelength response and low leakage current has been demonstrated. The additional studies that have been outlined above encompassing purification, LPE growth, and detector testing are essential for creating BIB detectors which meet all of the necessary criteria for far infrared applications.

References

M.G. Astles, Liquid Phase Epitaxial Growth of III-V Compound Semiconductor Materials and their Device Applications, Adam Hilger imprint by IOP Publishing Ltd., Bristol, 1990

B.J. Baliga, Epitaxial Silicon Technology, Chapter 3, “Silicon liquid phase epitaxy”, Academic Press, 1986, p. 177-232

E. Bauser, Crystal Growth of Electronic Materials, Chapter 4, “LPE-grown surfaces and growth mechanisms”, E. Kaldis, Ed., Elsevier Science, Amsterdam, 1985, p. 41-55

E. Bauser, Handbook of Crystal Growth, Chapter 20, “Atomic Mechanisms in Semiconductor Liquid Phase Epitaxy”, D.T.J. Hurle, Ed., Elsevier Science, Amsterdam, 1994, p. 880-939

E. Bauser, G.A. Rozgonyi, “A lateral microscopic growth model for heterogeneous impurity incorporation during Czochralski crystal growth”, Appl. Phys. Lett., Vol. 37, No. 11, 1980, p. 1001-1003

E. Bauser, H.P. Strunk, “Microscopic growth mechanisms of semiconductors: experiments and models”, J. Crystal Growth, Vol. 69, 1984, p. 561-580

E. Becklin, J.M.M. Horn, “Stratospheric Observatory for Infrared Astronomy (SOFIA)”, from ISO Surveys of a Dusty Universe, Proceedings of a Ringberg Workshop held at Ringberg Castle, Tegernsee, Germany, 8-12 November 1999, D. Lemke, M. Stickel, K. Wilke (Eds.), Springer-Verlag, Germany, 2000, p. 416-422

J.W. Beeman, W.L. Hansen, O.D. Dubon, E.E. Haller, “High performance antimony-doped germanium photoconductors”, Infrared Physics & Technology, Vol. 37, 1996, p. 715-721

A.C. Beer, R.K. Willardson, “Hall and Transverse Magnetoresistance effects for warped bands and mixed scattering”, Phyical Review, Vol. 110, No. 6, 1958, p. 1286-1294

R.J. Bell, Introductory Fourier Transform Spectroscopy, Academic Press, New York, 1972

J. Boussey, “Stripping Hall effect, sheet and spreading resistance techniques for electrical evaluation of implanted silicon layers”, Microelectronic Engineering, Vol. 40, 1998, p. 275-284

B. Brandl, V. Charmandaris, K. Uchida, J. Houck, “Extragalactic Spectroscopy with SIRTF / IRS”, from ISO Surveys of a Dusty Universe, Proceedings of a Ringberg Workshop held at Ringberg Castle, Tegernsee, Germany, 8-12 November 1999, D. Lemke, M. Stickel, K. Wilke (Eds.), Springer-Verlag, Germany, 2000, p. 402-407

T. Chu, R. Ray, “Resistivity measurements on germanium crystals by the spreading resistance technique”, Solid State Technology, September 1971, p. 37-40

B.D. Cullity, Elements of X-ray Diffraction, second edition, Addison Wesley, 1978

E.A. Davis, W.D. Compton, “Compensation dependence of impurity conduction in antimony-doped germanium”, Physical Review, Vol. 140, No. 6A, 1965, p. 2183-2194

E. Dwek, M. Fioc, F. Varosi, “The effect of dust evolution on the spectral energy distribution of galaxies”, from ISO Surveys of a Dusty Universe, Proceedings of a Ringberg Workshop held at Ringberg Castle, Tegernsee, Germany, 8-12 November 1999, D. Lemke, M. Stickel, K. Wilke (Eds.), Springer-Verlag, Germany, 2000, p. 157-165

W.D. Edwards, “Interaction between oxygen and aluminum in germanium”, J. Appl. Phys. Vol. 34, 1963, p. 2497-2498

A. Efstathiou, R. Siebenmorgen, M. Rowan-Robinson, “Models for the Infrared Emission from Starburst Galaxies”, from ISO Surveys of a Dusty Universe, Proceedings of a Ringberg Workshop held at Ringberg Castle, Tegernsee, Germany, 8-12 November 1999, D. Lemke, M. Stickel, K. Wilke (Eds.), Springer-Verlag, Germany, 2000, p. 141-148

T.A. Engh, Principles of Metal Refining, New York, Oxford University Press, 1992

G.G. Fazio, “Infrared array detectors in astrophysics”, Infrared Physics & Technology, Vol. 35, No. 2/3, 1994, p. 107-117

B. Fischer, E. Bauser, P.A. Sullivan, D.L. Rode, “Dopant tracing of terrace growth in GaAs LPE layers”, Appl. Phys. Lett., Vol. 33, No. 1, 1978, p. 78-80

J.D. Gilchrist, Extraction Metallurgy, 3rd edition, Permagon Press, New York, 1989

N.M. Haegel, *Performance and materials aspects of Ge:Be and Ge:Ga photoconductors for far infrared detection*, M.S. Thesis, University of California, Berkeley, 1983, unpublished

N.M. Haegel, E.E. Haller, “Ge:Be far infrared detectors”, Presented at the IR Detector Technology Workshop, Mountain View, CA, August 13-14, 1985

N.M. Haegel, J.E. Jacobs, A.M. White, “Modeling of steady-state field distributions in blocked impurity band detectors”, Appl. Phys. Lett., Vol. 77, No. 26, 2000, p.4389-4391

J. Haisma, B.A.C.M. Spierings, U.K.P. Biermann, A.A. van Gorkum, “Diversity and feasibility of direct bonding: a survey of a dedicated optical technology”, Applied Optics, Vol. 33, No. 7, 1994, p. 1154-1169

E.E. Haller, W.L. Hansen, “Impurities in high-purity germanium as determined by Fourier transform spectroscopy”, IEEE Trans. Nucl. Sci. NS-21, No. 1, 1974, p. 279-286

E.E. Haller, W.L. Hansen, F.S. Goulding, “Physics of ultra-pure germanium”, Advances in Physics, Vol. 30, No. 1, 1981, p. 93-138

E.E. Haller, W.L. Hansen, F.S. Goulding, “Photothermal Ionization Spectroscopy in semiconductors”, IEEE Trans. Nucl. Sci., NS-22, No. 1, 1975, p. 127-134

I. Hamberg, C.G. Granqvist, “Evaporated Sn-doped In_2O_3 films: Basic optical properties and applications”, J. Appl. Phys., Vol. 60, No. 11, 1986, p. R123-R159

W.L. Hansen, E.E. Haller, G.S. Hubbard, “Protective surface coatings on semiconductor nuclear radiation detectors”, IEEE Trans. on Nuclear Science, Vol. NS-27, No.1, 1980, p. 247-251

W.L. Hansen, E.E. Haller, Encyclopedia of Applied Physics, Vol. 7, VCH Publishers, Inc., 1993, p. 219-237

W.A. Harrison, Solid State Theory, Dover Publications, Inc., New York, 1980

J.E. Huffman, N.L. Casey, “Growth methods for high purity Ge and Ge:Ga homoepitaxy”, J. Crystal Growth, Vol. 129, 1993, p. 525-531

J.E. Huffman, A.G. Crouse, B.L. Hallek, T.V. Downes, “Si:Sb blocked impurity band detectors for infrared astronomy”, J. Appl. Phys., Vol. 72, No.1, 1992, p. 273-275

A.A. Immorlica, Jr., B.W. Ludington, “Diffusion coefficient and solubility of Ge and GaAs in Pb and application to LPE growth of Ge on GaAs”, J. Crystal Growth, Vol. 51, 1981, p. 131-139

T. Kajimura, K. Aiki, J. Umeda, “Nonradiative dark regions along surface ripples in GaP LPE layers”, Appl. Phys. Lett., Vol. 30, No. 10, 1977, p. 526-528

P. H. Keck, J. Broder, “The solubility of silicon and germanium in gallium and indium”, Physical Review, Vol. 90, No. 4, 1953, p. 521-522

M. Kessler, “The ISO mission and its surveys”, from ISO Surveys of a Dusty Universe, Proceedings of a Ringberg Workshop held at Ringberg Castle, Tegernsee, Germany, 8-12 November 1999, D. Lemke, M. Stickel, K. Wilke (Eds.), Springer-Verlag, Germany, 2000, p. 3-10

K. Kijima, N. Miyamoto, J. Nishizawa, “Observation of nucleus centers on solution-grown germanium epitaxial layers”, J. Appl. Phys, Vol. 42, 1970, p. 486-487

C. Kittel, Introduction to Solid State Physics, Sixth Edition, John Wiley & Sons, Inc., New York, 1986

SH.M. Kogan, T.M. Lifshits, “Photoelectric spectroscopy – a new method of analysis of impurities in semiconductors”, Phys. Stat. Sol. (a) Vol. 39, No. 11, 1977, p. 11-39

M. Konuma, E. Czech, I. Silier, E. Bauser, “Liquid phase epitaxy centrifuge for 100 mm diameter Si substrates”, Appl. Phys. Lett. Vol. 63, No. 2, 1993, p. 205-207

M. Konuma, I. Silier, A. Gutjahar, P.O. Hansson, G. Cristiani, E. Czech, E. Bauser, F. Banhart, “Centrifugal techniques for solution growth of semiconductor layers”, J. Crystal Growth, Vol. 166, 1996, p. 234-238

D. Lemke, M. Stickel, K. Wilke (Eds.), ISO Surveys of a Dusty Universe, Proceedings of a Ringberg Workshop held at Ringberg Castle, Tegernsee, Germany, 8-12 November 1999, Springer-Verlag, Germany, 2000

J. Leotin, “Far infrared photoconductivity studies in silicon blocked impurity band structures”, Infrared Physics & Technology, Vol. 40, 1999, p. 153-160

R. Linnebach, E. Bauser, “Low temperature liquid phase epitaxy of silicon”, J. Crystal Growth, Vol. 57, 1982, p. 43-47

Z.H. Lu, “Air-stable Cl-terminated Ge (111)”, Appl. Phys. Lett. Vol. 68, No. 4, 1996, p. 520-522

M.P. Lutz, *Development of ultra pure germanium epi layers for blocked impurity band far infrared detectors*, Ph.D. Thesis, University of California, Berkeley, 1991, unpublished

J.C. Mather, “Infrared measurements from the Cosmic Background Explorer (COBE)”, Infrared Phys. Technol., Vol. 35, No. 2/3, 1994, p. 331-336

H. Miyazawa, H. Maeda, “Anisotropic Hall Coefficients in n-type germanium”, J. Phys. Soc. Japan, Vol. 15, 1960, p. 1924-1939

G.E. Murch, A.S. Nowick, eds., Diffusion in Crystalline Solids, Academic Press, 1984

T. Nishinaga, T. Kazuno, T. Tanbo, J. Koide, K. Pak, T. Nakamura, Y. Yasuda, "Behavior of macrosteps and grooves during LPE growth as observed by photoluminescence images", J. Crystal Growth, Vol. 65, 1983, p. 607-610

C.S. Olsen, *Advanced Far Infrared Blocked Impurity Band Detectors based on Germanium Liquid Phase Epitaxy*, Ph.D. thesis, University of California, Berkeley, 1998, unpublished

M.D. Petroff, M.G. Stapelbroek, U.S. Patent No. 4-568-960

M.D. Petroff, M.G. Stapelbroek, "Responsivity and noise models of blocked impurity band detectors", unpublished report, IRIS Specialty Group on IR Detectors, 1984

M.D. Petroff, M.G. Stapelbroek, "Origin of low-frequency noise at intermediate infrared backgrounds in BIB detectors", unpublished report, IRIS Specialty Group on IR Detectors, 1984

W.G. Pfann, Zone melting, second edition, New York, Wiley, 1966

G. Pilbratt, "FIRST - Far Infrared and Submillimetre Space Telescope", Infrared Phys. Technol., Vol. 35, No. 2/3, 1994, p. 407-418

G. Pilbratt, "The FIRST mission", from ISO Surveys of a Dusty Universe, Proceedings of a Ringberg Workshop held at Ringberg Castle, Tegernsee, Germany, 8-12 November 1999, D. Lemke, M. Stickel, K. Wilke (Eds.), Springer-Verlag, Germany, 2000, p. 408-415

R.S. Popovic, Hall Effect Devices: Magnetic Sensors and Characterization of Semiconductors, Adam Hilger Series on Sensors, Bristol, 1991

J.H. Reuszer, P. Fisher, "An optical determination of the ground-state splittings of group V impurities in germanium", Physical Review, Vol. 135, No. 4A, 1964, p. A1125-A1132

G. Revel, J.-L. Pastol, J.-C. Rouchaud, R. Fromageau, "Purification of magnesium by vacuum distillation", Metallurgical Transactions B, Vol. 9B, 1978, p. 665-672

D.B. Reynolds, D.H. Seib, S.B. Stetson, T. Herter, N. Rowlands, J. Schoenwald, "Blocked impurity band hybrid infrared focal plane arrays for astronomy", IEEE Transactions on Nuclear Science, Vol. 36, No. 1, 1989, p. 857-862

G.H. Rieke, M.W. Werner, R.I. Thompson, E.E. Becklin, W.F. Hoffmann, J.R. Houck, F.J. Low, W.A. Stein, F.C. Witteborn, "Infrared astronomy after IRAS", Science, Vol. 231, 1986, p. 807-814

G.H. Rieke, "Surveys with SIRTF", from ISO Surveys of a Dusty Universe, Proceedings of a Ringberg Workshop held at Ringberg Castle, Tegernsee, Germany, 8-12 November 1999, D. Lemke, M. Stickel, K. Wilke (Eds.), Springer-Verlag, Germany, 2000, p. 394-401

D.L. Rhode, "Surface dislocation theory of reconstructed crystals: VPE GaAs", Phys. Stat. Sol. (a), Vol. 32, 1975, p. 425-434

F. Rosenberger, Fundamentals of crystal growth. I. Macroscopic equilibrium and transport concepts, Berlin, West Germany: Springer-Verlag, 1979

C.S. Rossington, *Germanium Blocked Impurity Band Far Infrared Detectors*, Ph.D. Thesis, University of California, Berkeley, 1988, unpublished

E. Rotsaert, P. Clauws, J. Vennik, "Absorption cross sections in the far-IR spectrum of elemental shallow donors and acceptors in germanium", J. Appl. Phys., Vol. 65, No. 2, 1989, p. 730-735

Z. Shi, W. Zhang, G.F. Zheng, J. Kurianski, M.A. Green, R. Bergmann, "The growth and properties of liquid phase epitaxial silicon in a forming gas ambient", J. Crystal Growth, Vol. 151, 1995, p. 278-284

B.I. Shklovskii and A.L. Efros, Electronic Properties of Doped Semiconductors, Springer-Verlag, Berlin, 1984

G. Sirmain, P. Etieve, W/ Knap, C. Meny, S. Pasquier, P. Adet, N. Fabre, A. Murray, M. Griffin, J. Leotin, "BIB photodetectors based on antimony doped silicon", Proceedings of an ESA symposium on photodetectors for space instrumentation, the Netherlands, 1992, p. 153-158

W.G. Spitzer, F.A. Trumbore, R.A. Logan, "Properties of heavily doped n-type germanium", J. Appl. Phys., Vol. 32, No. 10., 1961, p. 1822-1830

N.A. Stolwijk, H. Bracht, "Diffusion in Silicon, Germanium and Their Alloys", in Landolt Boernstein, New Series, Vol. III/33, Diffusion in Semiconductors and Non-Metallic Solids, ed. by D. L. Beke, Subvolume A: Diffusion in Semiconductors, Springer, Berlin, 1998, p. 1-257.

F.A. Trumbore, "Solid solubilities and electrical properties of tin in germanium single crystals", Journal of the Electrochemical society, Vol. 103, No. 11, 1956, p. 597-600

L.J. van der Pauw, “A method of measuring specific resistivity and Hall effect of discs of arbitrary shape”, Philips Res. Repts., Vol. 13, 1958, p. 1-9

J.R. Van Wazer, Phosphorus and its Compounds, Volume I: Chemistry, Interscience Publishers, Inc., New York, 1958

D.M. Watson, “Extrinsic germanium blocked-impurity-band detector arrays”, Proceedings of the S.P.I.E, Vol. 1874, 1993

D.M. Watson, M.T. Guptill, J.E. Huffman, T.N. Krabach, S.N. Raines, S. Satyapal, “Germanium blocked-impurity-band detector arrays: unpassivated devices with bulk substrates”, J. Appl. Phys, Vol. 74, No. 6, 1993, p. 4199-4206

I.C. Wu, J.W. Beeman, P.N. Luke, W.L. Hansen, E.E. Haller, “Ion-implanted extrinsic Ge photodetectors with extended cutoff wavelength, Appl. Phys. Lett. Vol. 58, No. 13, 1991, p. 1431-1433

D. Wynne, B. Cardozo, E.E. Haller, “GaAs thin film epitaxy and x-ray detector development”, Proceedings of the SPIE, hard x-ray, gamma ray, and neutron detector physics, 1999, Vol. 3768, p. 196-203

Appendix A. Depletion Width and Field Distribution in a BIB Detector

The electric field distribution in an ideal n-type BIB detector under reverse bias is given by the charge density (ρ):

$$\frac{dE}{dx} = \frac{\rho}{\varepsilon\varepsilon_0} = -\frac{eN_A}{\varepsilon\varepsilon_0} \qquad \text{eq. i}$$

where $\varepsilon\varepsilon_0$ is the dielectric constant of the material (16 for Ge), e is the electronic charge, and N_A is the acceptor concentration. There is no movable charge in the blocking layer

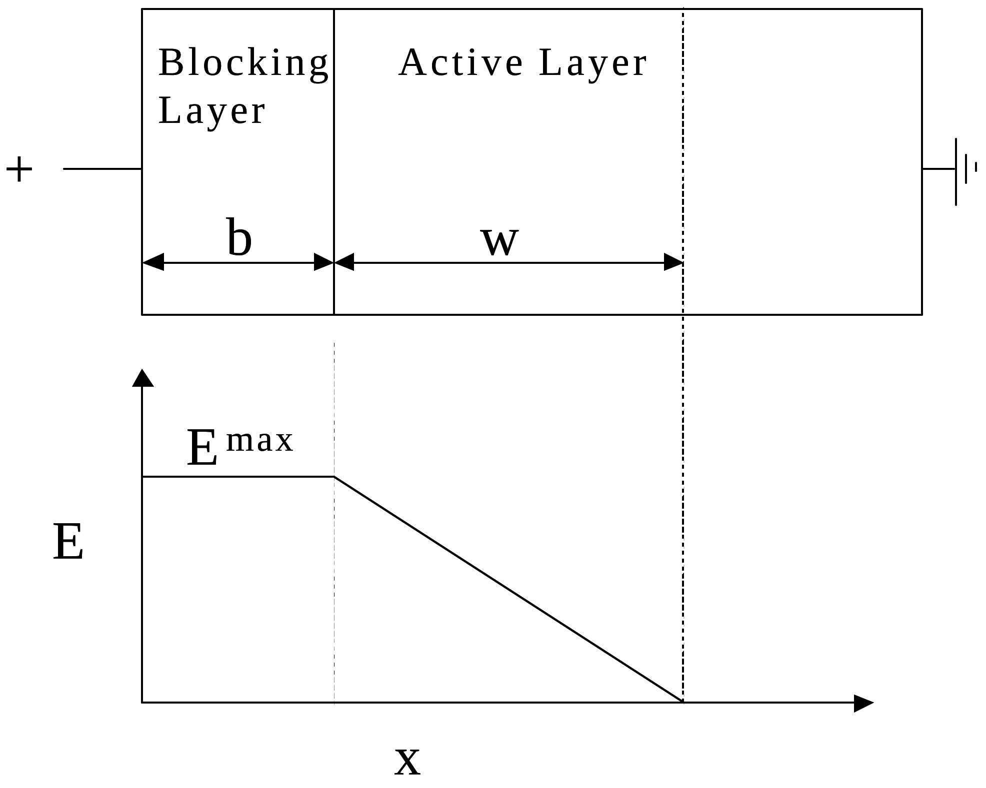

Fig. I. Electric field distribution in a reverse biased n-type BIB detector.

so the field is constant there and is defined as E^{MAX}. In the active layer, electrons can hop in the impurity band leaving behind ionized acceptors. The extent of the depletion width into the active layer is determined by the minority acceptor concentration. The applied bias determines the electric field in the active layer and blocking layer:

$$V = \int_0^w E dx + E^{\max} b \qquad \text{eq. ii}$$

where w is the depletion width and b is the blocking layer thickness. The built in potential is small and can be neglected. Using E= E^{MAX} when x=w, the solution to this equation gives the depletion width as a function of blocking layer thickness, acceptor concentration, and applied bias.

$$w^2 + 2wb - \frac{2\boldsymbol{ee}_0 V}{eN_a} = 0 \qquad \text{eq. iii}$$

$$w = \sqrt{\frac{2\boldsymbol{ee}_0 V}{eN_a} + b^2} - b \qquad \text{eq. iv}$$

This is the solution given by Petroff and Stapelbroek.

Appendix B. Hall Effect: Van der Pauw Method

Van der Pauw developed a method in 1958 for measuring Hall effect and resistivity of disc-like samples of arbitrary shape as shown in Fig. II.

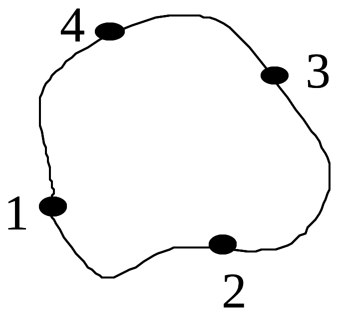

Fig. II. Van der Pauw geometry. Sample is a thin lamellae of arbitrary shape with 4 contacts placed at arbitrary positions on the periphery.

Van der Pauw showed that the Hall effect and resistivity of such an arbitrary sample can be determined provided the following conditions are met:

(1) The contacts are on the circumference of the samples
(2) The contacts are sufficiently small
(3) The thickness is homogeneous
(4) The surface of the sample is singly connected (no holes)

The Hall coefficient (R_H) is given by:

$$R_H = \frac{t\sum_{i=1}^{4}\Delta V_i}{4IB} = \frac{r_H}{ne} \qquad \text{eq. v}$$

where ΔV signifies the voltage difference measured between two contacts with the magnetic field on and off (or positive and negative), t is the thickness of the sample, I is the current, B is the magnetic field, n is the carrier concentration, e is the electronic charge, and r_H is the Hall scattering factor, also sometimes called the Hall factor. The carrier concentration can be calculated from the above equation. The contacts are switched such that four values for ΔV are averaged.

The Hall scattering factor (r_H) varies between approximately 0.8 and 1.4 for Ge and depends on the magnetic field, temperature, and sample orientation. In the high magnetic field limit (usually > 1T) r_H approaches 1. The Hall scattering factor for <111> Ge at 77 K in a 100G magnetic field is 0.83 for n-type Ge and 1.25 for p-type Ge. For complete data on hall scattering factors for n-type Ge see Miyazawa and Maeda, 1960 and for p-type Ge see Beer and Willardson, 1958. For variable temperature Hall measurements a scattering factor of 1 has been used. This introduces a small error since r_H is close to 1.

The resistivity can be determined by:

$$\boldsymbol{r} = \frac{\text{ðt}}{\ln 2}\frac{\sum_{i=1}^{4}|V_i|}{4I} f \qquad \text{eq. vi}$$

where the voltage is measured in two different contact configurations with two opposite current polarities giving 4 values of voltage. f is a function which varies between 0.3 and 1 and depends on the ratio of voltages in the two different contact configurations. If the two voltages are equal then f=1. For a close to square sample this generally holds true and f is neglected.

Mobility can be calculated from carrier concentration and resistivity.

$$\mu = \frac{1}{ne\rho} \qquad \text{eq. vii}$$

Sample thickness cancels out of the equation and therefore mobility is thickness independent.

The last point to note is that there is an error associated with the placement of contacts as it deviates from the criteria layed out by Van der Pauw [see Popovic, 1991 p. 240].

		$\frac{\Delta\rho}{\rho}$	$\frac{\Delta R}{R}$
(a)	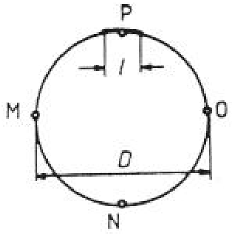	$\approx \frac{-l^2}{16D^2 \ln 2}$	$\approx \frac{-2l}{\pi^2 D}$
(b)	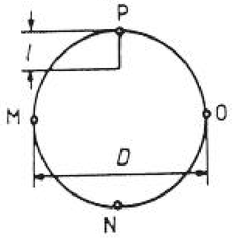	$\approx \frac{-l^2}{4D^2 \ln 2}$	$\approx \frac{-4l}{\pi^2 D}$
(c)	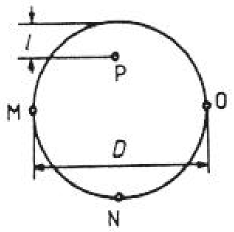	$\approx \frac{-l^2}{2D^2 \ln 2}$	$\approx \frac{-2l}{\pi D}$

Fig. III. Relative errors in resistivity and Hall coefficient caused by (a) finite size of contacts (l) along the sample circumference (b) finite size of contacts (l) toward the center, and (c) placement of the contacts off of the circumference [Adapted from Popovic, 1991]

To a first approximation the errors are additive for each contact. The largest error comes from case (c) where contacts are misplaced from the circumference. In this case, for l = D/3 for 4 contacts the error in Hall coefficient is ~ 80%.

Appendix C. Crystal Orientation by Laue X-ray Diffraction

In Laue diffraction an x-ray beam of white radiation is generated from a tube of a heavy metal target such as tungsten. The specimen is s single crystal or a large grain that is bigger than the incident beam. Using the diffraction equation:

$$n\lambda = 2d \sin \theta$$

one can see that each diffracted beam will have a different wavelength selected out by the d spacing and θ of each crystal plane. The Bragg angle (θ) is fixed by geometry.

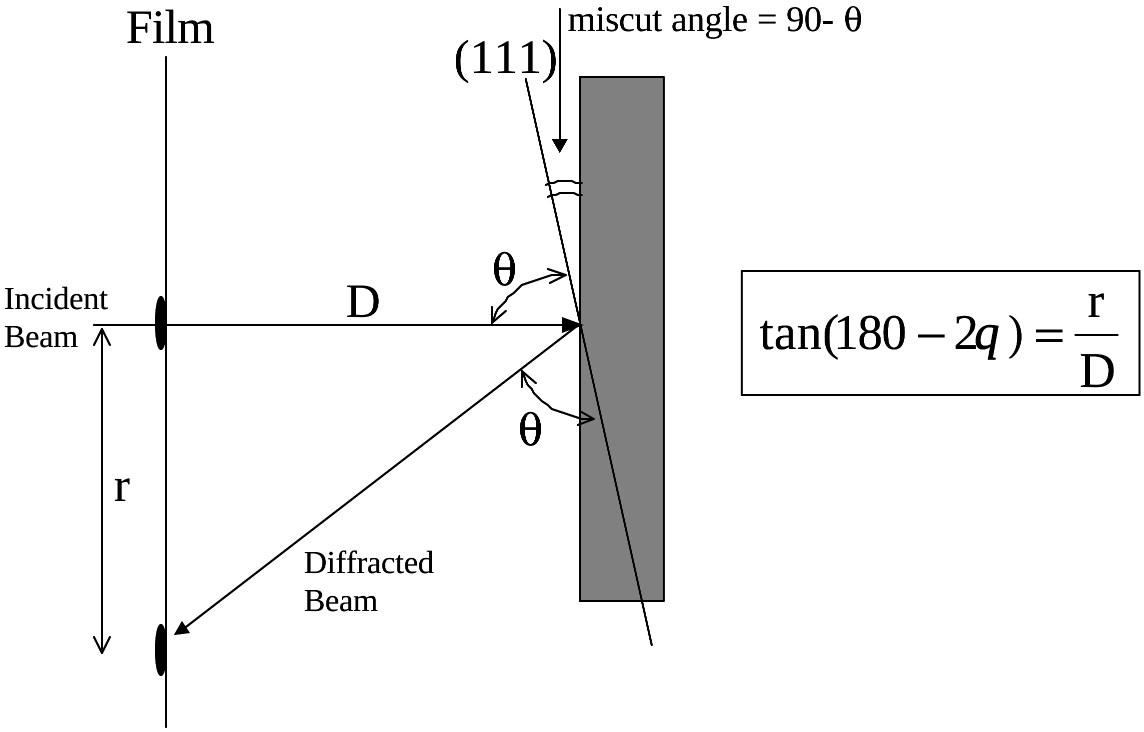

Fig. IV. Schematic of back reflection Laue x-ray diffraction. The substrate is shown on the right and the film or camera on the left.

Crystals with the same crystal structure but different d spacings will produce identical patterns with the only difference being the wavelength of the diffracted beam. The same holds true for a series of planes such as (100), (200), (300)…. They will all contribute to the same diffracted spot. For a complete treatment of x-ray diffraction, see Cullity, 1978.

The back-reflection Laue configuration is shown in Fig. IV. The beam is incident on the crystal through a hole in the center of the film or camera. The angle of the diffracted beam is determined by the Bragg equation and is shown here for the (111) plane of a miscut crystal. In this case, if the beam were precisely perpendicular to the (111) then the diffracted beam would line up with the incident beam and the miscut angle would be 0°. The position of the diffracted spot on the film is determined by the equation given in Fig. IV, and it depends on the camera length (D) and the distance from the spot to the center of the film (r). One can calculate the Bragg angle from the equation given in Fig. IV, however it is not possible to identify the plane in this way since the wavelength is unknown.

For crystal orientation purposes, we know that the crystal is oriented close to the (111). The Laue pattern can be identified as that of the diamond cubic structure for germanium. A diffraction pattern for a (111) oriented crystal is shown in Fig. V. The 3-fold symmetry of the crystal is evident. For a misoriented crystal, the distance from the 111 spot to the center of the film determines the Bragg angle. The misorientation angle, or angle that the crystal is tilted away from the (111), is simply 90° - θ. Practically, the central spot is large and measuring this distance accurately is difficult. To attain greater accuracy, lines are drawn through each hyperbola on the film (which can be

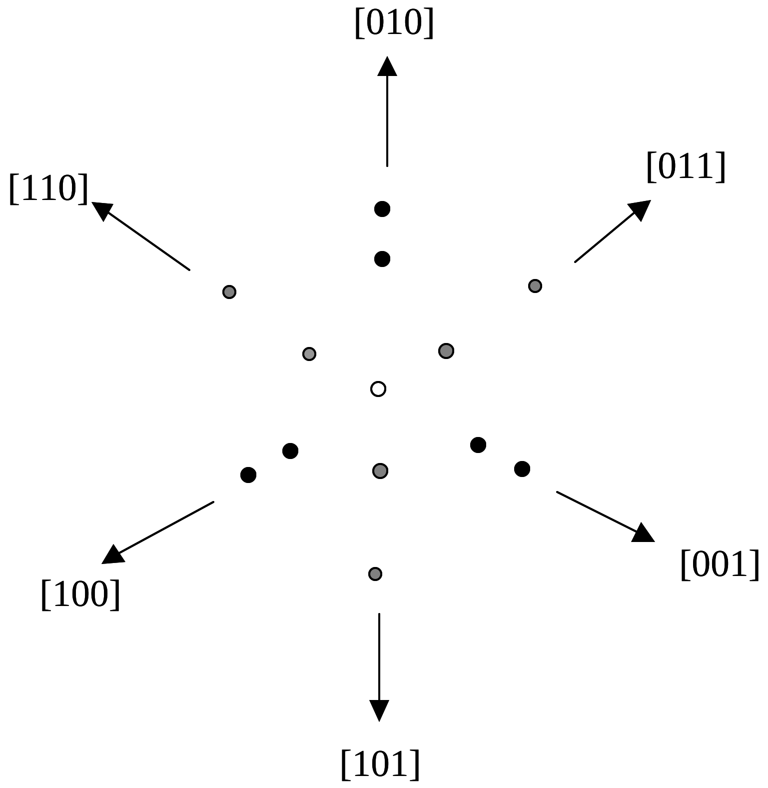

Fig. V. Sample Laue diffraction pattern for a <111> diamond cubic sample (not to scale). The central spot corresponds to the incident beam and overlaps with the 111 spot. Gray and black spots are used only to illustrate the 3-fold symmetry of the {111}.

approximated as a straight line since we are so close to the 111 zone). The intersection of these lines determines the location of the 111 spot. The crystal is then rotated 90°, 180° and 270°. Half of the distance between the 0° and 180° spot, for example, determines the misorientation angle. For precise orientation of crystals, the same procedure was used, but the crystal was rotated using a goniometer until the 111 spot lined up exactly with the center of the film.

Appendix D. Fourier Transform Infrared Spectroscopy

Fourier Transform Infrared Spectroscopy (FTIR) has been an important technique for measuring the spectral response of germanium in the far infrared. For an in-depth treatment of FTIR, see Bell, 1972. Photothermal ionization spectroscopy using FTIR is an invaluable technique for identifying impurities in high purity germanium [Haller, 1973]. Characterization of spectral response of far infrared detectors also relies on FTIR. In this work it is used for BIB detector spectral response measurements, PTIS, and

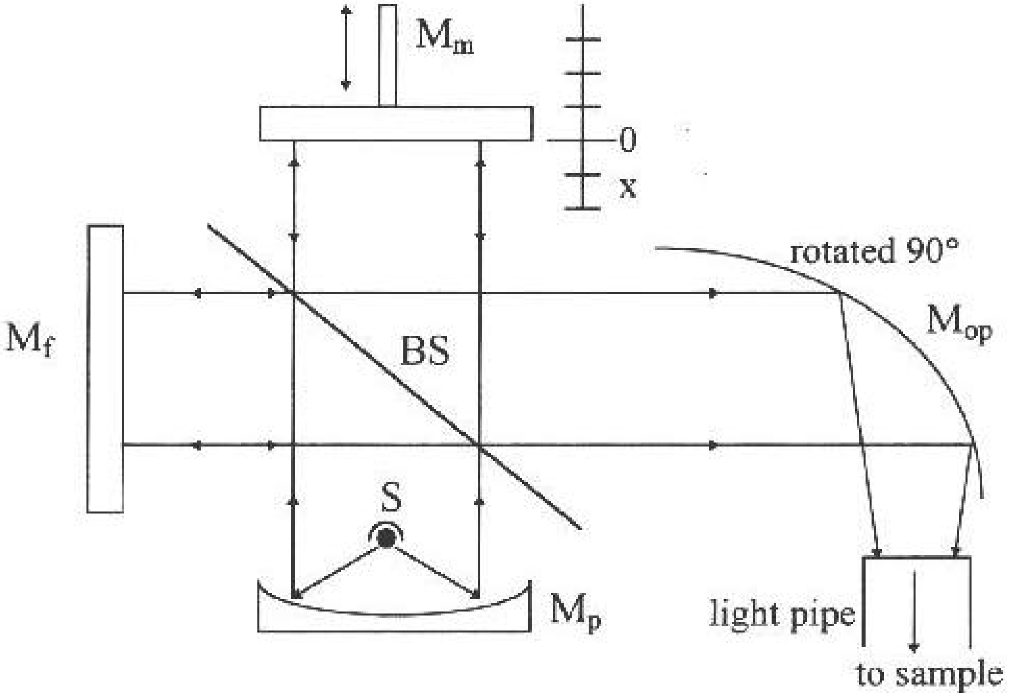

Fig. VI. Schematic of an infrared Michelson interferometer. S = light source, BS = beam splitter, M_p = parabolic mirror, M_f = fixed mirror, M_m = moveable mirror, x = position of the movable mirror, M_{op} is an off-axis parabolic mirror. [Olsen, 1998] transmission measurements. A schematic of a Michelson interferometer used for FTIR is shown in Fig. VI. It is operated in vacuum to eliminate water absorption lines.

An off-axis parabolic mirror (M_p) is used to create a parallel beam of light from a mercury arc lamp (S). A Mylar beamsplitter (BS) sends part of the beam to a fixed mirror (M_f) and part to a moveable mirror (M_m). The two beams recombine and interfere to form an outgoing beam with a spectrum determined by the position of the moveable mirror. A 20 cm long micrometer screw driven by a stepper motor moves the mirror. At the position where the distance from both mirrors to the beamsplitter are equal, the outgoing radiation is white (there is only constructive interference for all wavelengths between the two beams). This position is known as “zero path”. In all other mirror positions certain wavelengths will interfere constructively and others destructively. The outgoing beam is chopped at ~ 20 Hz, focused into a brass light pipe and guided into the sample dewar.

The photocurrent from the germanium detector in response to the light signal at different mirror positions is transformed to a voltage by a transimpedence amplifier. This signal is fed into a lock-in amplifier and into a computer, which collects output from the lock-in. The resulting plot of change in signal across the detector vs. mirror position is an interferogram. Fourier Transformation converts the interferogram into a frequency spectrum. Typically, a cosine transform is used, assuming that the interferogram is symmetric around zero path. A sine transform of a perfectly symmetric interferogram should be zero. If the phase of the interferogram is shifted slightly, this can be accounted for by using the information from a cosine and sine transform. An alternative is to use a

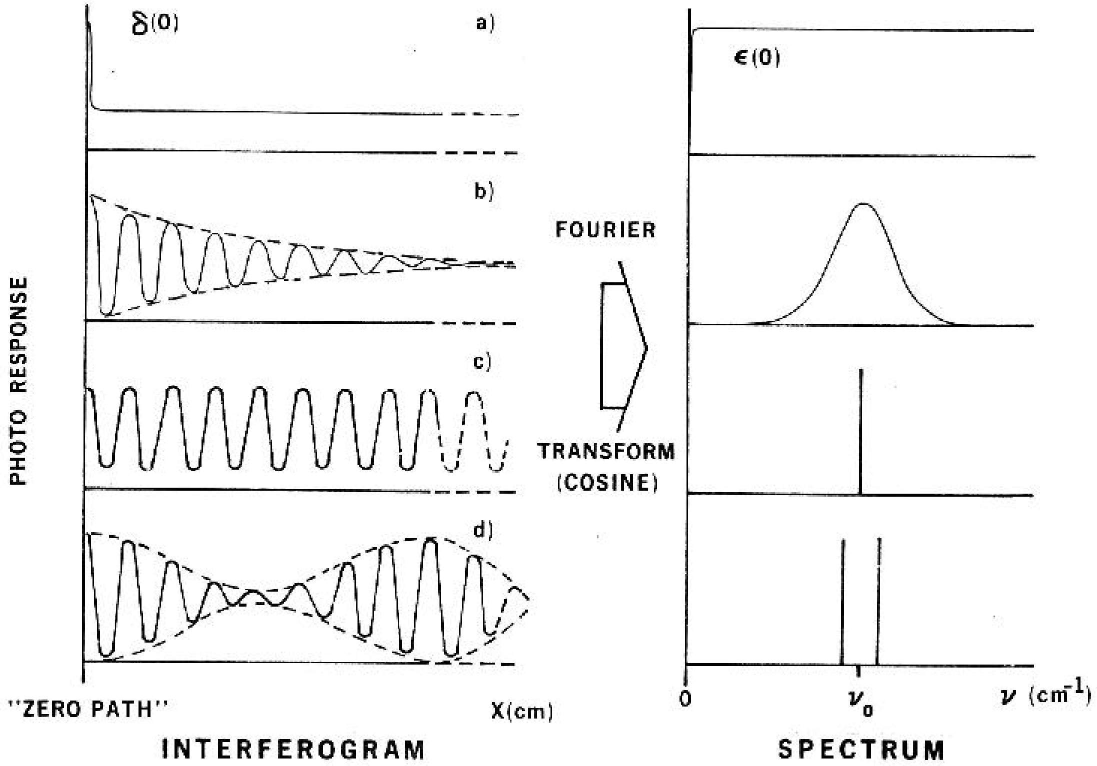

Fig. VII. Schematics of four sample interferograms and their spectra after Fourier transformation. (a) A δ response at zero path transformed into a white spectrum, (b) A decaying cosine function transforms to a broadband response (c) a cosine wave transforms to a single frequency (d) a cosine wave with a beating pattern gives sharp lines at two frequencies. [Haller, 1974]

power transform which will not be phase sensitive. In this work, the phase was adjusted accurately and cosine transforms were used.

Fig. VII illustrates the transformation of interferograms into spectra for several cases. A delta response at zero path transforms to white radiation at all frequencies. If the sample measured were to respond only to a single frequency, the interferogram would be a cosine wave. When Fourier transformed it would give a sharp peak at a single frequency. The response of a germanium photodetector is broadband, and so the interferogram is composed of many interfering cosine waves. It should be noted that the sensitivity of a photoconductor per frequency interval does not depend on photon energy. A photoconductor is a photon counter. Alternatively, a bolometer is sensitive to photon energy, so the same sample measured with a bolometer and a photoconductor will give different spectra. The response of a photoconductor to a specific photon energy can be measured using a narrow band filter with a known flux of photons impinging on the detector.

The beamsplitter is a sheet of Mylar of constant thickness, and therefore incurs Fabry-Perot interferences. For a 45° beamsplitter, the criteria for constructive and destructive interferences are [Bell, 1972]:

$$m\lambda = 2l\left(n^2 - \frac{1}{2}\right)^{\frac{1}{2}} \tag*{eq. viii}$$

m = 0, 1, 2, 3, ... for destructive interference
m = 1/2, 3/2, 5/2, … for constructive interference

Depending on the thickness of the beamsplitter there will be “zero” points in the spectra which match the Fabry-Perot minima. For the 0.001” thick Mylar beamsplitter (1 milB) used in this work, n ~ 1.85 and the first minimum should occur at 115 cm^{-1} for m=1. The observed minimum is at ~ 150 cm^{-1}, probably because the beamsplitter is actually thinner than 1 mil. This beamsplitter was chosen so as not to have a minimum in the region of interest.

Appendix E. Photothermal Ionization Spectroscopy

Photothermal Ionization Spectroscopy (PTIS) is an invaluable technique for identification of impurities in semiconductors. It is difficult to identify a specific shallow dopant in germanium using variable temperature Hall effect measurements because the

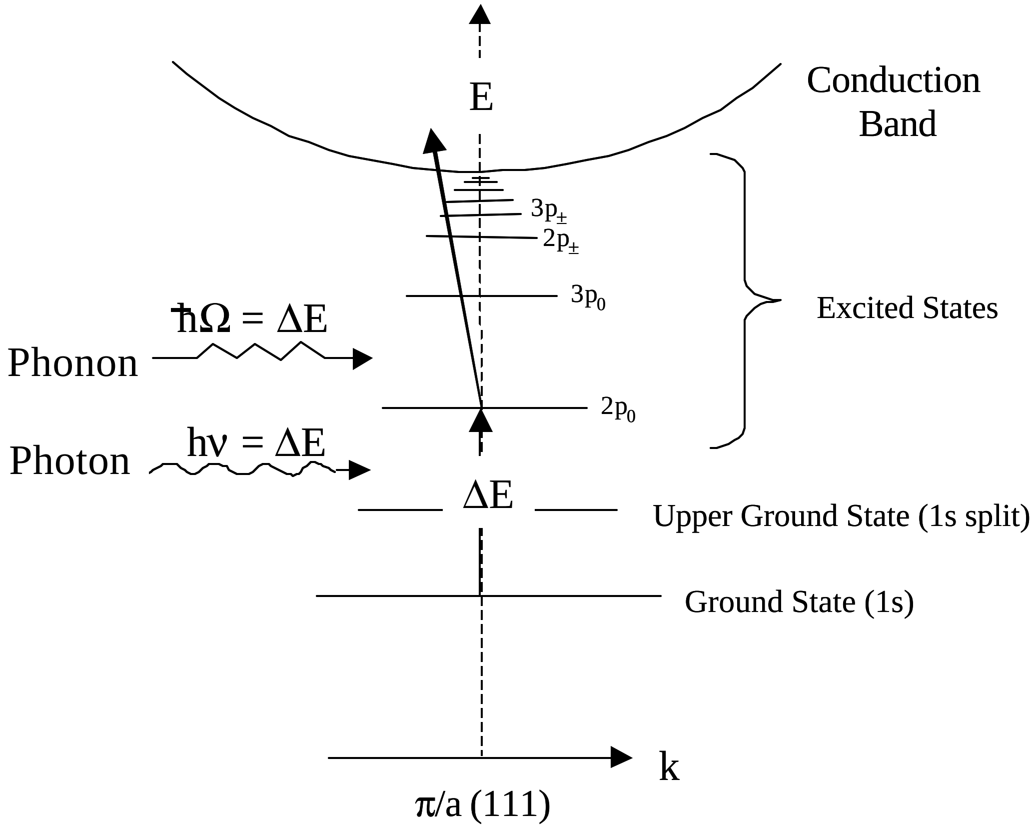

Fig. VIII. Process of Photothermal ionization shown for a shallow donor in germanium (not to scale). In step 1 a photon is absorbed with the energy (ΔE) to excite an electron from the ground state to a bound excited state. In step 2 a phonon is absorbed exciting the electron energy to the conduction band [Adapted from Haller, 1974].

ionization energies for different dopants are very close. PTIS takes advantage of the fact that each dopant has a unique ground state energy which makes the species immediately identifiable, while the bound excited states are identical. The difference in ground state energy comes about because in this state the electron wavefunction is s-like and is localized closest to the impurity atom. This makes the ground state energy sensitive to the chemical nature of the impurity. The excited states have much larger radii and are insensitive to the chemical nature of the impurity atoms.

Fig. VIII is a schematic of the two-step PTIS process for donors in germanium. In the first step, light impinging on the sample excites an electron from the donor ground state to an excited state. In the second step a phonon excites the electron into the conduction band. The process takes place at a temperature where sufficient phonons are present to excite the electron from the excited state into the conduction band. The probability of the second process (involving a phonon) increases with temperature. However, the temperature must be kept low enough such that most of the impurities are in their neutral state. An optimal temperature of around 8 K for germanium has been determined experimentally [Haller, 1974]. The PTIS process generates a photocurrent. A frequency spectrum is obtained using FTIR as described in Appendix E.

Appendix F. BIB Dewar Electronics

Germanium BIB detector characteristics were measured in an Infrared Labs HD-3 helium dewar. The dewar contains a copper cold stage that is cooled to 1.3 K by pumping on liquid helium in a reservoir. Detectors are electrically isolated from and heat sunk to the cold stage through a piece of sapphire mounted on brass.

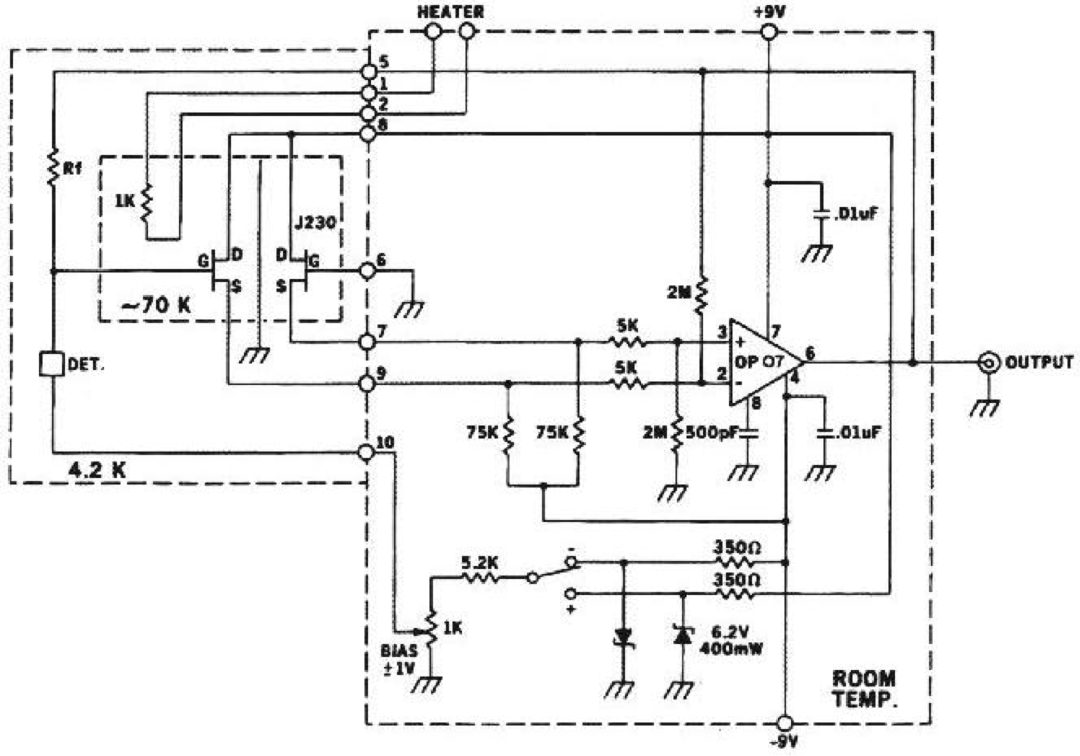

Fig. IX. Schematic of the transimpedance amplifier circuit used in BIB measurements.

A transimpedance amplifier (shown in Fig. IX) is used to transform the photocurrent (I_{signal}) out of the detector into a voltage (V_{out}). The circuit is designed to measure small currents (for example the dark current of the detector). The circuit contains a pair of cold matching JFETs with high impedance inputs and low offset. The op amp OP07 is chosen for its low noise and offset voltage. Current is measured via the voltage drop over a 10^{10} Ω feedback resistor, R_f. Currents can be measured between 10^{-9} and 10^{-14} A. The offset in the circuit at zero applied bias is -5.9 mV which must be subtracted from the output voltage for I-V measurements.